Norwegian University
of Life Sciences

Master's Thesis 2017 30 ECTS
Faculty of Science and Technology
Associate Professor Themistoklis Tsalkatidis

Evaluation of Crack Width Calculation Methods for Reinforced Concrete Structures exposed to Thermal Gradients using Nonlinear Finite Element Analysis

Oddgeir Ommelstad
Structural Engineering and Architecture
Faculty of Science and Technology

Preface

This is the final work of the Master program in Structural Engineering and Architecture at the Norwegian University of Life Sciences. After a total of 7.5 years of study, new challenges are waiting. I would like to thank all the lecturers for their sharing of knowledge and lectures during these years. An extra thank you to my supervisor Associate Professor Themistoklis Tsalkatidis for his administrative handling and correction of this task.

The thesis is also developed in collaboration with Multiconsult ASA. Their support and interest in the task has been very valuable, and I wish to thank them for believing that I could perform this task for them. I would like to send a special thank you to my co-supervisors Morten Engen and Reignard Tan who have helped with both expertise, corrections, exciting discussions and support during this working period.

In the end, I would like to thank Marie, Stella, my family and friends for their support through these years of study and during the work with this thesis.

Oddgeir Ommelstad

Abstract

Crack width calculations for reinforced concrete structures with imposed deformations are not fully specified in Eurocode 2. The lack of information has resulted in confusion about crack width calculations for reinforced concrete structures exposed to thermal gradients. Therefore, different engineers are using various approaches for implementation of load effects from thermal gradients. Use of restraint forces from linear finite element analysis and empirical calculations are two variants of these approaches. The restraint forces based on linear material behavior are criticized for being overestimated and the empirical calculations of restraint reinforcement strain are assumed uncertain for concrete structures with a limited crack propagation. The behavior of restraint forces from thermal gradients is explained in chapter 1.

A calculation procedure based on nonlinear finite element analysis in ANSYS Mechanical APDL was examined in this thesis. The evaluation of this calculation is based on an earlier experiment where thermal gradient effects on reinforced concrete structures were inspected. This experiment is introduced in chapter 2. The external restraint loads generated from the thermal gradients were registered indirectly in this experiment through the measurement of axial force in two pre-stressed tie-rods. In addition, maximum crack widths were illustrated for three of the load cases studied in the experiment.

The procedure used for calculation with nonlinear finite element analysis followed a three-step process. This procedure is described in chapter 3. The first step was to estimate the external restraint loads from steady-state temperature differentials using nonlinear finite element analysis. The nonlinear finite element analysis used in this project considered nonlinear material response and reduced material stiffness due to cracking of the concrete. The estimated tie-rod forces from this analysis were assessed using modelling uncertainties relative to the experimental tie-rod forces. These modelling uncertainties were also carried out for tie-rod force estimation based on linear finite element analysis. The approximation of restraint forces from nonlinear finite element analyses showed better accuracy relative to the experimental forces than approximated forces from linear finite element analyses. These results are shown and discussed in chapter 4.

The second and third step in the process were the implementation of external restraint loads in the crack width formula and the calculation of crack widths. Crack widths were calculated with four different approaches where the determination of the contribution from restraint forces varied. The basis for these contributions was either linear or nonlinear finite element analysis. The linear approaches were based on either an estimated restraint force or an empirical calculation of the restraint strain in the critical section. The nonlinear approaches were formed by the findings in this task. In chapter 5, these four calculations are compared with each other and with the maximum crack widths registered from the experiment.

Crack width calculations based on the empirical restraint strain using linear finite element analysis produced the most accurate results of conservative crack widths. Computations based on the procedure using nonlinear finite element analysis also showed relatively good results, and it is believed that this procedure can be even better with further investigation. The findings related to the calculation of crack widths for situations with thermal gradients are summarized in chapter 6, and the further work related to improvement of the nonlinear procedure are given chapter 7.

Sammendrag

Beregningen av rissvidder for armerte betongkonstruksjoner med påsatte deformasjoner er ikke fullstendig spesifisert i Eurokode 2. Den manglende informasjonen har ført til forvirring rundt beregningen av rissvidde for armerte betongkonstruksjoner utsatt for termiske gradienter. Derfor benytter ulike ingeniører forskjellige tilnærminger for implementering av lasteffekter fra termiske gradienter. Bruk av fastholdingskrefter fra lineære elementanalyser og empiriske beregninger er to varianter av disse tilnærmingene. Fastholdingskreftene som baseres på lineær materialoppførsel er kritisert for å være overestimert og de empiriske beregningene av fastholdt tøyning i armeringen antas å være usikre for betongkonstruksjoner med begrenset opprissing. Oppførselen til fastholdingskraften fra termiske gradienter er forklart i kapittel 1.

En beregningsprosedyre basert på ikke-lineære elementanalyser i ANSYS Mechanical APDL ble undersøkt i denne oppgaven. Evalueringen av beregningen er basert på et tidligere eksperiment hvor effektene av termiske gradienter på armerte betongkonstruksjoner er undersøkt. Dette eksperimentet er introdusert i kapittel 2. De eksterne fastholdingskreftene fra de termiske gradientene var registrert indirekte i dette eksperimentet gjennom målinger av aksialkraft i to forspente stag. I tillegg var maksimale rissvidder illustrert for tre av de studerte lasttilfellene i eksperimentet.

Prosedyren som ble brukt til beregning med ikke-lineære elementanalyser fulgte en tre-stegs prosess. Denne prosedyren er beskrevet i kapittel 3. Det første steget var å estimere den eksterne fastholdingskraften fra temperaturforskjeller i en likevektssituasjon ved hjelp av ikke-lineære elementanalyser. Den ikke-lineære elementanalysen som ble brukt i dette prosjektet tok hensyn til ikke-lineær material respons og stivhetsreduksjon i betongen på grunn av riss. Den estimerte stagkraften fra analysen ble vurdert ved hjelp av modelleringsusikkerheter i forhold til de eksperimentelle stagkreftene. Disse modelleringsusikkerhetene ble også estimert for fastholdingskrefter basert på lineære elementanalyser. Tilnærmede fastholdingskrefter fra ikke-lineære elementanalyser viste bedre nøyaktighet i forhold til eksperimentelle krefter enn tilnærmede krefter fra lineære elementanalyser. Disse resultatene er vist og diskutert i kapittel 4.

Det andre og tredje steget i prosessen var implementeringen av eksterne fastholdingskrefter i rissviddeformelen og beregning av rissvidder. Rissvidder ble beregnet med fire forskjellige tilnærminger hvor bestemmelsen av bidraget fra fastholdingskrefter varierte. Grunnlaget for disse bidragene var enten lineære eller ikke-lineære elementanalyser. De lineære tilnærmingene var basert på enten estimering av fastholdingskrefter eller empiriske beregninger av fastholdt tøyning i det kritiske tverrsnittet. De ikke-lineære tilnærmingene ble formet av funnene i denne oppgaven. I kapittel 5 er de fire beregningene sammenlignet med hverandre og med de maksimale rissviddene fra eksperimentet.

Rissviddeberegningene basert på den empiriske beregningen av fastholdt tøyning fra lineære elementanalyser produserte de mest nøyaktige og konservative rissviddene. Beregningene basert på prosedyren som bruker ikke-lineære elementanalyser viste også relativt gode resultater, og det er fortsatt tenkelig at denne prosedyren kan bli enda bedre med videre undersøkelse. Funnene relatert til beregningene av rissvidder for situasjoner med termiske gradienter er oppsummert i kapittel 6, og videre arbeid relatert til forbedringer av den ikke-lineære prosedyren er gitt i kapittel 7.

Contents

List of figures

List of tables

1 Introduction

1.1 Background

Limitation of crack widths is a control in the serviceability limit state to ensure the functionality, resistance and satisfactory appearance of a reinforced concrete structure (CEN 2004; Sørensen 2014). The control is usually stricter in gas and watertight structures where the functionality of reinforcement is vulnerable to leakage (Reinhardt 1991). For these structures the limitation varies between 0.20mm and 0.05mm depending on the water pressure (CEN 2006).

The calculation of crack widths should consider effects from both external forces and imposed deformations according to the design codes in Eurocode 2 (CEN 2004). Load effects from imposed deformations are caused by restraint of e.g. shrinkage and thermal expansion (Reinhardt 2014). These load effects are rather complex, and depends on the structural stiffness (Bruggeling 1987; Tavares & Camara 2010). They are also of particular interest in crack width calculations for liquid containing structures where the limit values are low (CEN 2006).

The load effects from thermal expansion are today usually calculated with the assumption of linear elastic material behavior (Brekke et al. 1994). These loads are either directly implemented in the crack width calculation or reduced before implementation. A direct implementation of these loads is criticized to be too conservative (Bruggeling 1991; Reinhardt 1991), and the reduced loads are calculated on an empirical basis (Brekke 2017; Det Norske Veritas 1980; Tavares & Camara 2010).

There is uncertainty attached to the empirical reduction of load effects from thermal expansion used in crack width calculations today (Brekke 2017). This uncertainty is associated to the validity of the empirical reductions in different structural problems. A load effect calculated directly from physical relations would have been preferred to avoid this uncertainty. Nonlinear finite element analyses taking into account stiffness reductions in the structure may be used for such calculations.

1.2 Previous work

The research in this thesis is focused on the implementation of restraint forces from imposed deformations in the crack width calculations. Imposed deformation and restraint forces from such deformations are studied by other researchers, and this research is important for the understanding of the complexity in the restraint force.

Because of the complexity of restraint forces, there was necessary to make some limitations in this thesis. One limitation was the exclusion of other imposed deformations than thermal deformations, which means that e.g. shrinkage was omitted. Another limitation was the exclusion of internal restraint forces from imposed deformations, which means that e.g. differences in thermal expansion between concrete and reinforcement were omitted.

In view of the limitations, the research was focused on the implementation of external restraint forces from thermal deformations in the crack width formula. Therefore, previous work on thermal deformations and external restraint forces are briefly presented in Sec. 1.2.1 and Sec. 1.2.2.

Another focus in this thesis was to implement external restraint forces in the crack width calculation from finite element analysis. A good approximation of these restraint forces depends on a reliable finite element model (Bathe 2014), and the material model for concrete is of importance for such approximations. Recent research on concrete material models in finite element analysis has made it possible to take into account more of the real concrete behavior. This research is briefly described in Sec. 1.2.3.

1.2.1 Thermal deformations

A material exposed to increasing or decreasing temperatures is known to expand or contract respectively (Tipler & Mosca 2008). This means that the volume of a reinforced concrete member will expand if the member is exposed to increased temperature. An increased temperature throughout the volume of the member will cause free expansion in all the spatial directions (El-Tayeb et al. 2017; Tipler & Mosca 2008).

A material exposed to different temperatures on two sides would not experience a uniform temperature throughout the volume, but rather a gradient in internal temperatures (Tipler & Mosca 2008). For a member of e.g. reinforced concrete, such gradients may be both linear of nonlinear throughout a cross section. These gradients would cause free bending of the member via internal restraint forces. This bending may be estimated based on the assumptions that plane sections remains plane (Ariyawardena et al. 1997; El-Tayeb et al. 2017).

A linear temperature gradient through the section would cause only free bending of the member in addition to free expansion, and a nonlinear gradient would cause both free bending and internal stresses. These internal stresses occurs due to the assumption that plane sections remains plane (Ariyawardena et al. 1997; El-Tayeb et al. 2017). A linear temperature gradient may be assumed in steady-state situations. Steady-state situation means that the surface temperatures has been constant over a longer period of time (Tipler & Mosca 2008).

Both uniform, linear and nonlinear thermal gradient should be taken into account in design of reinforced concrete structures (CEN 2003). The examinations in this thesis are limited to the elongations and bending caused by a linear thermal gradient. This gradient and the corresponding strains in a section are illustrated in Figure 1.

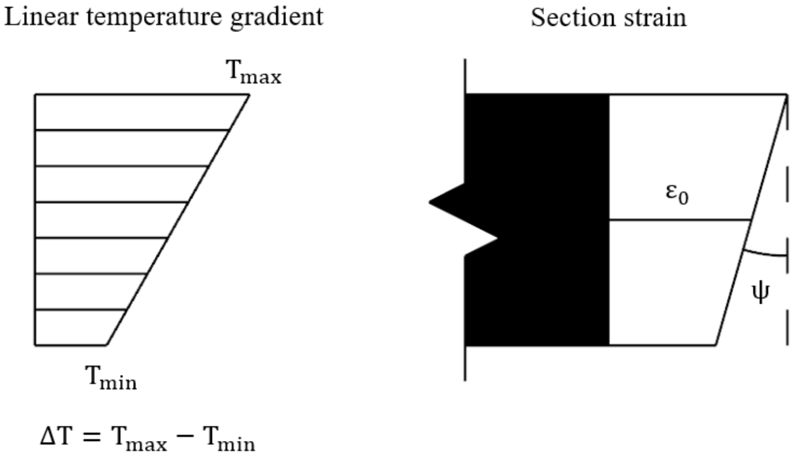

Figure 1: Linear temperature gradient with corresponding strain distribution for section.

The parameters ε_o and ψ given in Figure 1 are the average strain and curvature of the section due to thermal differentials respectively. The measure of the thermal gradient is given as the temperature difference between the maximum and minimum temperature in the section.

1.2.2 External restraint loads

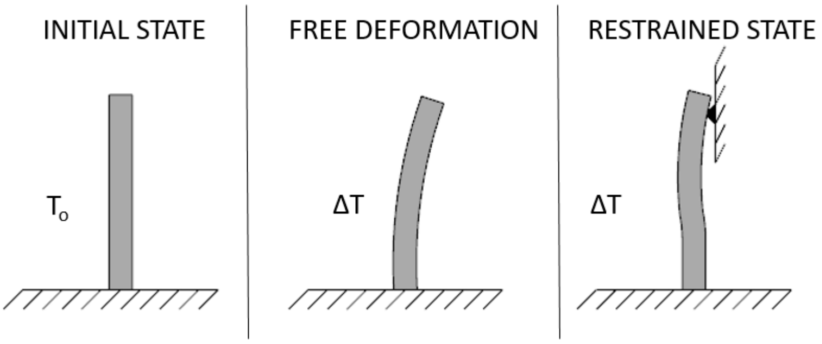

Figure 2: Initial state, free deformation and restrained state of concrete member.

External restraint loads occurs in systems where the free thermal deformations are restrained. A restraint may be e.g. the applied boundary conditions (Brattström & Hagman 2017; Nesset & Skoglund 2007). The boundary conditions may restraint both elongation and bending of a reinforced concrete member. The restraint of these free deformations may cause both external forces and moments (Ariyawardena et al. 1997; Nesset & Skoglund 2007). A restrained member is illustrated in Figure 2.

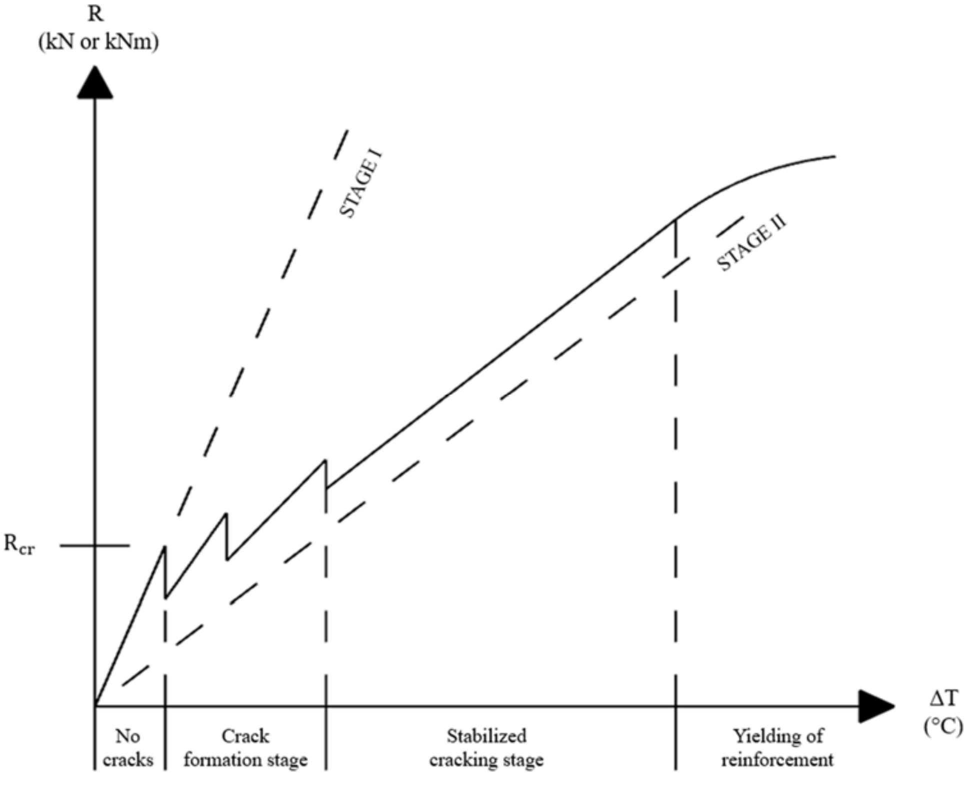

Figure 3: Development in external restraint loads.

The external restraint loads contributes to cracking of a structure (Ariyawardena et al. 1997; Nesset & Skoglund 2007). The magnitude of the external restraint loads is dependent on the stiffness of the structure (Alfredsson & Spåls 2008; Ariyawardena et al. 1997; Bruggeling 1987; Nesset & Skoglund 2007; Tavares & Camara 2010), and the structural stiffness decreases for each time of cracking (Li 2010; Sørensen 2014). This behavior is illustrated in Figure 3 (Bruggeling 1987).

The development in external restraint loads and cracking can be divided into four phases (Bruggeling 1987; Li 2010; Sørensen 2014). In the first phase, the external restraint load can be calculated based on the initial structural stiffness without cracks. This stiffness is also referred to as the Stage I stiffness (Li 2010; Tavares & Camara 2010).

The external restraint force based on Stage I stiffness may still cause cracking of the structure. The first crack occurs when an internal load combination inclusive the effects from external restraint loads exceeds a critical load combinations for the structure (Li 2010). This combination is given as R_{cr} in Figure 3. The critical load combination is where the maximum stress in the concrete equals the tensile strength of the concrete (Bruggeling 1987; Sørensen 2014). When the first crack is formed, the structural stiffness decreases and the crack formation stage is reached. In this phase, the external restraint load increases based on a reduced stiffness if the thermal gradients are increased. The restraint load increases until a new critical load combination is reached and then new cracks are formed (Bruggeling 1987; Li 2010). This sequence is repeated until the maximum number of cracks are formed in the structure.

When the final crack pattern is formed, the stabilized cracking stage is reached (Bruggeling 1987; Li 2010). This stage is characterized with a structural stiffness equal to the sum of the Stage II stiffness and a contribution from tension stiffening. The Stage II stiffness is equal to the stiffness of a cracked section where only reinforcement carries tensile forces (Li 2010; Sørensen 2014). In the stabilized cracking stage, the external restraint loads increases due to increased thermal deformations.

In the end of the stabilized cracking stage, the external loads have reached a level where the internal load combination causes yielding in the reinforcement. Additional forces would then cause mainly plastic deformations in the member, and the restraint forces will stabilize since the additional deformations are not restraint (Li 2010; Sørensen 2014).

The level of external restraint load reached in Figure 3 is not constant even though the applied thermal deformations remains constant. The reason for this is creep. Creep causes plastic deformations in a material because of a long-term loading. These plastic deformations cause relaxation of the restraint forces (Newman & Choo 2003; Reinhardt 1991).

Another aspect of creep is that the formation of plastic deformation accelerates if the structure is exposed to high temperatures (Ariyawardena et al. 1997; Bazant 1975). This is a general effect for all the loads applied to a heated structure.

The relation between cracks and external restraint loads is that cracks widen due to increased external restraint loads (Bruggeling 1987), but the cracks widths are also dependent on other loads and creep (CEN 2004; Miji Cherian & Ganesan 2014).

1.2.3 Material models for concrete in finite element analysis

The development in the external restraint force is dependent on cracking and tension stiffening. The material model for concrete is critical if these effects should be captured in a finite element analysis. The most common finite element analysis used for design today is linear finite element analysis (Brekke et al. 1994). These analyses are based on an elastic material behavior where stresses can increase indefinitely both in tension and compression.

The cracking behavior of concrete is not taken into account in the linear finite element analysis. This has led to nonlinear finite element analysis where some effects from cracking and tension stiffening are taken into account. It is expected that such nonlinear analysis would be used to a greater extend in the future (Vecchio 2001).

A material model according to Engen et al. (2017) that was originally intended for ultimate design of large reinforced concrete structures is used for approximation of restraint forces in this work. This material model takes into account the nonlinear stress and strain relations in concrete, cracking and compressive failures (Engen et al. 2017b). More details for the nonlinear material model are described during the section about the method.

1.3 Aim

The aim of the study in this thesis is to assess the use of nonlinear finite element analyses for calculation of external restraint loads imposed to reinforced concrete structures, and to assess the external restraint loads to be used in the crack width calculations.

The aim of this study can be divided into two main objectives, which are:

- Evaluation of approximated external restraint loads from nonlinear finite element analyses.
- Assessment of effects from external restraint loads to be used in the crack width formulas according to Eurocode 2 and NS3473.

These objectives are investigated based on an experiment performed by Vecchio and Sato (1990) with imposed deformations from thermal expansion. Both increased forces due to restraint and crack widths were registered in this experiment.

2 Case description

2.1 General

The case examined in this project was an experiment of thermal gradient effects on reinforced concrete frame structures performed by Vecchio and Sato (1990). In this experiment, three inverted frames of reinforced concrete were exposed to thermal gradients. The infliction of the thermal gradient was divided into load cases. In addition to increasing gradients, an increasing amount of force was applied to the columns by the pre-stressing of two tie-rods (Vecchio & Sato 1990). The setup of the experiment is illustrated in Figure 4.

The setup shows that thermal gradients in the experiment were applied to the structure by heating of water with a depth of 1500mm. This water was held inside the frame by walls connected to an external reaction frame. The only connection between the frame and wall was a flexible membrane. The restraint of deformation in the columns was applied through two tie-rods fastened near the end of the columns. These tie-rods were only fastened to the frame during Type II tests, and the columns were free to deflect in the Type I test (Vecchio & Sato 1990).

The frames were simply supported, with a pinned support beneath the column called C1 and a roller support beneath column C2. The difference between the three frames tested in the experiment was different amounts of reinforcement in the beam and columns. The three different constructions were named PF1, PF2 and PF3 (Vecchio & Sato 1990). The names for columns and frames are also used in this project and the differences in reinforcement are given in Sec. 2.2.

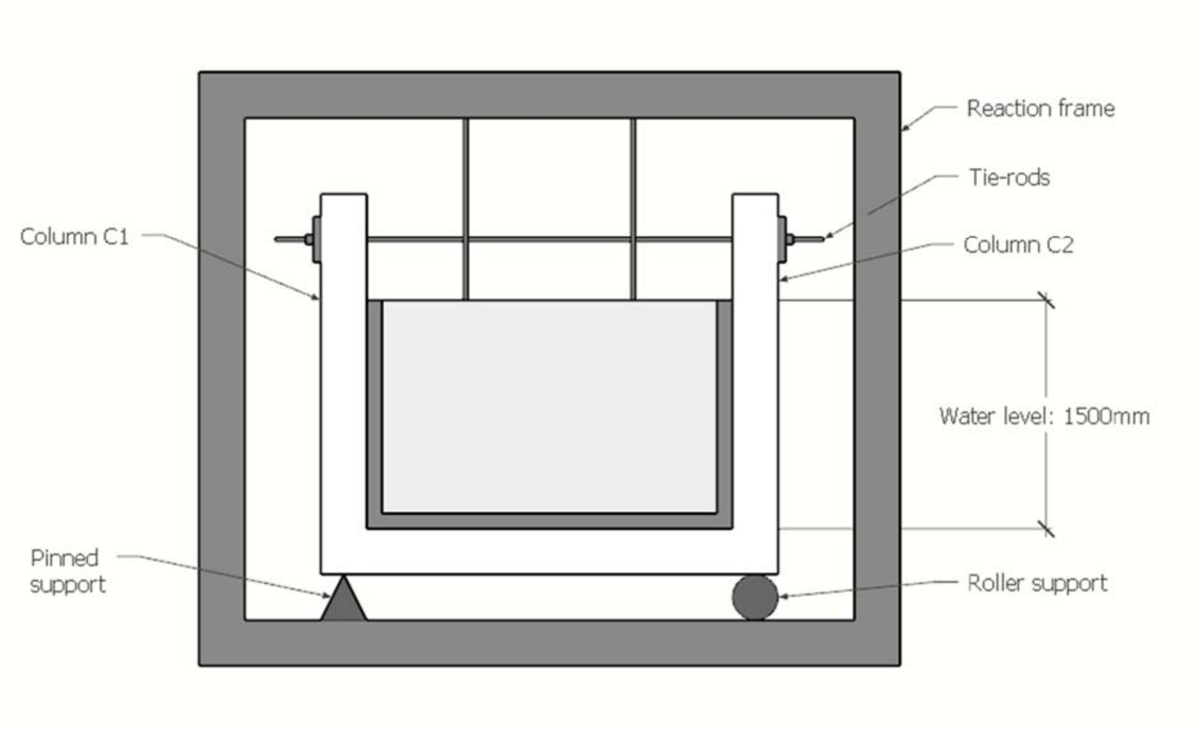

Figure 4: Setup of experiment.

2.2 Geometry

The frames used in the experiment had the same exterior dimensions. These dimensions were a height of 2500mm, a length of 3000mm and a width of 800mm. The thickness of the structural parts was 300mm and the tie-rods were fastened 300mm from the end of the columns (Vecchio & Sato 1990). These exterior dimensions are illustrated in Figure 5.

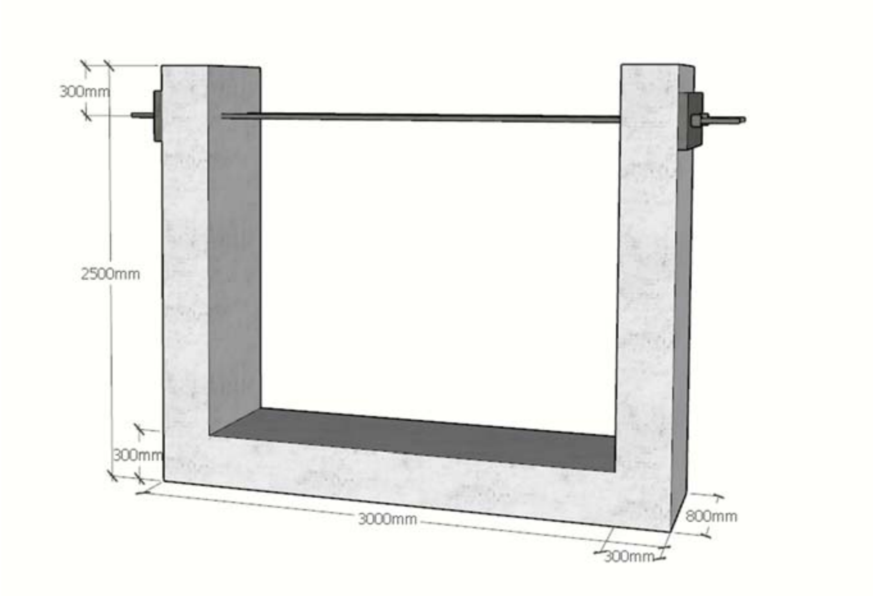

Figure 5: Exterior dimensions of experimental frame.

Inside the inverted frames, longitudinal reinforcement was applied with different amounts in the three frames. PF1 was equally reinforced in both columns and beam. PF2 was less reinforced in column C2 than the beam and column C1. PF3 was less reinforced in the beam than in the columns (Vecchio & Sato 1990). The geometrical properties for reinforcement are given in Table 1 and the reinforced cross section is illustrated in Figure 6.

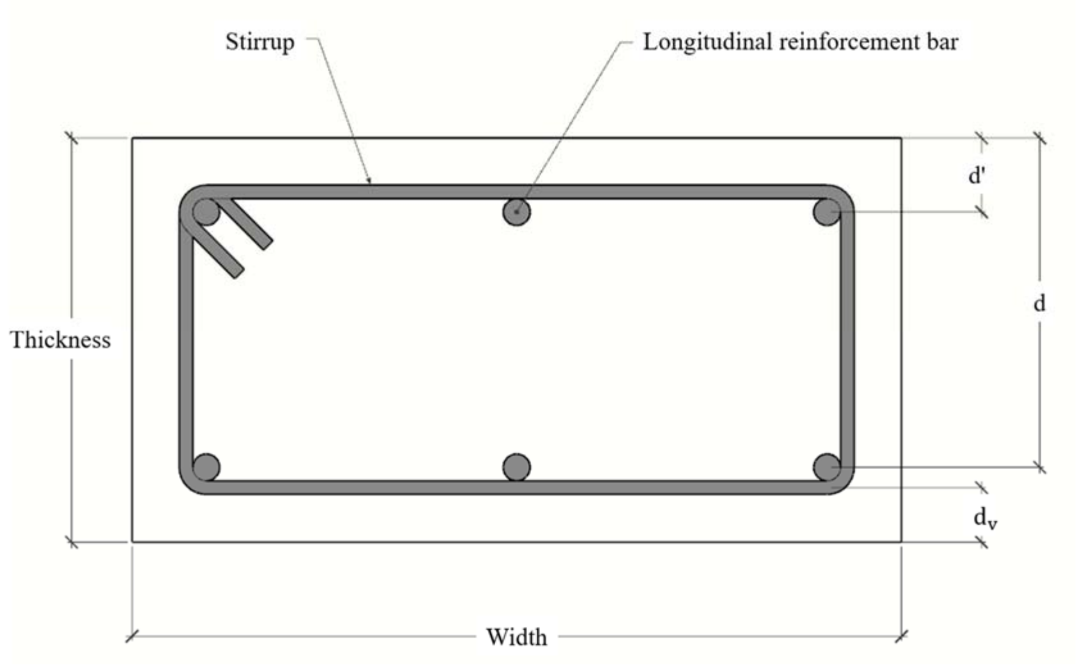

Figure 6: Reinforced cross-section.

The reinforcement bars used in the experiment were called #10, #20 and #25. The area of these bars were set to 100 mm^2, 300 mm^2 and 500 mm^2 respectively (Vecchio & Sato 1990). The same names and areas are used in this project. For layers of reinforcement with different bar areas, area of a bar was set equal to the average bar area.

The spacing between longitudinal reinforcement bars was not given in the article of Vecchio and Sato (1990). Since this was an input variable in the modelling of reinforcement, the rebars were spread to give the experimental area of reinforcement. This was done by spreading the bars equally over the width of the cross section. The equation for the spacing is given in Eq. (1).

$$s_l = \frac{b}{n_l} \tag{1}$$

Factors used in Eq. (1) are:

s_l	Spacing between reinforcement bars in the longitudinal direction (mm).
b	Width of frame (mm).
n_l	Number of longitudinal reinforcement bars in the layer.

Table 1: Geometrical properties for longitudinal reinforcement.

		LONGITUDINAL REINFORCEMENT		
		PF1	**PF2**	**PF3**
BEAM	**A_s' (mm^2)**	1200	1900	900
	d’ (mm)	55	50	50
	A_s (mm^2)	1200	1900	900
	d (mm)	245	250	250
	s_l (mm)	200	160	267
COLUMN C1	**A_s' (mm^2)**	1200	1900	1900
	d’ (mm)	55	50	50
	A_s (mm^2)	1200	1900	1900
	d (mm)	245	250	250
	s_l (mm)	200	160	160
COLUMN C2	**A_s' (mm^2)**	1200	900	1900
	d’ (mm)	55	50	50
	A_s (mm^2)	1200	900	1900
	d (mm)	245	250	250
	s_l (mm)	200	267	160

Unexplained parameters used in Table 1 are:

A_s'	Area of reinforcement in the top layer of reinforcement (mm^2).
d'	Center distance to reinforcement bar in top layer (mm).
A_s	Area of reinforcement in the bottom layer of reinforcement (mm^2).
d	Center distance to reinforcement bar in bottom layer (mm).

Shear reinforcement was also applied in the cross sections. This reinforcement was applied as stirrups around the longitudinal reinforcement. The area and spacing used for the stirrups are given in Table 2 (Vecchio & Sato 1990). The center distances from edge to stirrups were not given in the article by Vecchio and Sato (1990). Since these distances were used during modelling, it was assumed that the stirrups were in contact with the outer face of the #20 bars in the longitudinal direction. It was also assumed that the #10 and #20 bars had a diameter equal to 10mm and 20mm respectively. The center distance from edge to the stirrups was then calculated by Eq. (2).

$$d_v = d' - 0.5 \cdot (\emptyset_{\#20} + \emptyset_{\#10}) \tag{2}$$

New factors used in Eq. (2) are:

d_v	Center distance from edge to stirrup (mm).
$\emptyset_{\#20}$	Diameter of #20 reinforcement bars (mm).
$\emptyset_{\#10}$	Diameter of #10 reinforcement bars (mm).

Table 2: Geometrical properties for shear reinforcement.

		SHEAR REINFORCEMENT		
		PF1	**PF2**	**PF3**
ALL PARTS	**A_v (mm)**	100	100	100
	s_v (mm)	150	150	150
	d_v (mm)	40	35	35

Unexplained parameters used in Table 2 are:

A_v	Area of stirrup (mm^2).
s_v	Spacing between stirrups (mm).

All the reinforcement given in the article by Vecchio and Sato (1990) was applied in the structural finite element models.

2.3 Material properties

Material properties for the concrete and reinforcement used in the frames were tested in the experiment performed by Vecchio and Sato (1990). The tested material properties are shown in Table 3 and Table 4, and are used in this project.

Table 3: Material properties for concrete.

	CONCRETE		
	PF1	**PF2**	**PF3**
f_c (MPa)	42.4	48.4	30.1
f_{cr} (MPa)	3.12	3.80	3.1
E_c (GPa)	28.9	33.5	33.0
α_c (10^{-6}/°C)	9.86	11.9	12.1

Unexplained parameters used in Table 3 are:

f_c	Cylinder strength of concrete (MPa).
f_{cr}	Critical tensile strength of concrete (MPa).
E_c	Elastic modulus for concrete (GPa).
α_c	Thermal expansion coefficient for concrete (10^{-6}/°C).

The thermal diffusivity for concrete was also given in the article. This value was measured to 0.774 mm^2/s and was used to derive the thermal conductivity of the concrete. The thermal diffusivity was assumed equal for all the frames in the experiment (Vecchio & Sato 1990).

Table 4: Material properties for reinforcement.

	REINFORCEMENT		
	PF1	**PF2**	**PF3**
f_y (MPa)	448	450	448
E_s (GPa)	217	200	200
α_s (10^{-6}/°C)	12.4	12.0	12.0

Unexplained parameters used in Table 4 are:

f_y	Yielding strength of reinforcement (MPa).
E_s	Elastic modulus of reinforcement (GPa).
α_s	Thermal expansion coefficient for reinforcement (10^{-6}/°C).

The yielding stress tested for reinforcement was given for both #20 and #25 bars in the PF2 and PF3 frame. The values used in the model are given in Table 4. These values are the average yielding stress for the two bar dimensions.

2.4 Load cases

Ten load cases for each frame were investigated in the validation process of the model. The first load case investigated for the frames was a Type I test where the columns were free to deflect due to the applied thermal gradient, i.e. no pre-stressing applied. The thermal gradients used from this test were from a steady-state situation that occurred 18 hours after application of the gradient (Vecchio & Sato 1990). The thermal gradients were defined by the temperature on the inside and outside of the frame structures. The temperatures used to make gradients for Type I testes are given in Table 5.

The initial temperatures of the frames before heating were also given for each load case. These temperatures were measured on both the inside and outside of the frames. The initial temperatures given in the following tables are the mean temperature of the temperature on the inside and outside. The mean temperature was used as a reference temperature in the structural finite element analyses.

Table 5: Temperatures for Type I tests.

FRAME	LOAD CASE	TYPE I TEST			
		T_i (°C)	T_w (°C)	T_c (°C)	ΔT (°C)
PF1	**1**	19.9	89.2	35.6	53.6
PF2	**1**	14.5	90.7	32.6	58.1
PF3	**1**	16.3	91.8	31.9	59.9

Unexplained parameters used in Table 5 are:

T_i	Initial temperature of frame (°C).
T_w	Temperature on the inside of the frame - warm surface (°C).
T_c	Temperature on the outside of the frame - cold surface (°C).
ΔT	Steady-state thermal gradient through the cross section (°C).

In the Type II tests, pre-stress was applied to the frames through tie-rods. Three different levels of pre-stress were applied to the frames. For each level of pre-stress, multiple levels of thermal gradient were applied. The loads were applied to the frame with an increasing amount of force to cause increased crack propagation (Vecchio & Sato 1990). Nine load cases for each frame were examined for the Type II test in this project. These load cases are given in Table 6, Table 7 and Table 8.

Table 6: Temperatures and pre-stress for frame PF1 in Type II tests.

	LOAD CASE	TYPE II TEST				
		T_i (°C)	T_w (°C)	T_c (°C)	ΔT (°C)	F_{pre} (N)
PF1	**2**	16.5	25.0	15.7	9.3	3170
	3	15.0	65.0	23.6	41.4	3030
	4	13.3	91.1	29.6	61.5	3060
	5	16.5	35.5	20.7	14.8	22910
	6	15.7	56.0	25.9	30.1	22850
	7	14.6	92.4	31.5	60.9	23050
	8	15.8	35.9	20.8	15.1	38460
	9	14.9	54.1	24.2	29.9	38190
	10	16.9	93.9	34.0	59.9	39110

Table 7: Temperatures and pre-stress for frame PF2 in Type II tests.

	LOAD CASE	TYPE II TEST				
		T_i (°C)	T_w (°C)	T_c (°C)	ΔT (°C)	F_{pre} (N)
PF2	**2**	16.8	27.5	19.7	7.8	3720
	3	16.1	52.2	24.0	28.2	3890
	4	14.5	86.0	28.4	57.6	3540
	5	15.2	34.9	22.2	12.7	29550
	6	29.2	55.7	23.3	32.4	29530
	7	16.7	92.8	33.5	59.3	29470
	8	15.2	35.7	20.4	15.3	44060
	9	18.0	57.8	26.7	31.1	44430
	10	16.8	93.1	35.8	57.3	44160

Table 8: Temperatures and pre-stress for frame PF3 in Type II tests.

	LOAD CASE	TYPE II TEST				
		T_i (°C)	T_w (°C)	T_c (°C)	ΔT (°C)	F_{pre} (N)
PF3	**2**	15.7	25.7	18.9	6.8	4030
	3	14.3	65.3	22.3	43.0	4340
	4	14.2	83.3	27.6	55.7	3860
	5	12.1	34.1	16.4	17.7	21400
	6	14.0	54.1	22.2	31.9	21400
	7	14.5	92.8	30.4	62.4	20900
	8	13.2	35.0	19.5	15.5	33400
	9	15.5	55.1	23.9	31.2	33200
	10	16.0	93.5	32.0	61.5	32600

An unexplained parameter used in Table 6, Table 7 and Table 8 is:

F_{pre}	Applied pre-stress in tie-rods (N).

2.5 Crack widths

The article by Vecchio and Sato (1990) illustrated crack widths for three different load combinations for structure PF3. The maximum crack widths from these illustrations were registered. These crack widths are given in Table 9.

Table 9: Crack widths for frame PF3 registered in experiment.

LOAD CASE	TYPE II TEST
	w (mm)
4*	0.42
7	0.50
10	0.62

An unexplained parameter used in Table 9 is:

w Crack width (mm).

The first load case given in Table 9 was not one of the load cases picked in Sec. 2.4. This load case differed from the other load cases since the thermal gradient was held constant in 7 days (Vecchio & Sato 1990). The load case was inspected separately in this thesis just for examination of the crack widths. The load case was called 4* since it was a load case with similarities to load case 4. The temperatures and pre-stress applied in this load step are given in Table 10.

Table 10: Additional load case for frame PF3.

LOAD CASE	**TYPE II TEST**				
	T_i (°C)	**T_w (°C)**	**T_c (°C)**	**ΔT (°C)**	**F_{pre} (N)**
4*	14.4	93.1	30.9	62.2	3980

3 Method

3.1 General

A three-step process was used to calculate crack widths with effects from imposed deformations based on nonlinear finite element analyses. The imposed deformations considered in these calculations were the thermal expansion in the frames used in the experiment by Vecchio and Sato (1990). The first step in the three-step process was to approximate the external restraint forces from thermal expansion. These approximations were based on nonlinear finite element analyses. The nonlinear finite element analyses were based on nonlinear material behavior. The material model used for concrete in these analyses took into account nonlinear material response, cracking and compressive failure (Engen et al. 2017b).

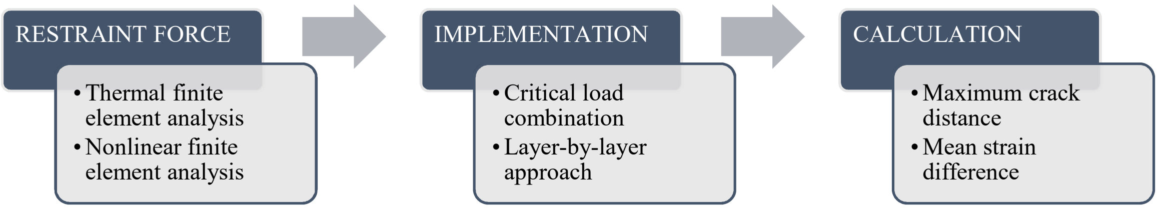

Figure 7: Three-step process for crack width calculation with thermal effects.

The external restraint forces approximated in the first step were used further in the second step. In this step, the external restraint force was used to approximate the strain distribution for a cracked cross section. This strain distribution was the basis for crack width calculations. Parameters as compression height, effective concrete area and reinforcement stress were calculated from this distribution. These parameters were further used in step three.

The third step was the calculation of the maximum crack width. This calculation was based on the design rules in Eurocode 2. The calculated crack widths were compared to measured crack widths from the experiment by Vecchio and Sato (1990). The three-step process with intermediate objectives is shown in Figure 7. These objectives are further explained in the next sections.

Approximations of the external restraint forces based on linear finite element analyses were carried out next to the nonlinear finite element analysis. The approximations from linear finite element analyses were compared to the approximations from nonlinear finite element analysis. The results from linear finite element analysis were also used to calculate crack widths based on an existing empirical method. These crack widths were compared to the crack widths calculated using nonlinear finite element analyses.

3.2 Finite element method

The finite element method was used for approximation of the external restraint force from thermal expansion. This method approximates a field variable like temperature or deformation within a real structure. The approximation takes place by meshing the real structural geometry into finite elements. The response of the field variable is then further approximated locally within the elements based on interpolation functions and material properties (Huebner et al. 2001).

The local element responses are then further assembled to approximate the response of the global system. This assembling process is based on continuity of the field variable between elements. An approximated solution of the field variable can then be found given a set of loads and boundary conditions. The solution can also be used for calculation of other related variables (Huebner et al. 2001). This procedure in the finite element method is illustrated in Figure 8.

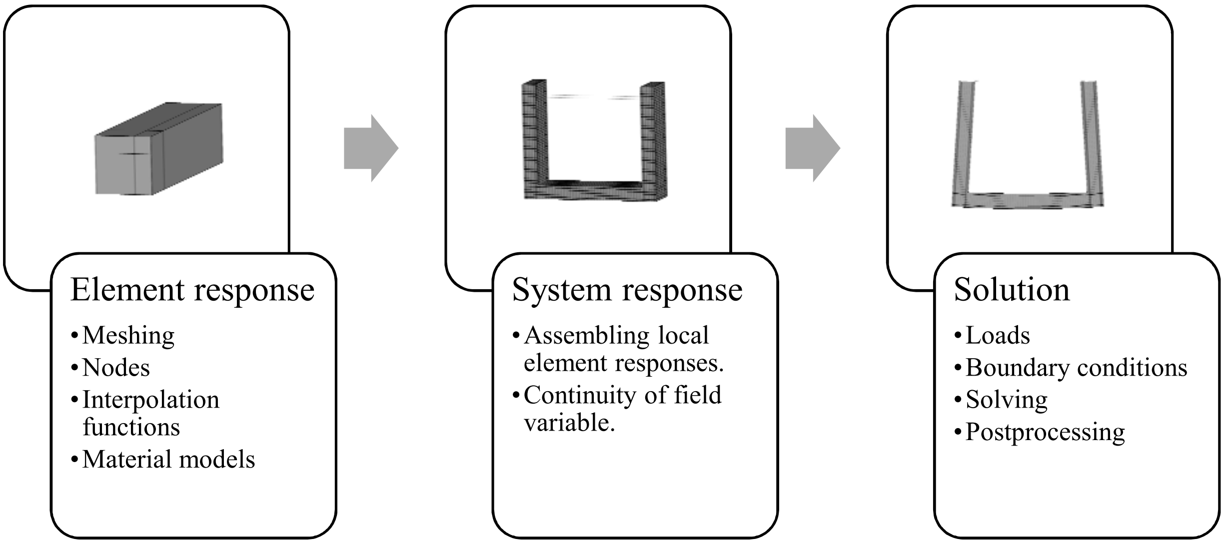

Figure 8: General procedure in finite element method.

The assembling process described above results in a mathematical representation of the system. The finite element programs are developed to solve complex variants of these mathematical representations. The reliability of the solutions is dependent on the assumptions made during modelling (Bathe 2014). This reliability of the finite element model is examined with a comparison of the results against the original experiment by Vecchio and Sato (1990). The modelling was focused on the use of measured parameters from the experiment. This focus was chosen to reduce the number of assumptions, and to capture more of the uncertainty in the used material model for concrete.

The process for finite element modelling in Figure 8 is used as a basis for explanation of the thermal and structural finite element analyses performed in this project. These explanations and assumptions during modelling are given in the next sections.

3.3 Thermal finite element analysis

The first objective in the first step of the three-step process was the approximation of temperatures within the frames. A thermal finite element analysis was performed for each examined load case to approximate a steady-state thermal gradient through the cross sections of the frames. The frame was meshed into 3D thermal elements. The elements were assigned conductivity, and temperatures were applied as boundary conditions in external nodes on the inner and outer surface of the frame.

A steady-state thermal gradient is a temperature distribution, which is independent of time. The distribution of temperatures was approximated based on Fourier's law of heat flow. This law states that heat will flow in the system if temperature differences are present. The steady-state gradient was then calculated by assuming that energy was conserved in the system (Hens 2010).

In this thermal finite element analysis, effects caused by convection, internal heat generation and radiation are neglected. These effects could have been taken into account by an extended analysis, but in this case, surface temperatures from a steady-state situation were given (Vecchio & Sato 1990). Because of this, it is assumed that the difference between these types of analyses is small in this particular case.

3.3.1 Thermal element response

The experimental geometry of the concrete was meshed into SOLID70 elements from the ANSYS element library. This element was used since the nodal temperature solution was compatible with the SOLID185 element used in the structural analysis. The SOLID70 and SOLID185 element were equal with respect to size, form and number of nodes. The size and form used for the elements were chosen due to approximation of deformations.

The SOLID70 element had eight external nodes with temperature as the only degree of freedom in each node. The distribution of temperatures within the element is approximated based on interpolation functions. These functions are adapted to the geometry of the element by a polynomial expression (ANSYS® Academic Research Mechanical Release 18.0). The element is illustrated in Figure 9.

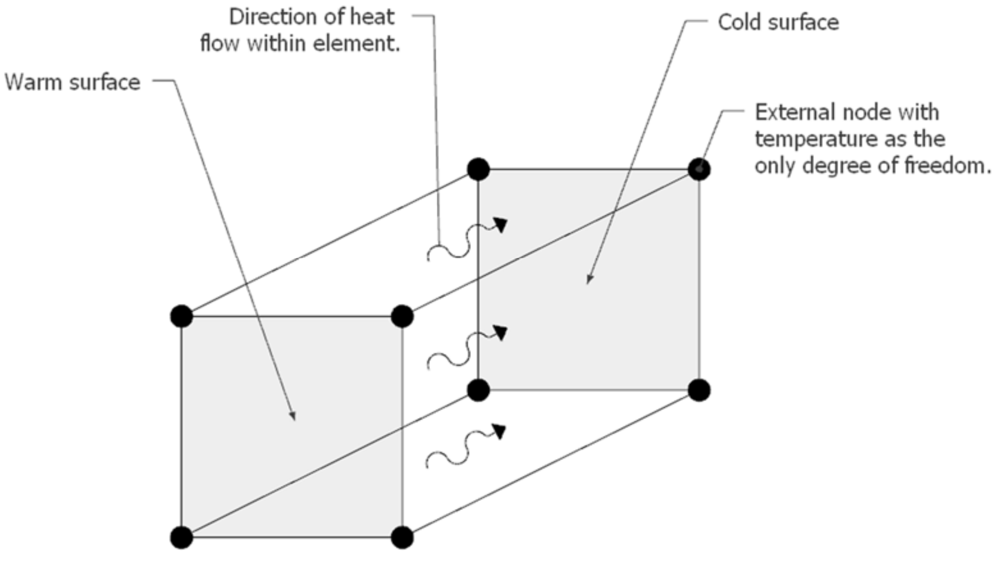

Figure 9: Eight-node thermal element used for thermal finite element analysis.

The heat flow within the elements is three dimensional, but occurs only in the directions where temperature difference is present. This is according to Fourier's law of heat flow. This law is the basis for a thermal finite element analysis (Huebner et al. 2001). Fourier's law is applied together with the law of conservation of energy to approximate a steady-state solution for the elements. Energy conservation ensures that the amount of heat within the element remains constant (Hens 2010; Huebner et al. 2001). This implies that heat flowing from one node in the element needs to be received by the other nodes in the element.

The heat flow within the element is approximated with the vector of nodal temperatures and a matrix describing the conductance of the material. The derivation of this conductance matrix for an element is shown in Eq. (3) (Huebner et al. 2001). This equation approximates the conductance related to conduction with the interpolation functions and the conductivity of the material.

$$[\mathrm{K_c}]^{(\mathrm{e})} = \int_{\Omega^{(\mathrm{e})}} [\mathrm{B}]^{\mathrm{T}}[\mathrm{k}][\mathrm{B}]\mathrm{d}\Omega \qquad (3)$$

The matrices used in Eq. (3) are:

$[\mathrm{K_c}]^{(\mathrm{e})}$	Element conductance matrix related to conduction.
$[\mathrm{B}]$	Temperature gradient interpolation matrix.
$[\mathrm{k}]$	Thermal conductivity matrix.
$\Omega^{(\mathrm{e})}$	Volume of element.

The only material property given as input in the calculation of the conductance matrix related to conduction was the conductivity of the concrete. This property was calculated from a given thermal diffusivity; see Sec. 2.3. The equation used for calculation of the conductivity is given in Eq. (4) (Byron Bird et al. 2002). The conductivity of the concrete was applied equal in all the directions of the material.

$$\mathrm{k} = \alpha \cdot \rho \cdot \mathrm{c} \qquad (4)$$

The factors used in Eq. (4) are:

k	Conductivity (W/m·°C).
α	Thermal diffusivity ($\mathrm{m^2/s}$) .
ρ	Density ($\mathrm{kg/m^3}$).
c	Specific heat capacity (J/kg·°C).

The density and specific heat capacity were needed to calculate the conductivity from thermal diffusivity. The density was set equal to 2400 $\mathrm{kg/m^3}$ by assuming normal concrete (CEN 2002a). The specific heat capacity of concrete was assumed constant and equal to 1000 J/kg·°C for the examined load cases (Klieger & Lamond 1994).

3.3.2 Thermal system response

The local responses of the elements were assembled into a global system response. This was done by adding the local conductance properties into their respective position in the global conductance matrix. The global conductance matrix made the nodal temperatures dependent on the heat flow through all elements connected to the node. In this way, it provide continuity of temperatures within the frame. The general equation for the system is given in Eq. (5) (Huebner et al. 2001).

$$[\mathrm{K_c}]\{\mathrm{T}\} = \{\mathrm{R_T}\} \tag{5}$$

The matrices and vectors used in Eq. (5) are:

$[\mathrm{K_c}]$	Global conductance matrix related to conduction (W/°C).
$\{\mathrm{T}\}$	Nodal temperature vector (°C).
$\{\mathrm{R_T}\}$	Nodal heat load vector from specified nodal temperatures (W).

3.3.3 Solution of thermal finite element analysis

The general equation is solved by setting either a temperature or a heat load for each node in the system. This was done in the project, by application of temperatures on the inner and outer surface of the frame. The temperatures used on these surfaces were taken from the article by Vecchio and Sato (1990); see Sec. 2.4. These temperatures were changed for each load case according to the given data.

The nodes on the inner surface of the frame were given high temperatures and the nodes on the outer surface were given low temperatures. Temperatures were applied in all nodes on the respective surfaces. This is a simplification of the real temperature distribution since the measured temperatures were from a region with water on the inside. The simplification was performed since no information was given about conditions above the water surface.

The temperature difference between the two surfaces generates heat flows in the system. The heat flow between the surfaces is illustrated in Figure 10.

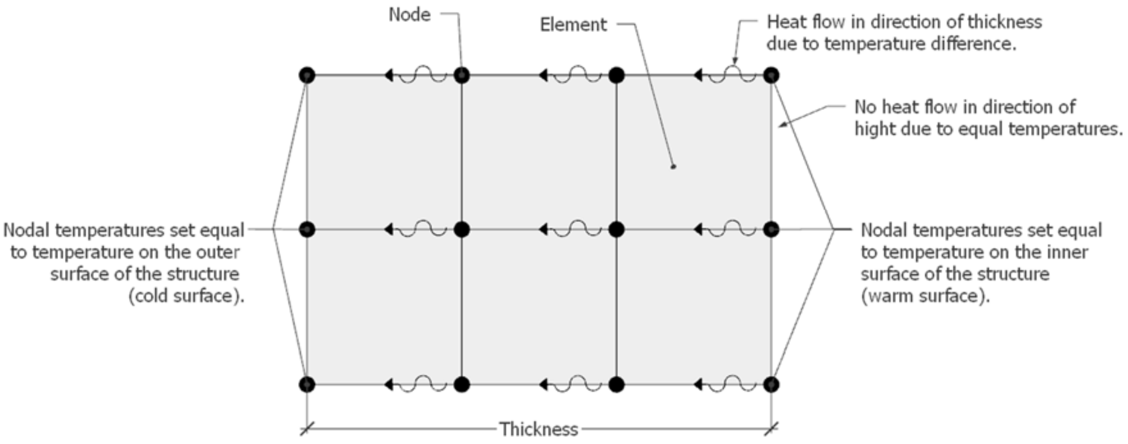

Figure 10: Heat flow between warm and cold surface.

The heat flow illustrated in Figure 10 is one-dimensional, but the nodes in the area around a corner would experience heat flow in two dimensions. This effect is caused by cooling from to surfaces.

In the nodes where temperatures are unknown, the heat load is set to zero. The calculation of an unknown temperature is then based on equilibrium between heats flowing in and out of the node due to the defined temperatures.

3.4 Structural finite element analyses

Two different structural finite element analyses were performed to approximate deformations in the structure. These were a linear finite element analysis (LFEA) and a nonlinear finite element analysis (NLFEA). The nonlinear finite element analysis was nonlinear due to material behavior. A nonlinear material model according to Engen et al. (2017) was used in the NLFEA. The NLFEA was the second objective in the first step of the three-step process, and the external restraint forces were indirectly registered from these analysis.

Reinforcement was embedded into the concrete elements in the structural analyses to give the system the behavior of a composite material. The reinforcement were modelled with an elastic behavior in the LFEA and a bilinear elasto-plastic behavior in the NLFEA.

The structural finite element analyses were performed for two load situations. In the first load situation, the thermal gradient was applied to an unrestrained frame together with self-weight and water pressure. In the second load situation, the frames were restrained by tie-rods attached to the columns. The loads involved in the second load situation were dead loads, water pressure, external and internal restraint forces and pre-stressing of the tie-rods. The two load situations were called Type I test and Type II test respectively. The external restraint forces were a part of the internal force in the tie-rods after application of the thermal gradient from the thermal finite element analysis in the Type II test.

A solution of the structural analyses was carried out based on force equilibrium for the system. The LFEA was solved based on force equilibrium for the linear-elastic material behavior, and the NLFEA was solved iteratively based on force equilibrium for the nonlinear material model using the Newton-Raphson method. The solution from NLFEA was accepted when an energy based convergence criterion was fulfilled. A convergence criteria and iteration process according to Engen et al. (2017b) were used in the solution of the NLFEA.

3.4.1 Structural element response

The structure was modelled with the real geometry from the experiment and meshed into SOLID185 elements. The SOLID185 element is the equivalent structural element to the thermal elements used in thermal finite element analyses. These elements were meshed with the same form and size.

The SOLID185 element is an eight node three-dimensional structural solid. Deformations within the element is approximated by use of three polynomial interpolation functions (ANSYS® Academic Research Mechanical Release 18.0). This element-type was used for the concrete parts of the structure. Within each element, the stresses were evaluated in eight integration points.

The size of the mesh was chosen with respect to the approximation of deformation in the NLFEA. Since cracks can occur in this analysis, the size of the mesh was influencing the crack propagation. A fine mesh was chosen, but still in a size where the assumed average material behavior could be assumed valid. The size of the elements is given in Figure 12 and a meshed frame is given in Figure 11. The element size gave four elements in the width of the frame and six elements in the thickness of the frame.

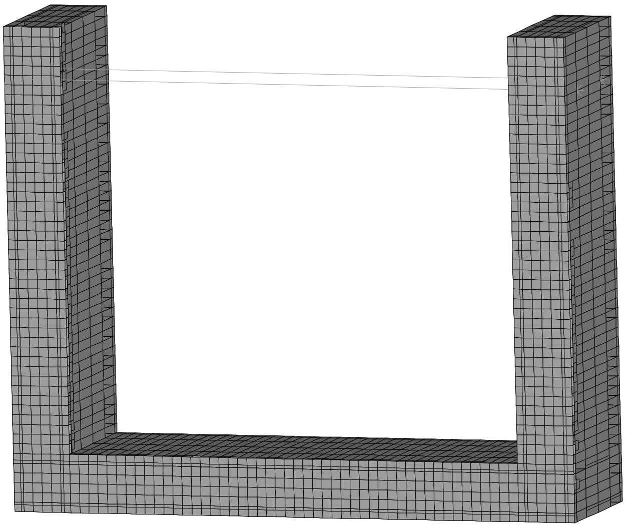

Figure 11: Meshed frame in structural finite element analysis.

Since the experimental structure was made of reinforced concrete (Vecchio & Sato 1990), reinforcement was embedded into the SOLID185 elements. The reinforcement was added as smeared layers with uniaxial stiffness. This was done by use of the REINF265 element from the ANSYS library. The nodes and degrees of freedom for this element are the same as for the related SOLID185 element (ANSYS® Academic Research Mechanical Release 18.0). A typical element used for reinforced concrete in the structural finite element analyses is illustrated in Figure 12.

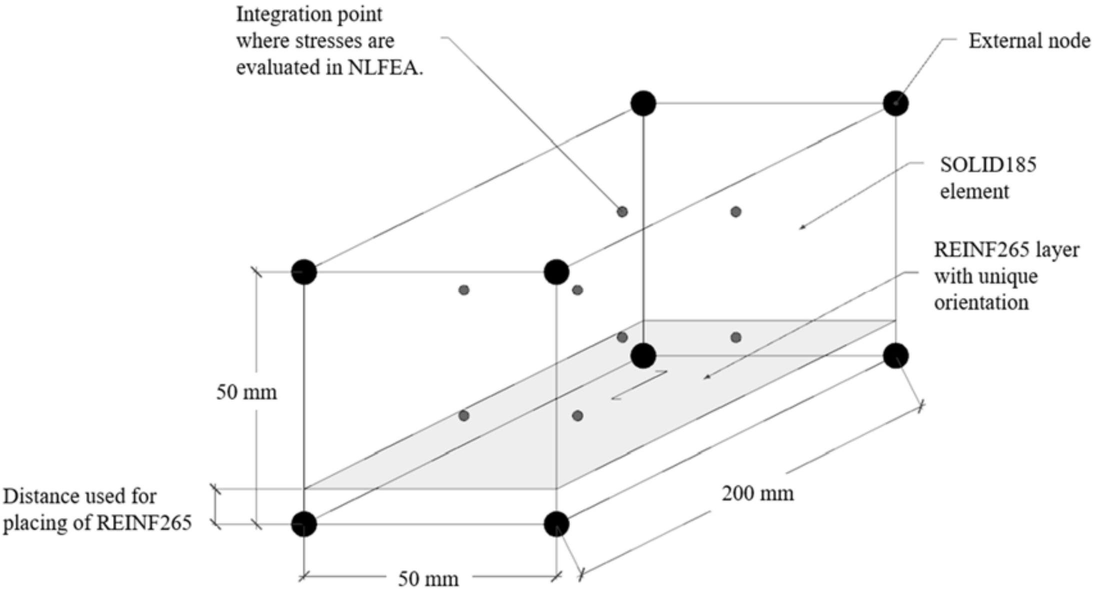

Figure 12: Reinforced concrete element used in LFEA and NLFEA.

The layers of reinforcement were defined by an area of the reinforcing bars and the spacing between these bars. This area was smeared out into a homogenous layer with an orientation of stiffness in the direction of the bars. The layers were placed within the concrete elements in a defined distance from one of the surfaces of the concrete elements. The area, spacing and location used for the reinforcement in the model are given in Table 1 and Table 2. The orientation of the reinforcement was defined in the global axes for the system due to the orientation of the cross sections.

The effect of REINF265 elements is a locally increased material stiffness in the direction of the reinforcing bars within the SOLID185 elements. This is taken into account in the calculation of the element stiffness given by Eq. (6).

$$[\mathrm{K}]^{(\mathrm{e})} = \int_{\Omega^{(\mathrm{e})}} [\mathrm{B}]^{\mathrm{T}}[\mathrm{C}][\mathrm{B}]\mathrm{d}\Omega \tag{6}$$

The matrices given in Eq. (6) are:

$[\mathrm{K}]^{(\mathrm{e})}$	Element stiffness matrix.
$[\mathrm{B}]$	Strain interpolation matrix .
$[\mathrm{C}]$	Linear material stiffness matrix.
$\Omega^{(\mathrm{e})}$	Volume of element.

The input needed to calculate the element stiffness were material stiffness properties of concrete and reinforcement. These properties were defined by the elastic modulus and the Poisson ratio of the materials in the LFEA. The elastic modules of the materials were extracted from the experiment by Vecchio and Sato (1990). The elastic modules used in the model are given in Table 3 and Table 4. The Poisson ratios were set equal to 0.2 for concrete and 0.3 for reinforcement (CEN 2004; CEN 2005). The material relations used for concrete and reinforcement in the LFEA are given in Figure 13 and Figure 14 respectively.

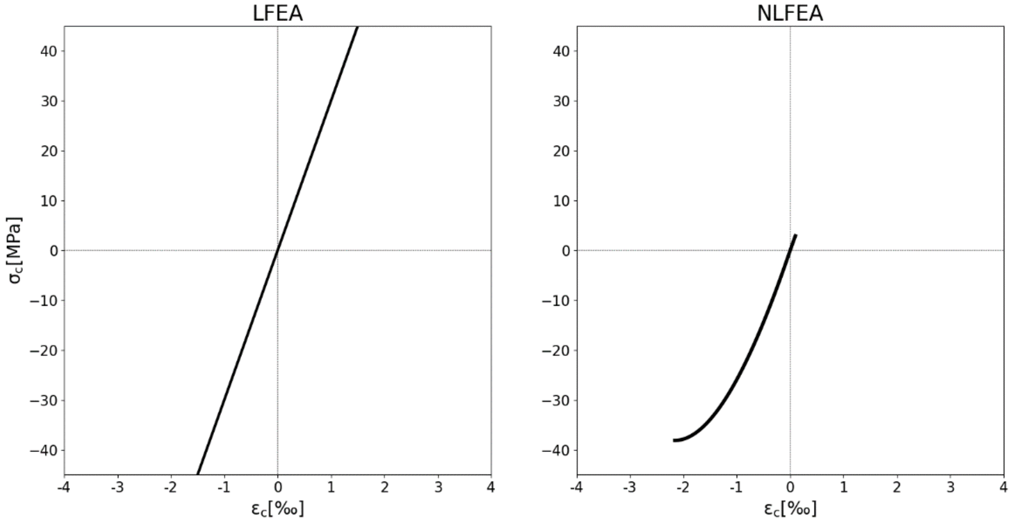

Figure 13: Material relations for concrete used in LFEA and NLFEA.

In the NLFEA, properties for concrete were defined by a user defined material model according to Engen et al. (2017). The input used for this model were the cylinder strengths of the concrete given from the experiment by Vecchio and Sato (1990). These strengths are given in Table 3. The implemented material model assigned nonlinear stress properties to the concrete. The nonlinearity also took into account tensile failure due to cracking and compressive failure due to crushing . The stiffness of concrete used in the calculated element stiffness equaled the initial secant stiffness for the given cylinder strength (Engen et al. 2017b). The material relation for concrete in the NLFEA is illustrated in Figure 13.

The stiffness properties of reinforcement in the NLFEA were defined with a user defined material model and a Poisson ratio equal to 0.3. The user defined material model for bilinear isotropic hardening was used for reinforcement. The reinforcement was given elastic behavior up to its yielding strength (ANSYS® Academic Research Mechanical Release 18.0). After yielding, a lower elastic modulus of 2 GPa was assumed to cause a yielding effect of the material. The elastic modulus used before yielding was equal to the modulus used in LFEA. The yielding strengths used for the model are given in Table 4 and the material relation used for reinforcement in the NLFEA is given in Figure 14.

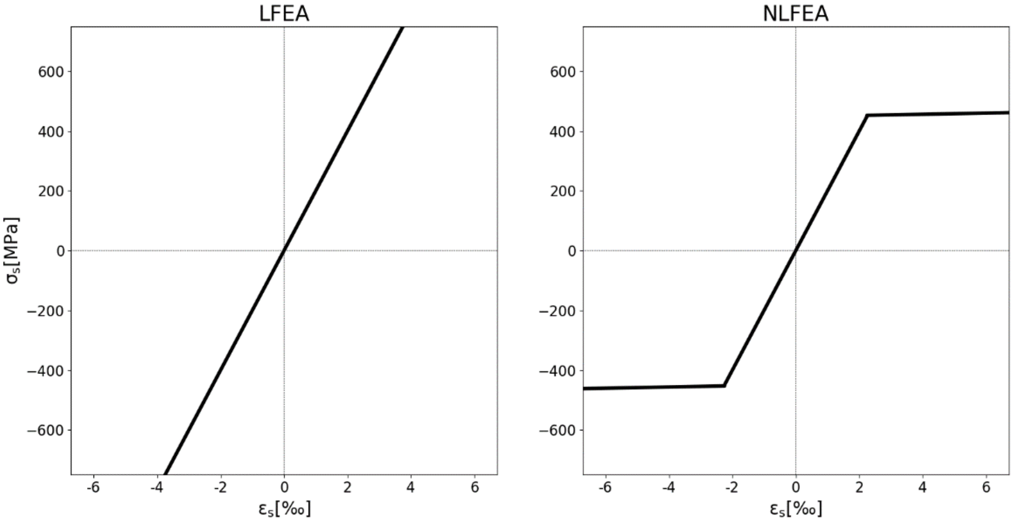

Figure 14: Material relations for reinforcement used in LFEA and NLFEA.

Due to the temperature rise in the reinforced concrete structure, thermal expansion coefficients were assigned to concrete and reinforcement elements. Measured values from the experiment by Vecchio and Sato (1990) were applied in the model. These values are given in Table 3 and Table 4.

In the load cases with pre-stress applied to the structure, tie-rods were modelled with LINK180 elements from the ANSYS library. These elements have three translational degrees of freedom in each of their two nodes, but only uniaxial stiffness. The element was also given a tension-only effect that made it function as a wire (ANSYS® Academic Research Mechanical Release 18.0). The element used for tie-rods is illustrated in Figure 15.

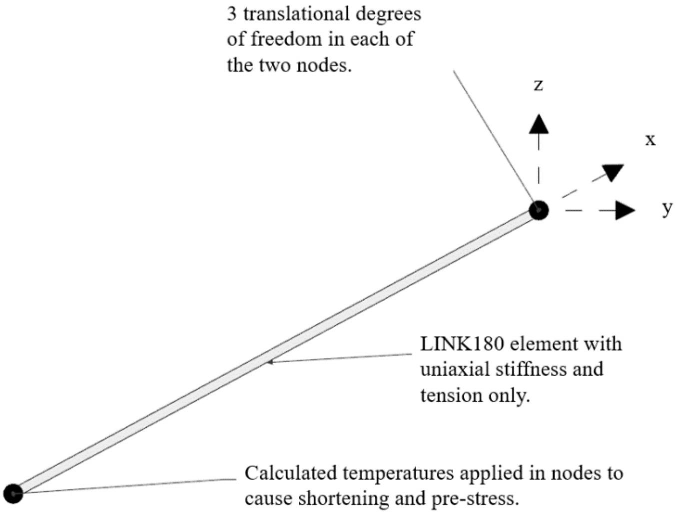

Figure 15: Tie-rod element used in LFEA and NLFEA.

The material properties of the LINK180 elements were assumed equal to reinforcement steel. This resulted in an elastic modulus of 200 GPa and a thermal expansion coefficient of 12 με/°C (CEN 2004). These elements were also assigned a cross sectional area equal to a circular section with diameter of 25 mm (Vecchio & Sato 1990).

The LINK180 elements were attached to the reinforced concrete structure by a multi-point constraint. This connection consists of a master node where the node of the LINK180 element is attached. Between the master node and multiple nodes on the reinforced concrete frame, it is a rigid connection. This constraint was replacing the force distribution function of a steel plate in the model. The multi-point constraint is illustrated in Figure 16.

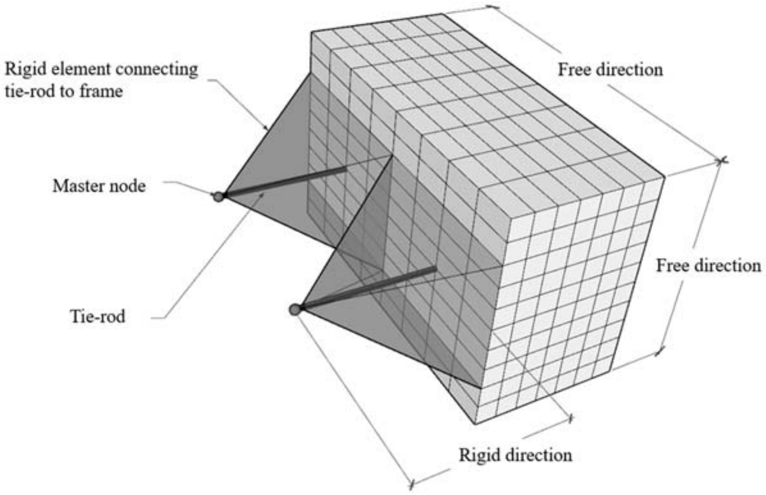

Figure 16: Multi-point constraint between tie-rod and reinforced concrete structure.

The rigid element in the multi-point constraint was only assigned rigidity in the direction of the tie-rod. This modification was done to prevent restraint forces in the reinforced concrete due to thermal expansion. With the modification, the connection surface between the rigid element and the reinforced concrete structure was free to expand in in-plane direction. The free and rigid directions of the multi-point constraint are illustrated in Figure 16.

3.4.2 Structural system response

After the local element stiffness matrices were calculated due to their material stiffness properties and geometries, they were assembled in a global stiffness matrix. This is done by adding the local stiffnesses into their respective positions in the global stiffness matrix. The global stiffness matrix makes the equilibrium of a node dependent on all the elements connected to the node. When the global stiffness matrix is assembled, the structural system can be described by the general equation given in Eq. (7) (Huebner et al. 2001; Stolarski et al. 2006).

$$[K]\{\delta\} = \{F\} \tag{7}$$

The matrices used in Eq. (7) are:

$[K]$	Global stiffness matrix (N/mm).
$\{\delta\}$	Vector of nodal deformations (mm).
$\{F\}$	Vector of nodal forces (N).

3.4.3 Solution of structural finite element analyses

To solve the general equation, loads, boundary conditions and proper solution methods needs to be applied. Loads and boundary conditions were assigned in the same way in both LFEA and NLFEA, but the solution process differed. Both application of loads, boundary conditions and solution methods are explained in the following sections.

When an approximated solution of the unknown deformations in the system is calculated, the solution could be used to calculate corresponding stresses, strains, reaction forces and internal forces for the system. These calculations were performed in the postprocessor in ANSYS.

3.4.3.1 Loads

Dead load, water pressure, pre-stress and thermal expansion were causing internal forces in the structures. This load situation was represented by body forces, surface forces and initial deformations on the model. These representations have different impacts on the elements. The impact on the element and loads associated to each representation are illustrated in Figure 17.

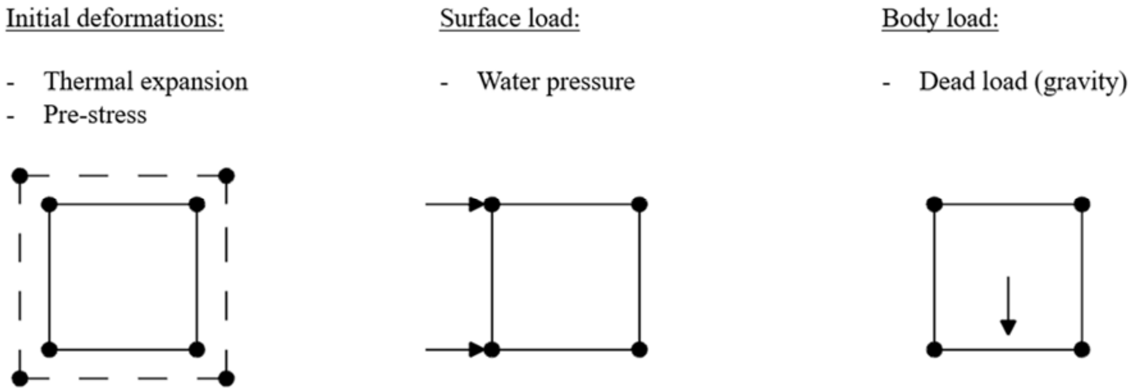

Figure 17: Load representations in structural finite element analysis.

Self-weight was applied in the model by the gravity of mass and densities of the structural elements. The gravity of mass was set to 9,81 m/s^2 (Tipler & Mosca 2008). The densities of concrete and reinforcement were set to 2400 kg/m^3 and 7775 kg/m^3 respectively (CEN 2002a).

Water pressure was added to the surfaces beneath water level on the inside of the frame. The loads on these surfaces were applied with a function of the distance beneath water level. This function is given in Eq. (8). The function gives the hydrostatic pressure in the water in a depth x. The density of water equal to 1000 kg/m^3 is used in this function (Tipler & Mosca 2008).

$$w(x) = \rho_w \cdot g \cdot x \tag{8}$$

The factors used in Eq. (8) are:

w	Hydrostatic pressure (MPa).
ρ_w	Density of water (kg/m^3).
g	Gravity of mass (m/s^2).
x	Distance beneath water level (m).

The hydrostatic pressures are applied on SURF154 elements attached to the surface of the SOLID185 elements. The SURF154 elements are only used to apply pressures normal to a surface, and adds no structural stiffness.

Temperatures were applied in the nodes of the reinforced concrete frame. The temperatures were implemented from the results of the thermal finite element analysis. The temperature difference between these temperatures and an initial reference temperature was causing thermal expansion in the reinforced concrete elements. The reference temperature was set to the initial temperature of the structure before heating. The reference temperatures used in each load case are given in Sec. 2.4. The thermal expansion was considered as initial deformations in the solution of the system.

Dead load, water pressure and temperatures were the only loads applied to the model in the approximations of free deformations. These approximations were called Type I analyses. In the Type II analyses, pre-stress was applied to the structure in addition to the other loads as a restraint of deformation. This pre-stress was applied through tie-rods that were attached between the columns of the frame.

The amount of pre-stress and the size of the thermal gradients differed in the applied load cases for Type II tests. The used gradient and pre-stress for different load cases are given in Sec. 2.4. The gradients and pre-stress were changed in the model by making separate analyses for each load case. An example of a nonlinear finite element analysis with corresponding thermal finite element analysis is given in Appendix A.3-A.6.

Pre-stress was applied to the structure by thermal contraction of the LINK180 elements. The temperature applied to the element was calculated to cause a given amount of pre-stress. The calculation of the temperature took into account the actual restraint of the tie-rods for a given pre-stress force and the slackening of the tie-rods due to the deformations from dead loads and water pressures. A detailed description of the temperature calculation is given in Appendix A.1.

All the forces applied in the model were assembled as nodal forces in the force vector of the general equation for the structural system. Surface forces and body forces were distributed directly into nodes, and initial deformations were converted to forces by related stiffnesses.

The loads were applied to the model in load steps. Five load steps were used in the LFEA and 30 load steps were used in the NLFEA. The loads were also applied in an order where dead loads and water pressure were applied first. Pre-stress was applied as the second load and finally the thermal gradient was applied. In these analyses, pre-stress and thermal gradients were applied sequential.

A second NLFEA was performed to examine the effect of load application. In this analysis, pre-stress and thermal gradients were applied parallel. The effect of load application was examined for the NLFEA since the principle of superposition is not valid for these analyses (Holand et al. 2000).

3.4.3.2 Boundary conditions

Boundary conditions in the structural analyses were restrained translations due to the supports of the frame. The frame was assumed simply supported by a pinned support and a roller support. These supports were placed in the center of the columns to prevent eccentricities. The support conditions were also applied throughout the width of the frame.

In the position of the pinned support, all nodes in the width were constrained in the vertical and horizontal direction of the frame. In the position of the roller support, all nodes in the width were constrained in the vertical direction. Since all forces on the structure were directed horizontal or vertical, out-of-plane constraints were only applied in one node for both the supports. The out-of-plane constraints were also applied in the same horizontal-vertical plane. This choice of out-of-plane constraints prevented restraint of thermal expansion in the out-of-plane direction.

Boundary conditions are used in in the general equation for the structural system to reduce the global stiffness matrix. This reduction process made it possible to solve the equation.

3.4.3.3 Solution process

The solution of the general equation for the structural system was found by inverting the global stiffness matrix. The inverted matrix was multiplied with the actual load vector to find an equilibrium solution for the nodal deformations in the structure. This is the whole solution process in the LFEA.

In the NLFEA, the same procedure was used to solve the general equation for the structural system. Since the solution in the LFEA was based on a constant material stiffness, an iteration process according to Engen et al. (2017) was used to approximate a nonlinear solution based on varying material stiffness. This iteration process was based on the Newton-Raphson method. In this process, the material was assigned an initial stiffness. Then the general equation for the structural system was used to approximate an equilibrium solution due to the initial stiffness. This solution was the first iteration in the solution process.

When the first iteration was done, an evaluation process of the stresses in the integration points was starting. In this evaluation, stresses were corrected due to the implemented nonlinear material model for concrete according to Engen et al. (2017). The evaluation of stresses also involved an update of material stiffness. The evaluation of stress in an integration point had four possible outcomes (Engen et al. 2017b):

1. If cracking or crushing did not occur, the stress was set to the actual nonlinear stress due to the related strain. The material stiffness was kept equal to the initial tangent stiffness.

2. If the nonlinear tensile stress exceeded the ultimate tensile strength of the concrete, a crack with a normal in the direction of the principal tensile stress was initiated. According to this, stress and the material stiffness normal to the crack were removed.
3. If the nonlinear compression stress exceeds the ultimate compression strength of the concrete, all material stiffnesses and stresses were removed.
4. If a crack was initiated in an earlier iteration and compressive strains normal to the crack occurred, the crack was closed and the material stiffness normal to the crack was restored.

After the evaluation of stresses, forces in the system were compared to the forces applied to the frame. A sufficient solution of the system was assumed when the forces in the system came close to an equilibrium with the applied forces. Equilibrium between the forces was assumed when an energy based convergence criterion was fulfilled. A criterion based on energy was chosen since a force criteria can be hard to fulfill due to cracking of the concrete (Engen et al. 2017b).

The energy criterion took into account both changes in deformations and residual forces in the system for each iteration. If the energy due to the last iteration was less than 1 ‰ of the energy due to the first iteration, an equilibrium solution was assumed. The energy criterion is given in Eq. (9) (Engen et al. 2017b).

$$\frac{\delta \mathrm{u}_i^{\mathrm{T}} \mathrm{R}_{\mathrm{res},i}}{\delta \mathrm{u}_1^{\mathrm{T}} \mathrm{R}_{\mathrm{res},1}} \leq 0{,}001 \tag{9}$$

Vectors used in Eq. (9) are:

$\delta \mathrm{u}_i^{\mathrm{T}}$	Vector of deformation increment due to iteration *i* (mm).
$\mathrm{R}_{\mathrm{res},i}$	Vector of residual forces due to iteration *i* (N).
$\delta \mathrm{u}_1^{\mathrm{T}}$	Vector of deformation increment due to iteration 1 (mm).
$\mathrm{R}_{\mathrm{res},1}$	Vector of residual forces due to iteration 1 (N).

When the energy criterion was fulfilled, the solution was accepted and the Newton-Raphson process ended. A new iteration in the Newton-Raphson method started if the criterion was not fulfilled until a maximum number of 40 iterations were reached.

The solutions for deformations from both LFEA and NLFEA were compared to deformations given from the experiment by Vecchio and Sato (1990). The solutions were also used to calculate internal forces in the system. The internal force in the tie-rods was of particular interest for the validation of the model due to Type II tests, since these tie-rod forces were registered in the experiment by Vecchio and Sato (1990).

3.5 Modelling uncertainty

The reliability of the finite element models was controlled after solution of the two systems. This was done by calculation of the modelling uncertainty for the approximations in the models. A modelling uncertainty was carried out based on an assumption of a lognormal distribution of the uncertainties. These distributions were calculated according to Engen et al. (2017a). The distributions were also corrected for a limited number of observations (Engen et al. 2017a).

$$\theta_i = \left(\frac{R_{exp}}{R_{FEA}}\right)_i \tag{10}$$

Factors used in Eq. (10) are:

θ_i	Modelling uncertainty for load case *i*.
$R_{exp,i}$	Expected force from experiment for load case *i*.
$R_{FEA,i}$	Approximated force from finite element analysis for load case *i*.

The expression for the modelling uncertainty is given in Eq. (10). The modelling uncertainty is given as the expected value from the experiment divided by the calculated value from the finite element analysis. The modelling uncertainty was calculated for both deformations and forces.

The lognormal distribution of the modelling uncertainty was based on an average value and a standard deviation for the selected load cases. These parameters were calculated according to Engen et al. (2017a). The correction of the distribution was performed since a limited number of load cases was examined. Base on this, the uncertainty in the modelling uncertainty was taken into account according to Engen et al. (2017a). Because more uncertainty was taken into account, the distributions became wider.

The modelling uncertainty for the models was examined for three deformations and one force given from the experiment by Vecchio and Sato (1990). The examined force was the sum of the internal forces in the tie-rods. The modelling uncertainty for this sum was calculated for load cases applied to the frames during Type II test.

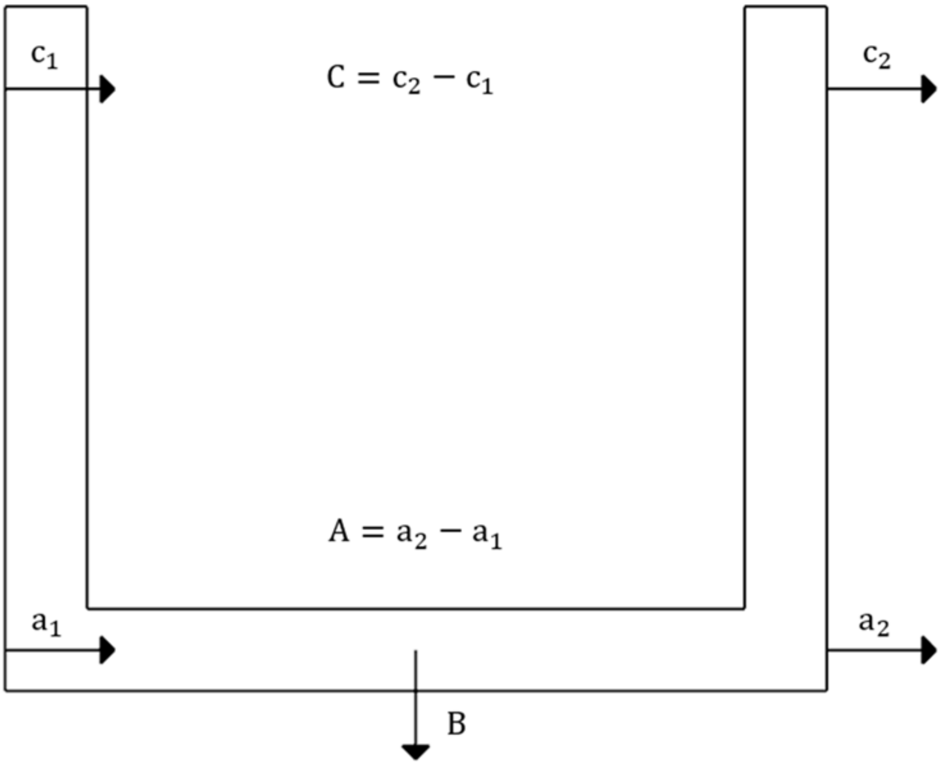

Figure 18: Registered deformations from structural finite element analysis.

The three examined deformations were:

A. Elongation of the beam in its axial direction. The values for deformation of the beam were measured in the center of the cross section. Positive values were related to expansion of the beam.
B. Deflection in the mid-span of the beam. The value was measured in the center of the cross section. Positive values were related to a downward deflection of the beam.
C. Relative deflection of columns in tie-rod level. The values were measured in the end nodes of the tie-rod elements. Positive value was related to an elongation of the tie-rods.

The modelling uncertainty for these deformations was calculated separately for load cases in Type I and Type II test. The modelling uncertainty due to load cases from Type I test showed uncertainty in approximation of free deformations, and the modelling uncertainty due to load cases from Type II test showed uncertainty in approximations of restrained deformations. The three deformations are illustrated in Figure 18 with their positive directions.

The modelling uncertainties were also calculated for both the LFEA and NLFEA. The modelling uncertainties from the LFEA were compared to the modelling uncertainties from NLFEA.

The modelling uncertainties and corresponding model reliability are discussed in Sec. 4.

3.6 Crack width calculation

The implementation of approximated external restraint forces in the crack width formula was the second step in the three-step process. The implementation was affected by the third step, which was a maximum crack width calculation based on Eurocode 2. The input needed in this calculation was crucial for the results needed in the implementation. The needed input showed that a strain distribution for a critical load combination in a cracked cross section gave sufficient results. Therefore, the critical load combinations and the corresponding strain distribution in Stage II were carried out.

The critical load combination was calculated in two different ways for the NLFEA. The first calculation used the tie-rod forces directly from the NLFEA. The other calculation used the same forces, but these forces were increased with a safety factor of 1.087. This factor took into account the modelling uncertainty of tie-rod forces and ensured a probability of 95 % conservative calculations of these forces. The critical load combinations included self-weight and water pressure in addition to the tie-rod forces. The calculations of these critical load combinations are described in Sec. 3.6.1.

The strain distribution corresponding to the critical load combination was found by a layer-by-layer approach. This approach used the principals of force and moment equilibrium for approximation of a linear strain distribution in a cracked cross-section (Collins & Mitchell 1991). The strain distribution was further used in the calculation of input parameters in the maximum crack width formula from Eurocode 2. The layer-by-layer approach is further explained in Sec. 3.6.2.

Implementations from the NLFEA were compared to two implementations from LFEA. The first of these implementations used the external restraint force approximated in the LFEA.

Except that the external restraint force was retrieved from the LFEA, the implementation was identical to the implementations based on NLFEA.

The second implementation from LFEA was used in a formula based on NS3473. The input needed in this formula was the Stage I restraint strain in the reinforcement from thermal expansion. This strain was calculated from the LFEA. In addition, the formula needed a strain distribution, which was calculated based on a critical load combination without restraint forces. The strain distribution was calculated by the layer-by-layer approach.

The four examined implementations of restraint forces are given in Table 11.

Table 11: Formula and restraint strain used in different implementations.

ANALYSIS	IMPLEMENTATION	FORMULA	RESTRAINT STRAIN
LFEA	**A**	Eurocode 2	Calculated from critical section loads
	B	NS3473	Scaled strain from critical section in LFEA
NLFEA	**C**	Eurocode 2	Calculated from critical section loads
	D	Eurocode 2 ($k_t = 0$)	Calculated from critical section loads with safety factor for tie-rod force

The third step in the three-step process was the calculation of maximum crack widths. The calculations were carried out based on input parameters from the four implementations. Input from implementation A, C and D was used in the formula from Eurocode 2 and input from implementation B was used in the formula based on NS3473.

Eurocode 2 uses a maximum crack distance and an average strain difference between reinforcement and concrete over the crack distance for calculation of the maximum crack width. The average strain difference is equal to the reinforcement strain in Stage II minus the contribution of tension stiffening over the crack distance (CEN 2004; Sørensen 2014). This approach was used as it is for implementation A and C, but the contribution of tension stiffening was neglected for implementation D. The maximum crack width formula from Eurocode 2 and corresponding input are further explained in Sec. 3.6.3.

The crack width calculation based on NS3474 consists of two parts. The first part has the same structure as the formula from Eurocode 2 with a maximum crack distance and a reduced reinforcement strain due to tension stiffening (Norges Standardiseringsforbund 2003). The second part is the implementation of restraint forces from imposed deformations. This part consists of a maximum crack distance and the Stage I restraint strain in the reinforcement from imposed deformations in the critical section. The restraint strain is also scaled with a factor of 2 to take into account the increased strains in a cracked section. The factor of 2 is an empirical factor (Brekke 2017; Det Norske Veritas 1980). The maximum crack formula based on NS3473 and corresponding input parameters are further explained in Sec. 3.6.4.

The four calculations of crack widths were compared to the maximum crack widths registered by Vecchio and Sato (1990); see Sec. 2.5. The results of these comparisons are given in Sec. 5.2.

3.6.1 Critical load combination

Critical load combinations were calculated for the three examined load cases for frame PF3. These critical combinations were assumed to be in the midspan of the beam. This assumption was made since both maximum loads and least stiffness are present in this section. The maximum cracks in the experiment by Vecchio and Sato (1990) were registered a little to the right of the midspan of the beam (Vecchio & Sato 1990).

The critical load combinations used for calculation of crack widths were the sum of two load combinations. The first load combination was the loads from self-weight and water pressure. This load combination was equal for all the four implementations. The calculation of this load combination was based on the LFEA. The procedure used for calculation of this load combination followed the calculation of the load combination for pre-stress and restraint forces in implementation A. The load combination from pre-stress and restraint forces was the second load combination in the sum that formed the critical load combination.

The load combination from pre-stress and restraint forces used in the critical load combination for implementation A was calculated from the cross sectional stresses in the LFEA. For this calculation, it was assumed that the stress distribution in the concrete was linear. The maximum and minimum concrete stress were registered in the critical cross section, and the slope for the stresses was calculated over the thickness. The registered stress values from the LFEA are illustrated in Figure 19.

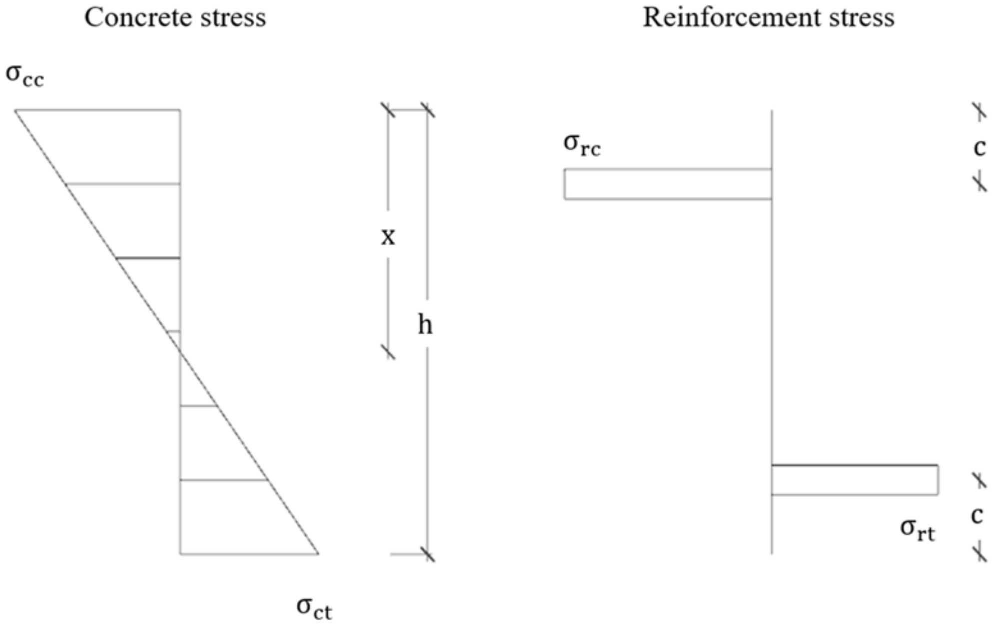

Figure 19: Stress distribution used for calculation of load combination from LFEA.

New factors used in Figure 19 are:

σ_{cc}	Maximum compression stress in concrete (MPa).
σ_{ct}	Maximum tension stress in concrete (MPa).

σ_{rc}	Maximum compression stress in reinforcement (MPa).
σ_{rt}	Maximum tension stress in reinforcement (MPa).
h	Thickness of frame (mm).
x	Compression height in cross section (mm).
c	Cover of reinforcement bar (mm).

The heights of the compression and tension zone for concrete were calculated based on the slope of concrete stresses. These heights were used together with the width of the cross section to calculate the compression and tension resultant of concrete. The resultant for reinforcement was calculated directly from the stress and the area of the respective reinforcement layers.

A summation of the force resultants in the cross section was used to find the acting axial force in the cross section, and a summation of the moment contribution from the resultants about the center of the cross section was used to find the acting moment. The resultants and moment arms for the stress distribution in Figure 19 are illustrated in Figure 20.

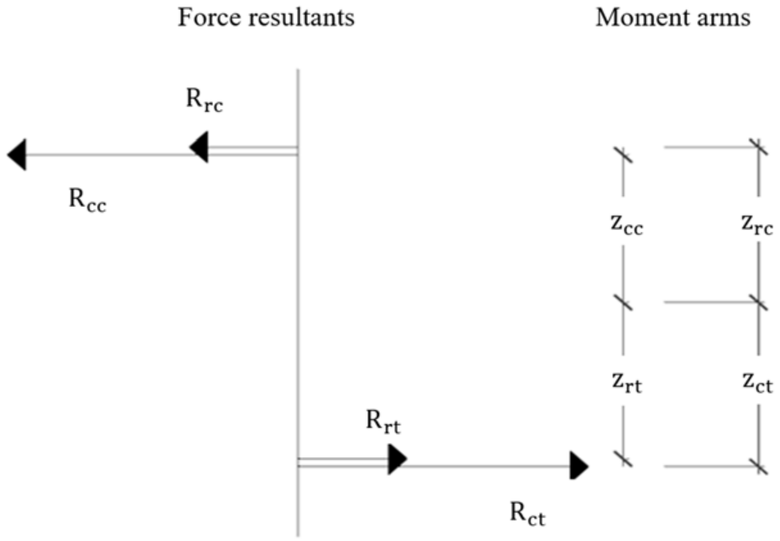

Figure 20: Resultants and moment arms in a cross section from LFEA.

New factors used in Figure 20 are:

R_{cc}	Resultant for compressive stresses in concrete (N).
R_{ct}	Resultant for tensile stresses in concrete (N).
R_{rc}	Resultant for compressive stresses in reinforcement (N).
R_{rt}	Resultant for tensile stresses in reinforcement (N).
z_{cc}	Moment arm for compression resultant of concrete (mm).
z_{ct}	Moment arm for tension resultant of concrete (mm).
z_{rc}	Moment arm for compression resultant of reinforcement (mm).
z_{rt}	Moment arm for tension resultant of reinforcement (mm).

The load combination from pre-stress for implementation B was found in the same way as for implementation A. This load combination was calculated from a LFEA where thermal gradients were not applied. In addition to the load combination from pre-stress, the tensile reinforcement strain from restraint forces was registered. This strain was found from a separate LFEA where only thermal gradients were applied. The registered strain was the strain corresponding to the stresses in the reinforcement. Both restraint strain and load combination were calculated in the same critical section in the midspan of the beam.

The calculation of the load combination from pre-stress and restraint forces for implementation C and D was based on hand calculations. The axial force in the tie-rods was used to calculate a corresponding moment and axial force in the midspan of the beam. The calculations were based on the free body diagram of the structure illustrated in Figure 21. The axial force in the cross section was found by force equilibrium and the moment was found by moment equilibrium about the center of the cross section.

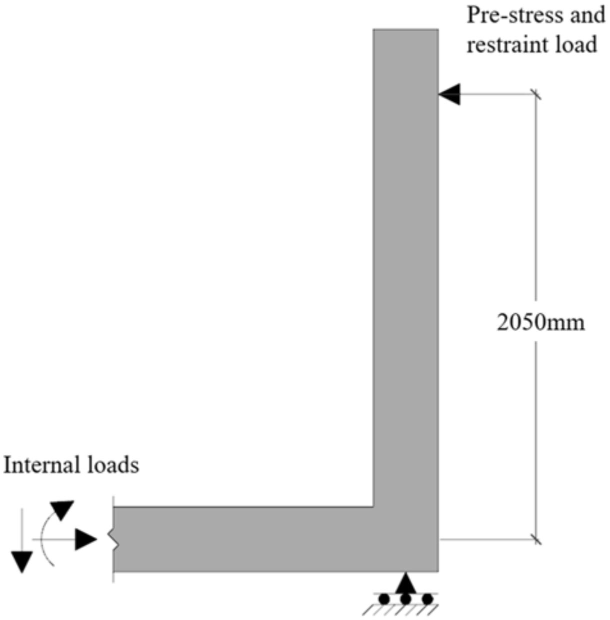

Figure 21: Free body diagram of frame exposed to pre-stress and restraint forces.

The tie-rod force used for calculation of the critical load combination differed in implementation C and D. The actual tie-rod force calculated by the NLFEA was used in the calculations for implementation C. This force was increased by a factor of 1.087 in the calculations for implementation D. This factor was equal to the 95% fractile of the modelling uncertainty.

The critical load combinations from pre-stress and restraint forces were added to the critical load combination from dead load and water pressure. The critical load combinations were then used to calculate the reinforcement stress and compression height in Stage II based on the layer-by-layer approach.

3.6.2 Layer-by-layer approach

A layer-by-layer approach was used to determine the strain in the reinforcement and the compression height in the cross section for a given load combination in Stage II. This method was based on a division of the cross section into layers (Collins & Mitchell 1991). The cross section was divided in the direction perpendicular to the axis of the moment acting on the cross section. The cross section was divided into 60 layers with a thickness of 5 millimeters. The principles of the layer-by-layer method are illustrated in Figure 22.

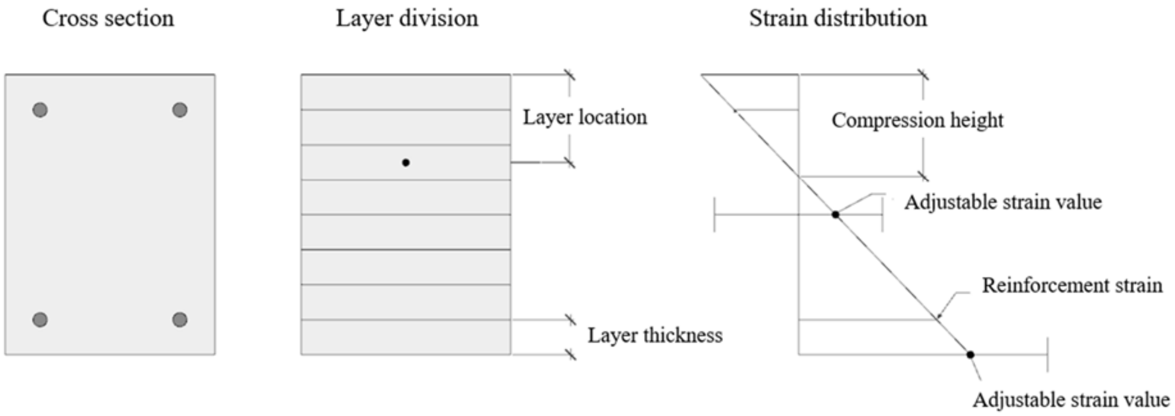

Figure 22: Layer division of cross section and linear strain distribution.

The strain distribution corresponded to the assumption of plane sections remaining plane. A linear distribution for the acting moment was then carried out by an iteration process, where two cross sectional strain values were adjusted until moment and force equilibrium were fulfilled. These equilibriums were assumed fulfilled when the sum of the internal and external moment were less than 0.1 kNm, and when the sum of the internal and external forces were less than 0.1 kN. A strain value on the edge of the cross section where tension stresses were present was adjusted to create moment equilibrium and an average strain value in the center of the construction was adjusted to create force equilibrium.

The internal forces were calculated from the stresses in the reinforcement and concrete. The stress in the reinforcement was calculated based on the strain associated to its location. The relation between stress and strain for reinforcement was assumed linear elastic, and was calculated based on Hooke's law. The elastic modulus used in the calculation was equal to 200 GPa.

The compressive stresses in the concrete layers were calculated according to the nonlinear material response in Eurocode 2 3.1.5. The material response was the basis for a function calculating stresses from the strain acting on a layer. This function is described in Appendix A.2. Tensile stresses in the concrete were neglected based on the assumption of a cracked cross section.

The internal forces were then carried out by multiplying the stresses with their corresponding areas. These multiplications gave the force resultants for the reinforcement and layer resultants for the concrete. The layer resultants were summed to form the total compression resultant for the concrete.

The internal moment was carried out by a summation of the moment contributions from all the internal force resultants. The moment arms for the resultants were given by their location relative to the center of the cross section.

When the equilibriums were fulfilled and the final strain distribution was found, a compression height was determined. This was done by registration of the location for all layers with negative strain values. These locations were given as a distance between the center of the layers and the edge of the cross section exposed to compression strains. The maximum distance registered and a half thickness of a layer were used as the compression height. The compression height is illustrated in Figure 22.

The stress in the tension reinforcement was found directly from the strain distribution that fulfilled the equilibriums. This stress and the compression height were used further in the calculations of the crack widths.

3.6.3 Crack width calculation based on Eurocode 2

Crack widths for implementation A, C and D were calculated based on the crack width formula given in Eurocode 2. The general formula for these calculations is given in Eq. (11) (CEN 2004). This formula is based on a maximum crack spacing and the average strain difference between steel and concrete over this length.

$$w_k = s_{r,max} \cdot (\varepsilon_{sm} - \varepsilon_{cm}) \tag{11}$$

Factors used in Eq. (11) are:

w_k	Crack width (mm).
$s_{r,max}$	Maximum crack spacing (mm).
ε_{sm}	Average strain in reinforcement between cracks due to the actual load combinations, including effects from imposed deformations and tension stiffening.
ε_{cm}	Average strain in concrete between cracks.

The formula for the maximum spacing between cracks is given in Eq. (12) (CEN 2004).

$$s_{r,max} = k_3 \cdot c + k_1 \cdot k_2 \cdot k_4 \cdot \emptyset / \rho_{p,eff} \tag{12}$$

New factors given in Eq. (12) are:

k_1	Factor taking into account the bond between concrete and reinforcement.
k_2	Factor taking into account the strain distribution in the cross section.
k_3	Constant coefficient from Eurocode 2.
k_4	Constant coefficient from Eurocode 2.
c	Cover of reinforcement bar (mm).
$\emptyset$	Diameter of reinforcement bar (mm).
$\rho_{p,eff}$	Ratio between area of reinforcement and effective concrete area.

A number of coefficients in the calculation of maximum crack spacing were constant. The values of these parameters are given in Table 12.

Table 12: Constant parameters in maximum crack spacing from EC2 for frame PF3.

Parameter	Value
k_1	0.8
k_2	0.5
k_3	3.4
k_4	0.425
c	40 mm
Ø	20 mm

For the inspected frame, the factor k_1 was set equal to 0.8 based on the assumption of rebars with good bonding to the concrete, and the factor k_2 was set equal to 0.5 since the critical cross section was exposed to bending.

The cover and diameter of the rebars were set equal to 40mm and 20mm respectively. This was based on the assumption that a #20 rebar was equal to a rebar with diameter of 20mm. The covering of the rebars was calculated as the distance between the edge of the cross-section and the edge of the rebar.

The maximum crack spacing for structure PF3 was given by Eq. (13) when all the predefined factors were taken into account.

$$s_{r,max} = 136\text{mm} + 3.4\text{mm}/\rho_{p,eff} \tag{13}$$

The area ratio between the reinforcement and the effective concrete area in the cracked section was determined from the strain distribution found with the layer-by-layer approach. The effective concrete area corresponding to the strain distribution was found with Eq. (14) (CEN 2004). The compression height from the layer calculations was used in this formula together with some geometrical properties from the cross section of structure PF3. The geometrical properties are given in Table 13.

$$A_{c,eff} = \min\left(2.5 \cdot (h-d), \frac{(h-x)}{3}, \frac{h}{2}\right) \cdot b \tag{14}$$

Table 13: Geometrical properties in calculation of effective concrete area for frame PF3.

Parameter	Value
h	300 mm
d	250 mm
b	800 mm

After calculation of the effective concrete area, the effective area ratio in a cracked section was found as $A_s/A_{c,eff}$. The area of reinforcement was set equal to the total area of reinforcement in tension.

The maximum crack spacing was multiplied with the average strain difference between reinforcement and concrete over a length equal to the maximum crack spacing. This strain difference was found with Eq. (15) from Eurocode 2 (CEN 2004).

$$(\varepsilon_{sm} - \varepsilon_{cm}) = \frac{\sigma_s - k_t \cdot \frac{f_{ct,eff}}{\rho_{p,eff}} \cdot \left(1 + \alpha_e \cdot \rho_{p,eff}\right)}{E_s} \geq 0.6 \cdot \frac{\sigma_s}{E_s} \tag{15}$$

New factors used in Eq. (15) are:

σ_s	Stress in reinforcement in a cracked section (MPa).
k_t	Factor taking into account the load duration.
$f_{ct,eff}$	Effective concrete tension strength (MPa).
α_e	Ratio between elastic modulus of reinforcement and elastic modulus of concrete.
E_s	Elastic modulus of reinforcement (MPa).

Some of the parameters in the calculation of the average strain difference were constant in all calculations. These parameters are given in Table 14.

Table 14: Constant parameters in average strain difference from EC2 for frame PF3.

Parameter	Value
k_t	0.6
$f_{ct,eff}$	3.1 MPa
α_e	6.06
E_s	200 GPa

The stress in the reinforcement in a cracked section was calculated based on the strain distribution from the layer-by-layer approach. The strain corresponding to the location of the reinforcement was used to calculate the stress based on Hooke's law. The elastic modulus for reinforcement used in this equation was set equal to the elastic modulus for structure PF3 given in Sec. 2.3.

The stress in the reinforcement varied in implementation A, C and D due to the critical load combination used in the layer-by-layer approach. This variation in the reinforcement stress and some minor changes in the effective area ratio were the only factors causing different crack widths between implementation A, C and D. These factors were also the only factors causing different crack widths for the three examined load combinations for frame PF3.

The effective tension strength of concrete used in Eq. (15) was set equal to the mean tension strength of the concrete according to Eurocode 2 7.1 (2) (CEN 2004). This mean tension strength was assumed equal to the cracking strength reported by Vecchio and Sato (1990). Based on this, the effective tension strength for structure PF3 was set equal to 3.1 MPa.

The ratio between the elastic modules for reinforcement and concrete was based on the elastic modules for structure PF3 reported by Vecchio and Sato (1990), and the factor k_t was set equal to 0.6 assuming short-term loading of the structure. The effective area ratio used in Eq. (15) was the same ratio that was used in Eq. (13).

3.6.4 Crack width calculation based on NS3473

Crack width calculations based on implementation B were carried out with the formulas given in NS3473 and an extension for restraint strains from imposed deformation. This empirical formula[1] is given in Eq. (16). The formula had the same structure for external forces as Eq. (11) with a maximum crack distance and average strain difference over this length. The crack width from external forces is given as w_o in Eq. (16) (Norges Standardiseringsforbund 2003).

The extension part w_t in Eq. (16) differed from w_o in the way that restraint strains in the reinforcement were scaled with a factor F_t set equal to 2. The principle behind this factor is to transfer restraint strains from an uncracked section to a cracked section. The factor of 2 was based on a derivation of a similar factor from Dr. Techn. Olav Olsen (Brekke 2017). The implementation of strains from thermal expansion as an own part in Eq. (16) was similar to the treatment of shrinkage in NS3473 (Norges Standardiseringsforbund 2003).

$$w = w_o + w_t = 1.7 \cdot k \cdot r \cdot \varepsilon_s \cdot s_{rm} + 1.7 \cdot k \cdot F_t(\varepsilon_0, \kappa) \cdot \varepsilon_t \cdot s_{rm} \tag{16}$$

Factors used in Eq. (16) are:

w	Total combined crack width (mm).
w_o	Crack width from external static loads (mm).
w_t	Crack width from external restraint forces due to thermal gradient (mm).
k	Reduction factor for increased cover.
r	Static strain reduction factor taking into account tension stiffening.
ε_s	Static strains from external loads.
s_{rm}	Mean distance between cracks (mm).
$F_t(\varepsilon_0, \kappa)$	Coefficient taking into account increased restraint strain in a cracked section.
ε_t	Restraint strain from applied thermal gradient.

The reduction factor, k, was set equal to 1. This factor is used in NS3473 for reduction of crack width due to a higher covering of reinforcement than the nominal covering. There is no knowledge about the nominal cover for the frames used in the experiment by Vecchio and Sato (1990), and the reduction factor is not present in the calculations based on Eurocode 2. Therefore, a reduction factor of 1 was used to reduce the differences between the formulas from Eurocode 2 and NS3473.

The strain from the external loads was carried out based on the layer-by-layer approach with the actual load combination from dead load, water pressure and pre-stress in the critical cross section. The restraint strain from imposed deformations was found directly from the reinforcement in a LFEA where only thermal strains were applied to the model.

---

[1] This empirical formula is an interpretation of the crack width calculation with restraint loads from thermal gradients used in design of offshore structures since early 1990s. The perception of the calculation is based on a derivation from Dr. Tech. Olav Olsen and design rules from Det Norske Veritas (Brekke 2017; Det Norske Veritas 1980). The purpose of the formula is to reduce crack widths calculated from linear finite element analyses when restraint loads from thermal movement are present.

The mean distance between cracks and the reduction factor for tension stiffening were calculated with Eq. (19) and Eq. (17) respectively (Norges Standardiseringsforbund 2003).

$$r = 1 - \frac{\beta_s \cdot \sigma_{sr2}}{\sigma_{s2}} \tag{17}$$

New factors used in Eq. (17) are:

β_s	Factor taking into account the load duration.
σ_{sr2}	Stress in the reinforcement in a cracked section when the section loads corresponds to maximum tension stress in the uncracked structure (MPa).
σ_{s2}	Stress in the reinforcement for a cracked section with the actual load combination (MPa).

The stress in the cracked section for the actual load combination was calculated from the corresponding strain calculated with the layer-by-layer approach. Hooke's law and the elastic modulus of the reinforcement were used for this calculation.

The stress in the reinforcement causing maximum tensile stresses in the uncracked structure was calculated by Eq. (18). This formula is also a part of Eq. (15) from the calculation based on Eurocode 2 (CEN 2004) .

$$\sigma_{sr2} = \frac{f_{ctm}}{\rho_{p,eff}} \cdot \left(1 + \alpha_e \rho_{p,eff}\right) \tag{18}$$

The factors used to calculate σ_{sr2} are explained and given in connection with Eq. (15). The area ratio between reinforcement and the effective concrete area was calculated from the strain distribution in the layer-by-layer approach used to calculate σ_{s2}.

The factor β_s, which take into account the load duration, was set to 0.6 assuming short-term loading.

The mean crack spacing used in Eq. (16) was calculated with Eq. (19) from NS3473.

$$s_{rm} = s_{ro} + \left(\frac{f_{tk}}{\tau_{bk}}\right) \cdot k_b \cdot k_c \cdot h_{cef} \cdot s_b / (\pi \cdot n \cdot \emptyset) \tag{19}$$

New factors used in Eq. (19) are:

s_{ro}	Constant length with loss of bond (mm).
$\left(\frac{f_{tk}}{\tau_{bk}}\right)$	Effective ratio between tension and bond strength.
k_b	Coefficient taking into account the reduction of bond due to bundles.
k_c	Coefficient taking into account the strain distribution in the cross section.
h_{cef}	Effective height of concrete in the tensile area of the cross section (mm).
s_b	Center distance between rebars (mm).
n	Number of rebars in bundle.
$\emptyset$	Diameter of rebar (mm).

Several parameters used in the calculation of the mean crack spacing were constant during crack width calculation for frame PF3. These parameters are given in Table 15.

Table 15: Constant parameters in mean crack spacing from NS3473 for frame PF3.

Parameter	Value
s_{ro}	40 mm
$\left(\frac{f_{tk}}{\tau_{bk}}\right)$	0.75
k_b	1
s_b	267 mm
n	1
$\emptyset$	20 mm

The constant length with loss of bond was set equal to the covering of the reinforcement according to NS3473. The ratio between the tension strength of concrete and the bonding strength was set equal to 0.75 based on an assumption of deformed bars.

The cover and diameter of the rebars used in Eq. (19) were set equal to 40mm and 20mm respectively. The number of rebars in a bundle and the coefficient k_b were set to 1 since no bundles were used in the experiment by Vecchio and Sato (1990). The spacing between rebars was found in Table 1 and was set equal to 267 mm for the beam.

The coefficient k_c was calculated from the strain distribution used to calculate σ_{s2}. This coefficient was calculated based on the highest and lowest strain in the effective area of concrete. The formula for the effective height and factor k_c given in NS3473 are given in Eq. (20) and Eq. (21) respectively. The strains used in the calculation of the factor k_c are also illustrated in Figure 23 (Norges Standardiseringsforbund 2003).

$$h_{cef} = \min\left(2.5 \cdot (h - d), (h - x), \frac{h}{2}\right) \tag{20}$$

The geometrical properties used in the calculation of the effective height were identical to the properties used for the effective concrete area in the calculation based on Eurocode 2. These properties are given in Table 13.

$$k_c = \frac{(1 + \varepsilon_{II}/\varepsilon_I)}{2} \tag{21}$$

New factors used in Eq. (21) are:

ε_{II}	Lowest strain in effective concrete area.
ε_I	Highest strain in the effective concrete area.

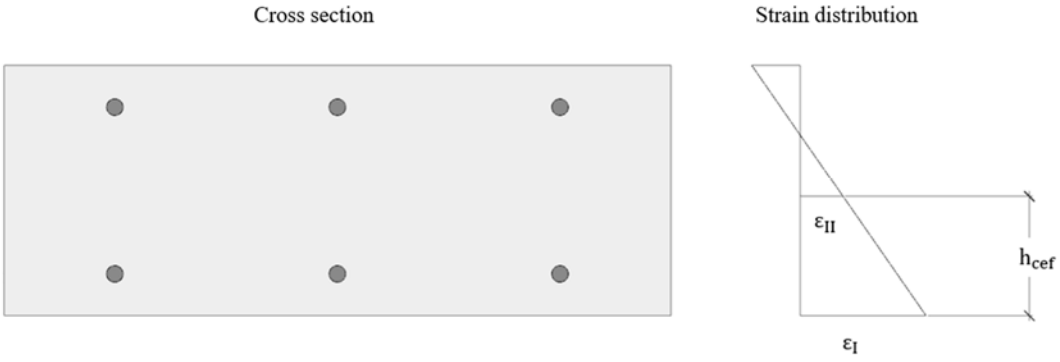

Figure 23: Strain values used in calculation of k_c.

The highest and lowest strain value used in the calculation of k_c were found from the strain distribution calculated with the layer-by-layer approach.

4 Finite element model

4.1 General

The model reliability in the NLFEA was examined with calculation of the modelling uncertainty for three deformations and the tie-rod force in the frames. The results from these calculations are given in Sec. 4.2.

These results are focused on the tie-rod forces since these forces are used further in the crack width calculations. Results for all the three deformations are only given for a Type I test where free deformations due to thermal expansion were examined. The only result presented for approximation of deformation during Type II test is deformation B. The other deformations were neglected due to systematical deviations in the results. The reasons for these deviations are discussed in Sec. 4.4.

The model reliability for approximation of tie-rod forces is discussed in Sec. 4.3. This is indirectly also a discussion for the approximation of external restraint forces, since these forces are a part of the tie-rod force.

Modelling uncertainties and approximations for LFEA are presented next to the results from NLFEA. The model reliability due to approximation of external restraint forces in these two analysis is discussed in Sec. 4.3.3.

4.2 Results from finite element modelling

The modelling uncertainties and approximations of tie-rod forces are given in Sec. 4.2.1. The modelling uncertainty for the tie-rod force was investigated in general, for different levels of pre-stress and for different load applications. In addition, the increase in tie-rod force was investigated for different magnitudes of thermal gradient.

The selected approximations of deformations are presented in Sec. 4.2.2. The selected deformations are the free thermal deformations for the frames without restraint, and deformation B during load cases with restraint.

4.2.1 Tie-rod force

The internal force in the tie-rods was approximated both with a linear and nonlinear finite element analysis. These internal forces were registered in all the nine load cases for each of the three frames given in Sec. 2.4. The approximated values were compared to the real values with a scatterplot against the experimental values. These scatterplots are given in Figure 24.

The scatterplot in Figure 24 showed a clear difference between the approximation from LFEA and NLFEA. The results from the LFEA indicated a conservative calculation of tie-rod forces. This can be seen in the left scatterplot of Figure 24. Points to the right for the diagonal line in the scatterplot indicates a higher approximated value than the experimental value. Therefore, the points to the right for the diagonal line are conservative.

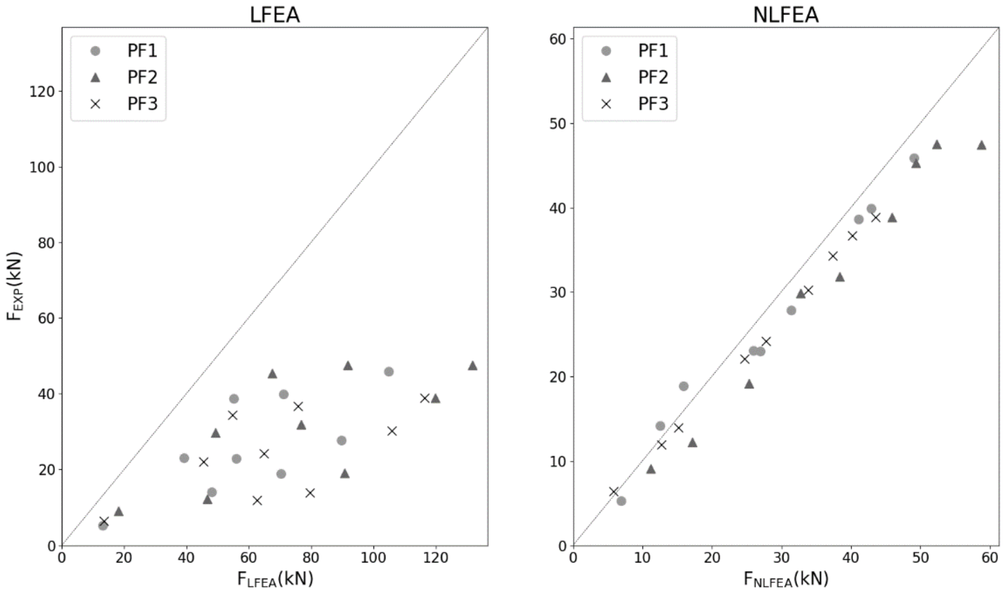

Figure 24: Comparison of tie-rod force from FEA and experiment.

The scatterplot for results from the LFEA also indicates a high overestimation of tie-rod forces for some observations. These observations are represented by the points furthest to the right. Since the tie-rod forces are connected to the stiffness of the frame, this overestimation also indicates an overestimation of stiffness in the frame.

The results in Figure 24 are also separated for the three examined frames. Few systematical differences were observed between the frames, but it was noticed that the most conservative force calculations belonged to frame PF2 and PF3. A common feature for these frames was that one member had reduced stiffness relative the other members.

The right scatterplot in Figure 24 shows the same internal force approximated with a NLFEA. These results showed approximations closer to the experimental values. Points close to the diagonal line in the scatterplot indicate an approximation close to the experimental value. Approximations from the NLFEA were in general closer to the experimental values than the approximations in the LFEA.

The results from NLFEA also showed mostly conservative calculations of tie-rod forces, but three observations were registered as non-conservative. These observations are localized to the left of the diagonal line in the scatterplot for NLFEA. It was also noticed that these non-conservative observations belonged to load cases with a low level of pre-stress.

The most overestimated tie-rod force in NLFEA belonged to structure PF2. This force was calculated for a load case with a high level of pre-stress. A closer examination of this load case showed yielding of reinforcement for the critical section in the NLFEA. Yielding of reinforcement was also registered in the experiment for this load case (Vecchio & Sato 1990).

The results plotted in Figure 24 were further used to calculate a modelling uncertainty based on the procedure in Sec. 3.5. The modelling uncertainties for approximation of the tie-rod force in LFEA and NLFEA are given in Figure 25. These figures illustrate the distribution of the modelling uncertainty and the associated mean, standard deviation and coefficient of variation.

A mean modelling uncertainty below one indicates a systematic overestimation of tie-rod forces in the finite element model.

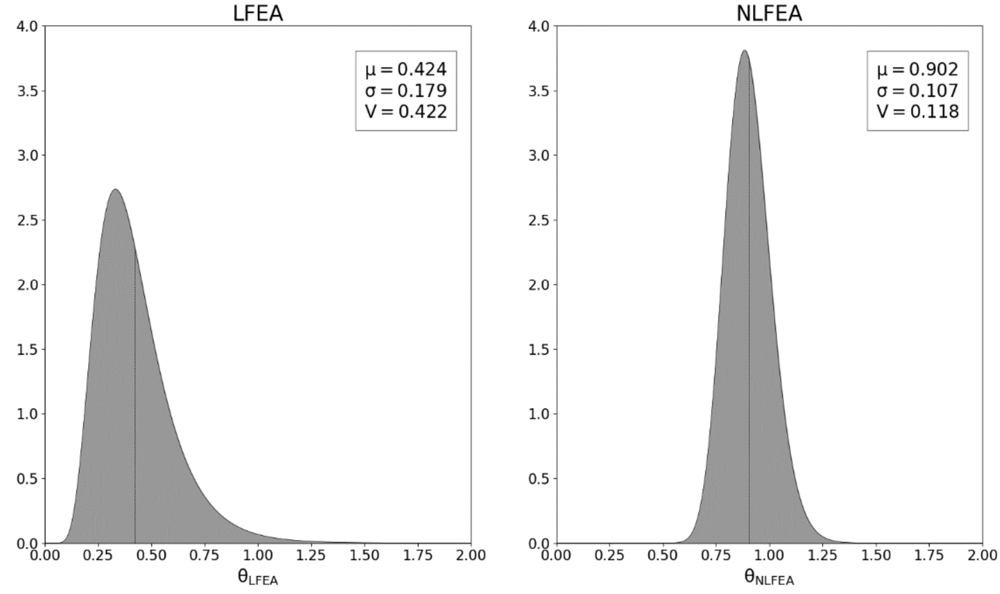

Figure 25: Modelling uncertainties for tie-rod force.

The modelling uncertainty for the LFEA shows a mean value of 0.424, a standard deviation of 0.179 and coefficient of variance of 0.422. The average modelling uncertainty from these results indicates more than a doubling of the tie-rod forces relative to the registered forces from the experiment. This means that the LFEA in general overestimates both restraint forces from imposed deformations and the stiffness in the structure.

The results from the NLFEA shows an average modelling uncertainty of 0.902. The associated standard deviation was 0.107 and the coefficient of variance was 0.118. The average modelling uncertainty indicates a conservative approximation of tie-rod forces, but the probability for modelling uncertainties above 1 is higher than for LFEA. Therefore, it is a higher risk of non-conservative calculations for NLFEA than LFEA. The probability of non-conservative calculations in the lognormal distribution for NLFEA is 17.5 %, and the same percentage for the LFEA is only 1 %.

Since there was a risk of non-conservative force calculations in the NLFEA, a modelling uncertainty corresponding to the 95 % fractile was calculated. The value for this modelling uncertainty was 1.087, and it was further used as explained in Sec. 3.6.1.

The risk of non-conservative observations was also the motivation for a further examination of the modelling uncertainty from NLFEA. In this examination, the modelling uncertainty was carried out for different levels of pre-stress. The distributions for these modelling uncertainties are given in Figure 27. The division in pre-stress levels was carried out to represent different stages of cracking in the structure.

A low level of pre-stress was assumed to represent the crack formation stage of the structure. The medium level of pre-stress was assumed to represent the transition zone between crack formation and stabilized cracking, and the high pre-stress was assumed to represent the stabilized cracking stage. These assumptions were made based on crack patterns from the NLFEA and crack patterns illustrated in the article about the experiment (Vecchio & Sato 1990). The typical crack patterns registered for the three pre-stress levels in the NLFEA are shown in Figure 26.

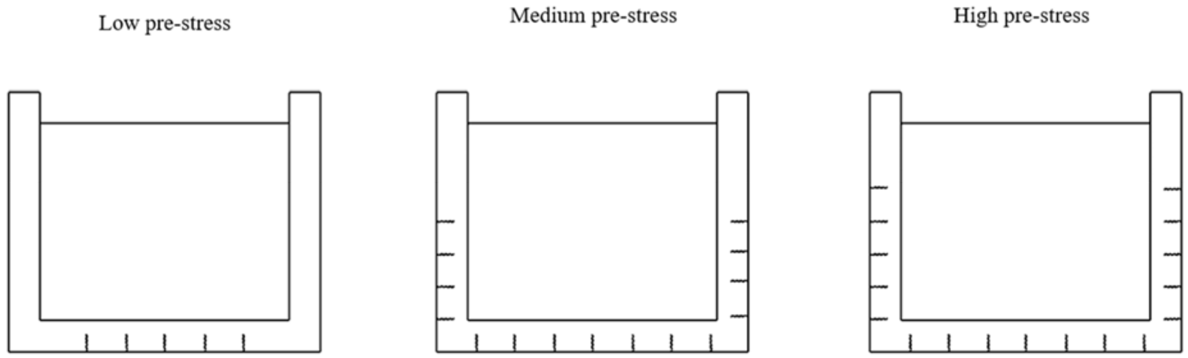

Figure 26: Typical crack patterns for different pre-stress levels in NLFEA.

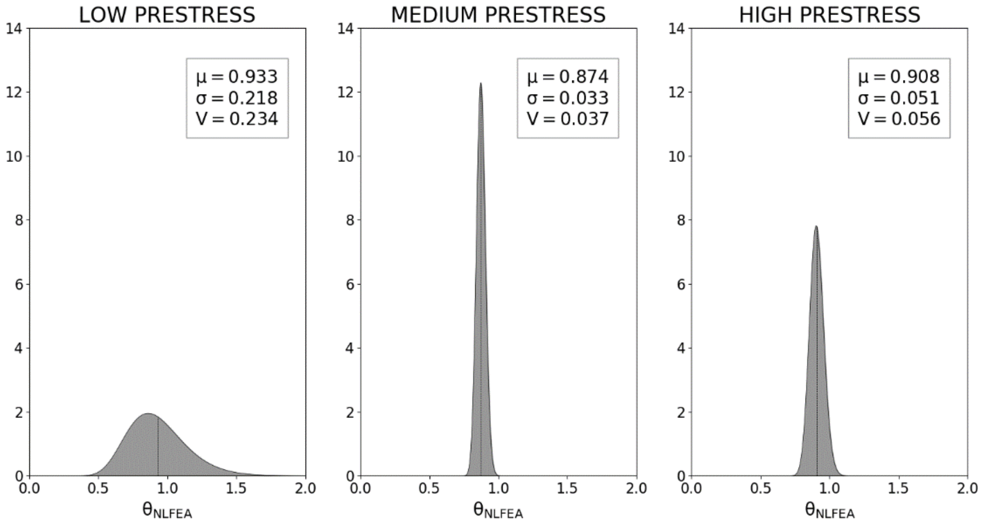

Figure 27: Modelling uncertainties for tie-rod force with various pre-stress level.

Differences in modelling uncertainty were observed after division into levels of pre-stress. The variation in modelling uncertainty was observed to be highest in the load cases with a low level of pre-stress. This can be seen in the leftmost distribution in Figure 27. A high variation is characterized by a flat and wide distribution for the modelling uncertainty.

The average value of modelling uncertainty for low levels of pre-stress indicated conservative force calculations for the tie-rods, but since the variation was high, there was a significant risk of non-conservative calculations. The distribution showed a probability of non-conservative calculations at almost 35 % for these load cases.

The modelling uncertainty for medium and high levels of pre-stress showed a small variation in the results, and almost all approximations for these pre-stress levels can be assumed conservative based on the distributions. This division of the modelling uncertainty indicated a better approximation of restraint forces in the stabilized cracking stage than in the crack formation stage.

The cracking of the structure was observed to effect the approximation of tie-rod forces in both Figure 27 and Figure 29. In Figure 29, the effect of load application was examined. The different load applications are described in Sec. 3.4.3.1. The different load applications were examined due to observations of different crack patterns from pre-stress and internal restraint forces. These observations were seen both in a crack plot from NLFEA and in the crack patterns given in the article from the experiment by Vecchio and Sato (1990). The cracking caused by internal restraint forces was not registered in the NLFEA under the Type II test with sequential load application. These cracks were formed under the Type I test in the experiment, and were present in the Type II test in the experiment (Vecchio & Sato 1990). A parallel load application of pre-stress and thermal gradient was examined to make both types of cracking. The cracks from restraint forces and pre-stress are illustrated for a corner of the frame in Figure 28 (Vecchio & Sato 1990).

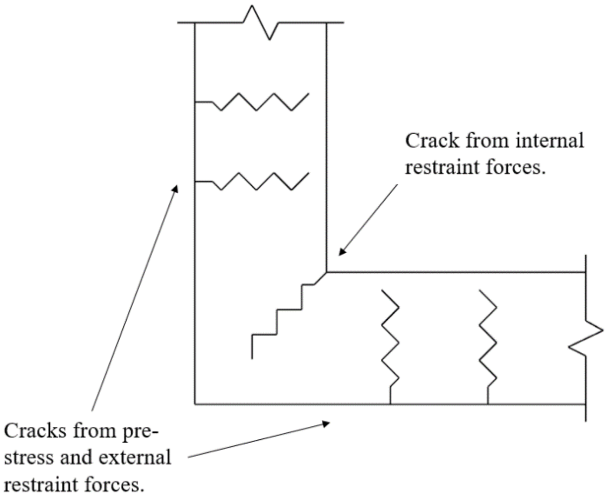

Figure 28: Experimental cracking registered in corners of frame .

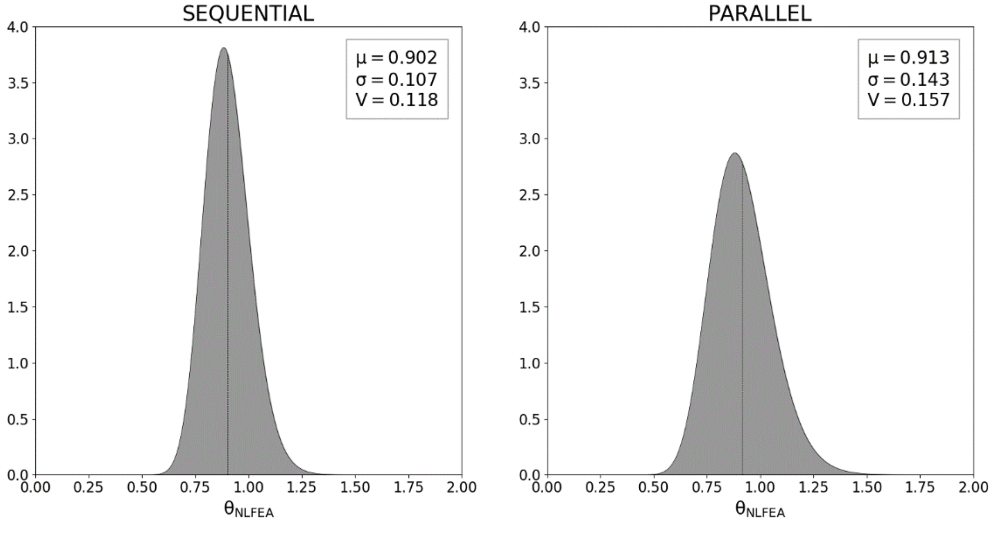

Figure 29: Modelling uncertainties for tie-rod force with different load applications.

The modelling uncertainty examined earlier in this section is related to a load application where pre-stress and thermal gradients were applied sequential. This load application was compared to an application where pre-stress and thermal gradient were applied parallel. The distributions of modelling uncertainty for these load applications showed almost no difference in the average modelling uncertainty, but the parallel application had a higher variation.

In this case, a higher variation means a higher number of non-conservative force calculations for the tie-rods. Based on the distribution for simultaneous application, almost 25 % of the calculations may lead to non-conservative forces. The corresponding estimate from the earlier examined load application was 17.5 % non-conservative calculations.

The change in the internal force in the tie-rods due to the applied thermal gradient was also examined. These results were carried out to examine how stiffness reductions in the system effected the actual force in the tie-rods. A typical change in the tie-rod force for different thermal gradients is illustrated in Figure 30.

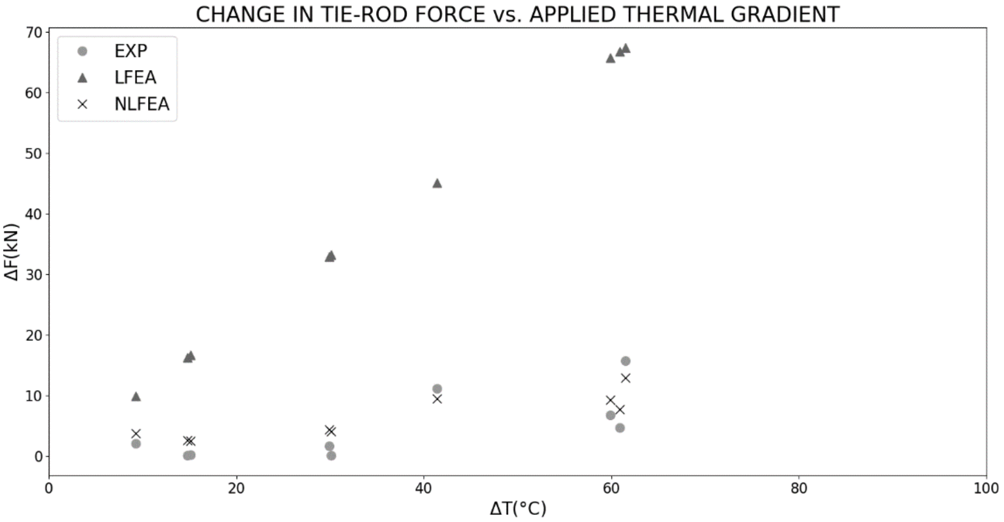

Figure 30: Increase in tie-rod force for different thermal gradient in frame PF1.

The change in the tie-rod force due to imposed deformation was linear for a LFEA. This can be seen from the triangular points in Figure 30. This linear increase in forces occurs because of a constant stiffness in the system. The increase in forces registered in the experiment differed from this linear relation. The relation for the forces in the experiment by Vecchio and Sato (1990) is given by the circular points in Figure 30. The difference between force increase in the LFEA and the experiment indicated that the restraint forces are stiffness dependent.

The relation between forces approximated by NLFEA and the thermal gradient is also given in Figure 30. This relation was observed to be closer to the actual relation registered in the experiment from Vecchio and Sato (1990). The relations given in Figure 30 are based on observations for frame PF1, but similar relations were observed for the other frames.

4.2.2 Deformation

Results for the three deformations explained in Sec. 3.5 were also obtained from the finite element analyses. These deformations were first examined in a Type I test where the tie-rods were unconnected. This test was performed once for each of the three structures. The results from the tests are given in Figure 31.

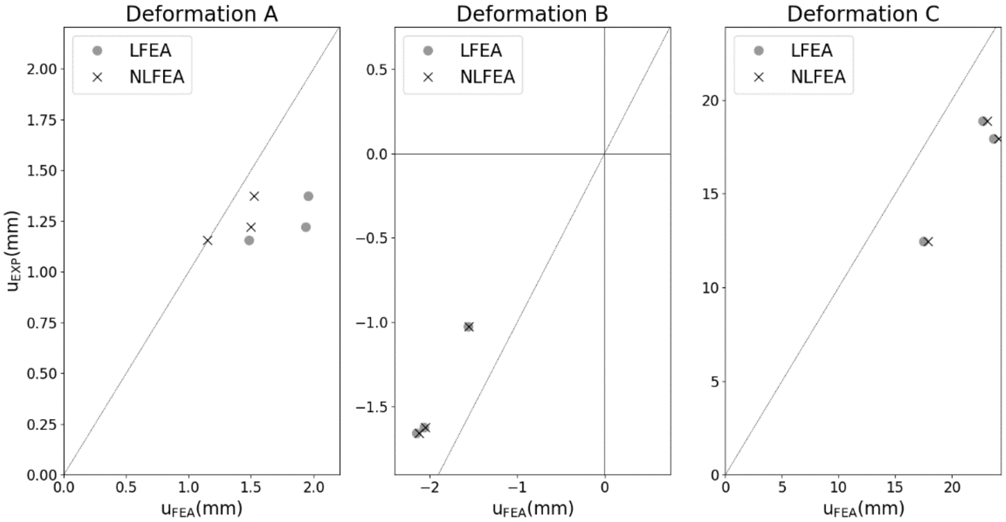

Figure 31: Comparison of deformations from Type I test.

The results given in Figure 31 showed an overestimation of the axial elongation of the beam represented by the leftmost scatterplot. The value for these deformations was approximated better by the NLFEA than the LFEA. The average modelling uncertainties for the axial elongation were 0.909 for the NLFEA and 0.704 for the LFEA.

The approximation of deformation B and C was almost equal for the NLFEA and LFEA. Both the finite element analyses overestimated the deflection in the midspan of the beam, represented by the scatterplot in the middle of Figure 31. The deflection in the columns in the rightmost scatterplot was also overestimated by both the finite element analyses. The average modelling uncertainties for the NLFEA and LFEA were almost 0.750 for both these deformations.

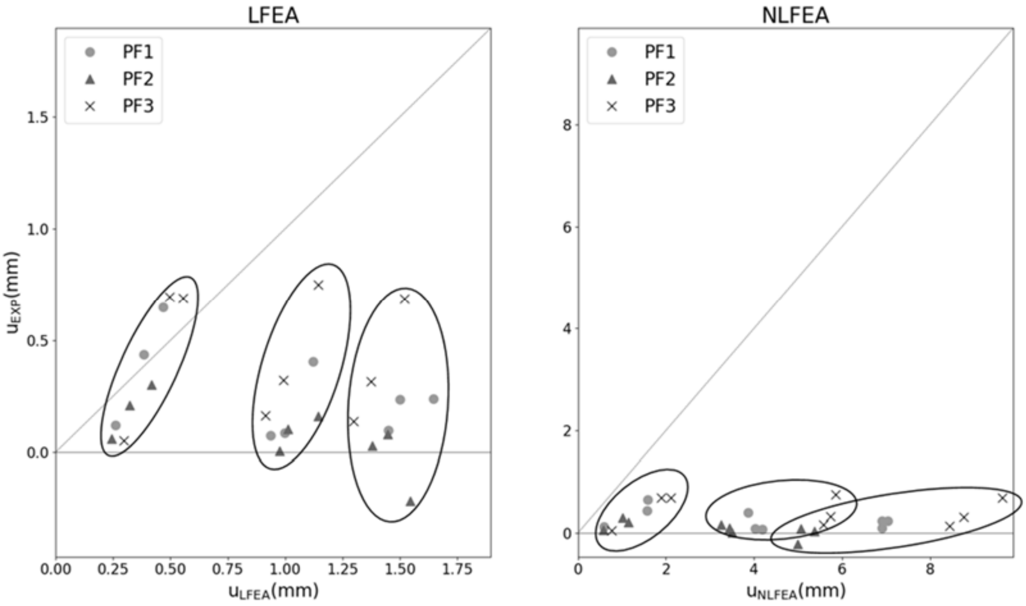

Figure 32: Comparison of deformation in midspan of beam with illustrated pattern.

After the Type I test, the pre-stressed tie-rods were connected to the structures. The combination of pre-stress and restraint from these tie-rods changed the deformations in the structures. The approximated deformations for these load cases varied, and there was observed systematical differences between approximated values and experimental values from the experiment by Vecchio and Sato (1990).

The approximated values for the deflection in the midspan of the beam are the only results given in this thesis due to the systematical failures observed in the results. These results are given in Figure 32. The reason for the systematical failures are discussed in Sec. 4.4.

The results for the approximation of the deflection in the midspan of the beam showed an overestimation of deformation in the finite element analyses. The exceptions were four calculations from LFEA. There was also a pattern in the observations where approximations for load cases with a high level of pre-stress were most overestimated. This pattern is illustrated in Figure 32 for both the finite element analyses.

4.3 Discussion about estimation of tie-rod force

The NLFEA approximated values for the tie-rod force close to the experimental values. It is important to be aware of the fact that the tie-rod force is a combination of external restraint forces and pre-stress. Therefore, the uncertainties are effected of both the estimation of restraint forces and pre-stress. The restraint forces could not be separated from the tie-rod forces since the application of the thermal gradient also reduced the pre-stress due to stiffness reduction from crack propagation. The reduced pre-stress was not given in the article from the experiment by Vecchio and Sato (1990).

The results for the tie-rod force still provided an indication of the uncertainty in restraint modelling. This is valid since the initial state before application of the thermal gradient was close to the initial state used in the experiment by Vecchio and Sato (1990). The only difference between these initial states was a small inaccuracy in the pre-stress modelling in the NLFEA. It is assumed that this inaccuracy is caused by different responses in the structure for the thermal contraction of the tie-rod and the applied load used to calculate the thermal contraction of the tie-rod in Appendix A.1. The difference in response caused a slightly different crack pattern in the NLFEA and thus a slightly different pre-stress.

In the end, the modelling uncertainty for the tie-rod force is a product of three modelling uncertainties. These are the modelling uncertainties for initial pre-stress, restraint force and reduced pre-stress. The modelling uncertainty for the initial pre-stress given in Table 16 is in average only 1 %, and may be neglected. In addition, the modelling uncertainty of the reduced pre-stress depends on the crack pattern caused by the restraint force. Therefore, the calculated modelling uncertainties for the tie-rod force are mainly caused by the uncertainty of the restraint force, even though it cannot be deducted as a separate uncertainty.

Table 16: Modelling uncertainty of initial pre-stress.

NAME	SYMBOL	VALUE
Average	**μ**	0,988
Standard deviation	**σ**	0,020
Coefficient of variance	**V**	0,020

The uncertainty in the approximated tie-rod force caused by mainly restraint forces is discussed in the following sections. This uncertainty is used as an indication of the uncertainty in the restraint force approximation. The discussions are focused on trends in restraint approximation rather than the absolute values of the modelling uncertainty since these uncertainties are composed.

4.3.1 General uncertainty in use of NLFEA

Two observations from the results in Sec. 4.2.1 are assumed representable for a general uncertainty in the approximation of restraint forces with NLFEA. These observations are the high uncertainty in tie-rod forces for load cases in the crack formation stage and the increased uncertainty due to load application.

4.3.1.1 Uncertainty in crack formation stage

The high uncertainty in the estimation of tie-rod forces in the crack formation stage is assumed a consequence of varying tension strength in the concrete. The variation of tension strength in the concrete can be assumed normally distributed (Nesset & Skoglund 2007; Sørensen 2014). The crack formation that occurs in the NLFEA is based on an excess of the tensile strength of concrete corresponding to the nominal compression strength from the experiment used as input in the material model. This tensile strength is constant and the normal distribution of strengths is neglected. In contrast, the experimental crack formation would occur in the section where the stress first exceeds the sectional tensile strength. This effect may cause both conservative and non-conservative calculations of the restraint force in the crack formation stage. Conservative calculations would occur in situations where the NLFEA underestimates the number of cracks in the structure. The effect of varying tension strength on the estimation of restraint force is illustrated in Figure 33.

The first crack formation in Figure 33 shows a deviation where the tensile strength in the NLFEA overestimates the tensile strength in the structure. The effect of overestimated tensile strengths is overestimated restraint loads. In the second crack formation, the NLFEA underestimates the tensile strength in the structure and thus the restraint loads. These deviations are assumed present in the NLFEA, since the tensile strength used in the model corresponds to a nominal tensile strength. A conservative approach in further work may be to use the tensile strength equal to the 95 % fractile of the normal distribution of tensile strengths.

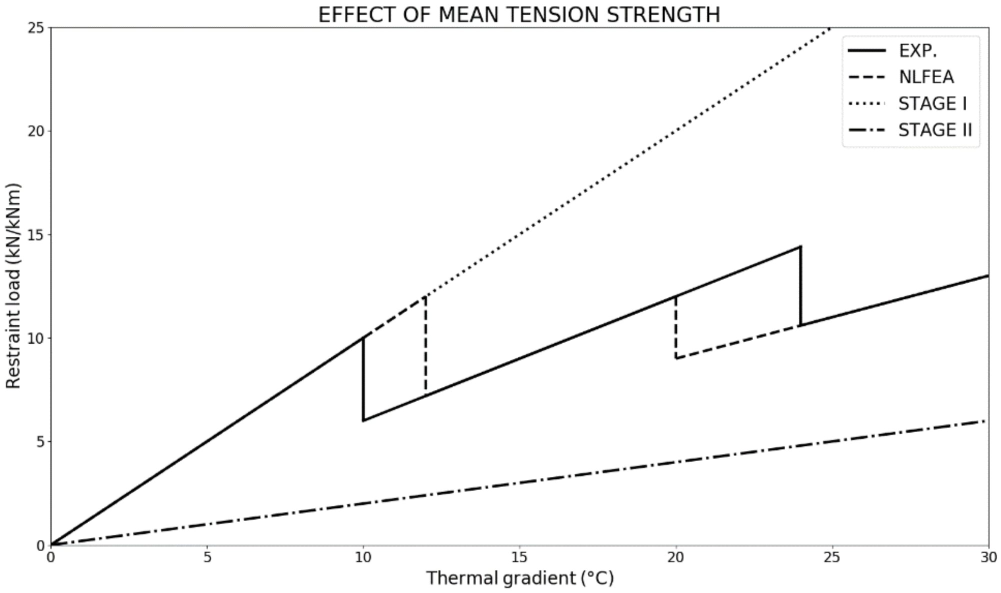

Figure 33: Effect of deviation in tension strength between NLFEA and experiment.

Another parameter that may affect the uncertainty of the restraint force in the crack formation stage is the use of smeared cracking in the NLFEA. The smeared cracking used in the NLFEA reduces the stiffness of concrete in parts of the structure, which are not cracked in the experiment. These stiffness reductions affects the restraint forces since the tension stiffening contribution from concrete is reduced. An underestimated stiffness leads to an underestimated restraint force according to the theory in Sec. 1.2. This underestimation of restraint force may be present until a new crack is formed in the real structure. The effect of smeared cracking on the approximation of the restraint force is illustrated in Figure 34.

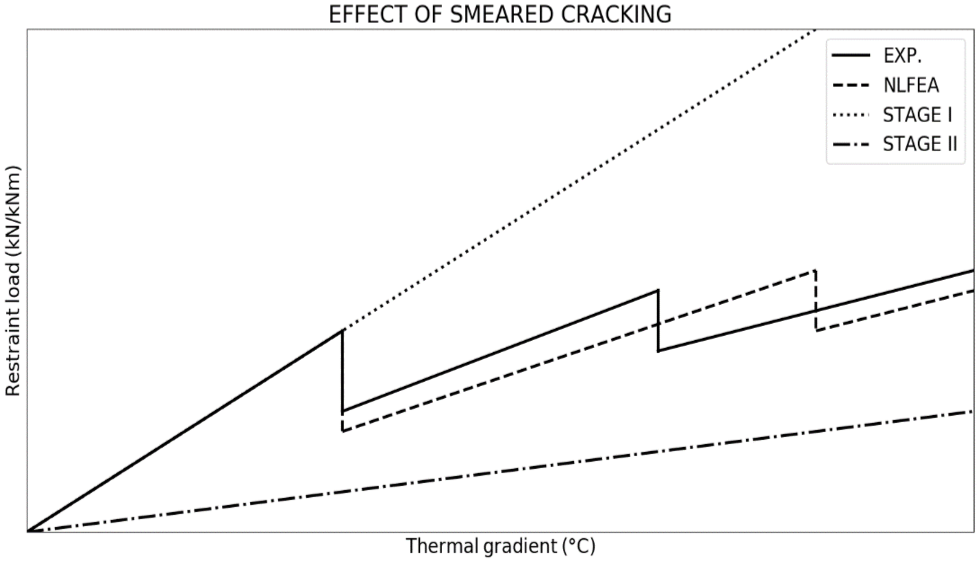

Figure 34: Effect of smeared cracking on restraint forces in crack formation stage.

It is recommended to avoid the use of an underestimated restraint forces from the crack formation stage in further calculations. Load combinations used in the serviceability limit state are lower than the load combinations used for design of the structure in the ultimate limit state (CEN 2002b). Based on this, it is more likely that the restraint force is calculated for a load combination in the crack formation stage when NLFEA is used for crack width calculations. Therefore, the use of NLFEA for calculations in serviceability limit state is dependent on a safety factor, which takes into account these uncertainties in the restraint force.

4.3.1.2 Uncertainty for different load applications

The increased uncertainty in the estimation of tie-rod forces from a parallel application of loads, given in Figure 29, seems to be caused by different crack formation for restraint loads and pre-stress. In the load application where pre-stress and thermal gradient are applied sequential, the stiffness reductions are determined mainly by the pre-stress. In the parallel application, the stiffness reductions are determined partial by pre-stress and partial by restraint forces. Since the variation in modelling uncertainty is higher for a parallel application, cracking from restraint forces seems to affect the numerical calculation of restraint more than cracking from pre-stress.

For the examined case, it seems correct to use an application where loads are placed sequential since the pre-stress is applied before the thermal gradient in the experiment by Vecchio and Sato (1990). Nevertheless, it can be argued for parallel load application since the structure was exposed to a high thermal gradient during the Type I test without pre-stressing. Therefore, eventual cracking from internal restraints during the Type I test is neglected with an application where the pre-stress and the thermal gradients are applied sequential.

In a design of a real structure, it is not able to predict the application of loads fully. Therefore, it is necessary to make further investigations of how to apply loads in a NLFEA to ensure conservative calculations of restraint forces. Examinations of the importance and development of internal cracking from restraint forces are necessary for conservative assumptions.

4.3.2 Case dependent uncertainty in use of NLFEA

There were also several assumptions taken in the modelling process that may have affected the numerical calculation of the restraint force. These effects are assumed case dependent since more information may be available in a design process. Some of these effects were mentioned in Sec. 4.3.1 like the application of loads and the uncertainty in pre-stress application. Other case dependent effects are presented in this section.

4.3.2.1 Modelling of thermal gradient

A simplification is made in the numerical calculation of the thermal gradient in this thesis. The thermal gradient is applied over the whole length of the columns in the structure. In the experiment, this gradient was limited to the length in contact with water. The temperature difference above water level was not described in the article by Vecchio and Sato (1990). It is valid to assume that this length also was affected by the heat generation in the water, but it is uncertain to what extent it is affected.

The simplification is assumed to affect the results from the NLFEA. It is believed that this effect increased the thermal gradient in the length of the column above water level relative to the experiment. The increased gradient in the length between the water level and the tie-rod increased the restraint forces generated in the tie-rod. Ultimately, this leads to an increased probability for conservative calculations of the restraint force.

The increased probability of conservative calculations needs to be taken into account in the assessment of the results from NLFEA. The effect from this assumption is still assumed small since the only contribution to the tie-rod force is caused by the additional curvature of the length between water level and the tie-rod. It is assumed that the elongation of this length has no affection on the tie-rod force.

The simplified application of thermal gradients was made to avoid internal cracking of the concrete in the transition zone between water and air. This effect was registered in the NLFEA when the linear gradient was applied only below water level and the initial temperature was applied above water level. A transient temperature analysis may be used to estimate a more realistic temperature for the transition zone, but the information about the surroundings of the structure was limited in the article by Vecchio and Sato (1990).

4.3.2.2 Modelling of tie-rod

The material properties of the tie-rods used in the experiment by Vecchio and Sato (1990) were not given in the article. Therefore, the material properties for the tie-rods are set equal the material properties for the reinforcement in this thesis. The restraint force generated in these tie-rods is directly affected of the used elastic modulus. An exaggeration of the elastic modulus for the tie-rod is expected to cause higher restraint forces than the experimental measurements.

4.3.2.3 Creep

The structures were exposed to both high temperatures and a constant load situation over time in the experiment by Vecchio and Sato (1990). It is known that creep occurs in materials exposed to long-term loading, and this effect is accelerated due to increased temperatures (Ariyawardena et al. 1997; Bazant 1975). The effect of creep is plastic deformations over time due to a constant load. Such effects may be favorable in situations with restraint forces from imposed deformations since these plastic deformations would reduce the restraint force. The reduced restraint forces would increase the probability for conservative estimations of the restraint force from NLFEA. This effect was observed by Zhou and Vecchio for the case examined in this thesis (Zhou & Vecchio 2005).

The cracks in the concrete are expected to contract due to the reduced restraint loads. The contraction is an effect of reduced elastic deformations in the structure. Although, restraint forces are reduced, parts of the corresponding crack widths may remain due to plastic deformations from creep (Miji Cherian & Ganesan 2014).

4.3.3 Uncertainty in NLFEA versus LFEA

The uncertainty in the modelling of the tie-rod force is significantly lower for NLFEA than LFEA. The main reason for this is that the LFEA do not take into account the reduction of restraint force due to stiffness reductions in the structure. The effect is clearly shown in Figure 30 where the increase in tie-rod forces in the LFEA is proportional to the applied thermal gradient. This increase is not observed in the experiment by Vecchio and Sato (1990).

The approximations from the NLFEA are closer to the experimental values. This can also be seen in Figure 30. The NLFEA seems to be a better alternative than LFEA for estimations of the restraint force. The use of the restraint force from numerical calculations in design requires conservative calculations. This is considered in further calculations by implementation of the modelling uncertainty.

A conservative restraint force based on the modelling uncertainty is unfavorable in a design perspective since it requires information about the actual response in the structure. Simplified methods that secure conservative approximations are preferred in the future.

4.4 Discussion about estimation of deformations

The approximated deformations from the finite element analysis are not close to the experimental values by Vecchio and Sato (1990). In the Type I test, the numerical estimations are closer to the experimental values than in the Type II test. This effect is caused by the pre-stress applied in the Type II test. A grouping pattern is observed in the results in Figure 32 for different levels of pre-stress. An attempt to remove this grouping was performed by measuring only deformations that occurred after the time of pre-stressing. This attempt removed the grouping, but there was still a significant difference between the numerical calculations and the experiment.

Lack of information in the article by Vecchio and Sato (1990) is assumed the reason for the remaining deviations. Information is missing mainly for the description of the deformation in the midspan of the beam and the relative deflections of the columns. The problem with these descriptions is that there is no description of the initial situation. The tested initial situations for the estimated deformations in this thesis are an unloaded structure and a structure exposed to pre-stress, water pressure and self-weight. None of these situations gave deformations close to the deformations measured in the experiment. The frames used in the experiment were also loaded and unloaded several times and this may have caused plastic deformations in the frames.

The relative deflection of the columns is not only ambiguous due to the initial load situation, but it is neither described what the deflection is measured relative to. This may also cause a systematical failure in the results. Because of these deviations, which can be traced back to ambiguous descriptions, it is assumed that the models are valid regardless of deformations, since the calculation of tie-rod forces is good. There may also be other factors that affect the deformations e.g. creep, elastic modulus of tie-rods and crack formation stage. A phenomenon like creep may for example have a greater effect on deformations than tie-rod forces since some of the measured deformations are close to zero.

5 Crack width calculation

5.1 General

Approximated tie-rod forces from the NLFEA were implemented in the crack width formula from Eurocode 2, and crack widths were calculated for three load cases from the experiment by Vecchio and Sato (1990). These crack widths were compared to the maximum crack widths registered in the experiment.

In addition, two implementations based on LFEA were used. These implementations are described in Sec. 3.6. The calculations based on implementations from NLFEA and LFEA were all compared with the experimental crack widths and with each other. Results from all the implementations and crack width calculations are given in Sec. 5.2.

The results from all implementations are discussed separately and against each other in Sec. 5.3. This discussion was focused on calculations based on NLFEA versus calculations based on LFEA.

5.2 Results from crack width calculations

The implementation of tie-rod forces was based on a critical load combination with effects from external restraint forces and a strain distribution for a cross section in Stage II. The critical load combinations used for approximation of the strain distribution are given in Sec. 5.2.1. The load combination for implementation B was separated from the others, since this implementation separates contributions from external static forces and external restraint forces.

The strain distribution for a section in Stage II was approximated for the critical load combination with a layer-by-layer approach. This strain distribution was the origin to the input parameters in the crack width calculations. The input parameters in all four implementations are given in Sec. 5.2.2. The input parameters for implementation B are again separated from the others due to a higher number of input parameters.

The maximum crack distances and crack widths from the four implementations in this research are given in Sec. 5.2.3. The maximum crack widths registered in the experiment are also given as a basis for comparison.

5.2.1 Load combination

Load combinations were calculated for the critical cross section in frame PF3 due to three different load cases. The calculated load combination for implementation A was based on the LFEA, and the load combinations for implementation C and D were based on the NLFEA. The results from these calculations are given in Table 17.

Table 17: Load combinations used in crack width calculation A, C and D.

LOAD CASE	**A**		**C**		**D**	
	N (kN)	**M (kNm)**	**N (kN)**	**M (kNm)**	**N (kN)**	**M (kNm)**
4*	84	180	8	44	9	47
7	101	213	25	79	28	85
10	111	233	35	99	38	107

The load combinations in Table 17 clearly showed that the loads were lower in the NLFEA than in the LFEA. The difference between load combinations was observed to be highest for load case 4*, which was a load case examined just for estimation of crack widths. The amount of loads in this load case was almost equal to the loads in load case 4, and on this basis it is called 4*. In load case 4*, the axial force in the LFEA was 10.5 times the force in NLFEA, and the moment in LFEA was 4.1 times higher than in the NLFEA.

The difference between the load combinations in implementation C and D was caused by the implementation of the modelling uncertainty. The effect of this implementation was increased section loads.

The input used in implementation B were both a load combination from static loads and the restraint strain in the reinforcement from imposed deformations. The load combinations and strains used for these calculations are given in Table 18.

Table 18: Load combinations and strains used in crack width calculation B.

LOAD CASE	**B**		
	N (kN)	**M (kNm)**	**ε_t (10^{-6})**
4*	-5	17	290
7	12	50	291
10	24	72	287

The load combinations used for implementation B were lower than for the other implementations. These loads were lower since effects from imposed deformations were treated separately. The restraint strains in implementation B were almost equal to each other for the three load cases.

5.2.2 Input parameters from layer-by-layer approach

Reinforcement stress, compression height and effective concrete area were calculated with the layer-by-layer approach for all four implementations. In implementation B, the strain distribution was also used for calculation of the reinforcement strain due to static forces and the factor k_c. The factors calculated for implementation A, C and D are given in Table 19 and the factors for implementation B in Table 20.

Table 19: Factors calculated from strain distribution for implementation A, C and D..

LOAD CASE	**A**			**C**			**D**		
	σ_s (MPa)	**x (mm)**	**$A_{c,eff}$ (mm^2)**	**σ_s (MPa)**	**x (mm)**	**$A_{c,eff}$ (mm^2)**	**σ_s (MPa)**	**x (mm)**	**$A_{c,eff}$ (mm^2)**
4*	823	60	64000	206	55	65333	220	55	65333
7	977	60	64000	365	55	65333	392	55	65333
10	1071	60	64000	456	55	65333	493	55	65333

Table 20: Factors calculated from strain distribution for implementation B.

LOAD CASE	B				
	ε_s (10^{-6})	σ_s (MPa)	x (mm)	$A_{c,eff}$ (mm^2)	k_c
4*	420	84	50	100000	0,748
7	1163	232	55	100000	0,745
10	1659	332	55	100000	0,744

An interesting observation from the results in Table 19 was the magnitude of the reinforcement stress. These stresses were higher than the yielding stress of reinforcement for implementation A. Yielding stress was not registered in the experiment by Vecchio and Sato (1990). The maximum reinforcement stresses calculated for implementation C and D were also right above the yielding stress. This showed that experimental stress levels in the reinforcement were overestimated with the calculations based on Eurocode 2, but reinforcement stress close to the yielding stress was observed for load case 10 in the NLFEA.

The stress levels in Table 20, for calculations based on NS3473, were calculated without the restraint forces from imposed deformations. The maximum level of stress was equal to 446 MPa when stress from the restraint strain was taken into account. This value was still right below the yielding stress of the reinforcement equal to 448 MPa.

The calculated compression height was almost equal for the implementations in the formula from Eurocode 2, but the implementation for the formula in NS3473 had a higher compression height. This effect was caused by different formulas for the compression height in Eurocode 2 and NS3473.

5.2.3 Crack distance and crack width

The factors from the layer-by-layer approach calculations were used to calculate the maximum crack spacing for the structure. Values for this crack spacing are given in Table 21.

Table 21: Maximum crack spacing for crack width calculation A, B, C and D.

LOAD CASE	A	B	C	D
	$s_{r,max}$ (mm)	$s_{r,max}$ (mm)	$s_{r,max}$ (mm)	$s_{r,max}$ (mm)
4*	378	575	383	383
7	378	573	383	383
10	378	573	383	383

There was only small differences in the maximum crack spacing between implementations based on Eurocode 2, but the implementation based on NS3473 used a higher crack spacing.

The maximum crack spacing was used to calculate the crack width based on the methods described in Sec. 3.6.3 and Sec. 3.6.4. The results from these calculations are given in Table 22.

Table 22: Crack widths from calculation A, B, C and D and experiment.

LOAD CASE	EXP.	A	B	C	D
	w (mm)	w_k (mm)	w (mm)	w_k (mm)	w_k (mm)
4*	**0,42**	1,28	0,43	0,24	0,42
7	**0,50**	1,57	0,60	0,42	0,75
10	**0,62**	1,75	0,71	0,59	0,94

The crack widths calculated based on implementation A showed an overestimation relative to the registered crack widths from the experiment by Vecchio and Sato (1990). The calculated crack widths from this implementation were more 2.5 times the experimental values. This value indicated a very conservative calculation of crack widths, and this effect was mainly caused by the load combination used in the calculations.

Crack widths from implementation B were closest to the actual crack widths from the experiment. The crack widths calculated were also conservative compared to the experimental values. The calculated crack width for the load case 4* was almost equal to the experimental width, and there may have been a risk of non-conservative calculations for similar cases.

Implementation C showed non-conservative crack width calculations. The calculated crack width for load case 4* was 43 % below the experimental value. Since underestimation was a general problem in this implementation, a new implementation was proposed in implementation D.

The crack widths calculated based on implementation D were conservative for all load cases. The calculated crack width for load case 4* was equal to the experimental width, and there was no additional safety present in this calculation. For the other load cases, the implementation overestimated crack widths more than implementation B. The average overestimation of crack widths was 34 % for this implementation compared to 12 % for implementation B.

5.3 Discussion about implementation of external restraint load

The different implementations of restraint forces from thermal expansion in the crack width formula are discussed in this section. The implementations are discussed separately in Sec. 5.3.1-5.3.4, and the use of an implementation based on NLFEA as opposed to other implementations is discussed in Sec. 5.3.5.

5.3.1 Implementation A

The implementation of the total restraint force from a LFEA in the crack width formula highly overestimates the real crack widths. This was expected since the restraint forces used in the calculations do not consider the reduction of restraint forces from reduced structural stiffness due to crack propagation. This implementation is also presented in Sec. 1.1 as the criticized implementation (Bruggeling 1991; Reinhardt 1991). The criticism of this implementation seem to be justified by the calculated crack widths in this work.

Based on the calculated crack widths from implementation A, it is recommended to avoid use of total restraint forces calculated with LFEA. These restraint forces lead to overestimated crack widths. Since additional reinforcement is a measure used for reduction of crack width, this may lead to an overuse of reinforcement.

5.3.2 Implementation B

The empirical calculation based on NS3473 also shows conservative calculations of the crack widths in this case. Although the calculations are conservative, they are close to the experimental widths. The crack width calculated for load case 4* is almost equal to the maximum crack width registered for the load case in the experiment. Since this calculation is nearly conservative, there may be a risk of underestimated crack widths if several load cases are being investigated.

The reduced overestimation in the crack width calculation for load case 4* may be caused by several factors. Creep can be such a factor since load case 4* was exposed to a high thermal gradient in 7 days. The other examined load cases were exposed to a thermal gradients only for 24 hours (Vecchio & Sato 1990). Creep in the materials may cause plastic deformations in the cracked sections, which make the calculations less conservative since creep is not considered in the calculations.

Another factor, which can contribute too little overestimation in load case 4*, is the factor F_t equal to 2. Detailed documentation of the background for this factor has not been found, but a derivation of a comparable factor from Dr. Techn. Olav Olsen was examined. This derivation mentions that the factor is not conservative for structures with only slightly reduced stiffness from cracking. The forces in load case 4* results in cracking of the beam, but almost no cracking in the columns. Therefore, the load case is located almost halfway in the crack formation stage. The non-conservative region for the factor F_t seems to be in a region with lower structural stiffness than the stiffness corresponding to load case 4*, but further investigation should be performed to verify this.

5.3.3 Implementation C

A direct implementation of the estimated tie-rod force from a NLFEA gives non-conservative crack widths for all the examined load cases. It is believed that this effect is caused by the assumptions underlying the formula from Eurocode 2. This formula assumes a calculation of the reinforcement strain where tension stiffening is not considered. Therefore, the maximum contribution from tension stiffening is deducted from the reinforcement strain within the formula (CEN 2004).

A full deduction of tension stiffening from the reinforcement strain, which originates from restraint forces in NLFEA, is assumed not valid. The reason for this is that the restraint force is calculated based on the available tension stiffening in the nonlinear finite element model. The tension stiffening in the NLFEA is not equal to the maximum tension stiffening. A maximum tension stiffening effect is only present if all crack distances are equal the maximum crack distance and if the crack propagation is discrete. The cracking in the NLFEA is smeared and this results in longer average crack distances than in the experiment and no localization of cracks. Therefore, the reinforcement strain from the NLFEA is lower than the strain required as input in the formula in Eurocode 2. The lack of tension stiffening in the calculation of reinforcement strain was handled conservatively in implementation D by ignoring the reduction from tension stiffening.

Another problem for implementation C is that restraint forces are not always conservatively calculated from the NLFEA. This problem was discussed in Sec. 4.3. The risk of unsafe force calculations was considered in implementation D by use of the modelling uncertainty for the structure.

5.3.4 Implementation D

Implementation D was formed by the findings in this research. This resulted in a calculation where the used restraint forces were increased due to the modelling uncertainty and where the crack width formula ignored tension stiffening. Conservative crack widths were found with this approach. Even though the calculations were conservative, it was observed that load case 4* would have been non-conservative if the modelling uncertainty was not implemented. This was observed despite the fact that the restraint force for load case 4* was conservatively calculated in the first place. This indicates that also other factors, which are not taken into account in this thesis, are affecting the crack widths. One of these factors is the creep mentioned in Sec. 4.3.2.3 and Sec. 5.3.2.

The ignored tension stiffening in the crack width formula resulted in crack widths for load case 7 and 10 with a high degree of overestimation. Because of this, the omission of tension stiffening seems to be too conservative. Therefore, it is recommended to perform further research on the contribution from tension stiffening in order to consider this in a better way.

5.3.5 Implementation from NLFEA versus other implementations

An implementation of forces from NLFEA leads to more accurate calculations of crack widths than the implementation of forces from LFEA. This results in having outcomes closer to the experimental crack widths and less overestimation. In this way, overuse of reinforcement to reduce crack widths can be prevented.

Nevertheless, it seems like the empirical formula used for crack width estimations gives similar or more realistic crack widths than the implementation from NLFEA used in this thesis. Because of this, further investigations are needed to calculate more accurate crack widths using NLFEA. An investigation of tension stiffening contributions in the NLFEA would be of interest for further research.

It is another suggestion to perform further calculations to ensure that both the empirical calculations and the calculations based on NLFEA are conservative for several load cases and structures. Load case 4* and 10 in this thesis are critical since load case 4* may be influenced by creep, and load case 10 is almost at the limit of yielding of the reinforcement. Therefore, load case 7 is the best comparison basis for the calculations. This load case leads to conservative results when used with both the empirical formula and the implementation from NLFEA.

6 Conclusion

A procedure for crack width calculation with effects from thermal gradients using NLFEA was developed in this thesis. The calculation showed conservative results for all the three examined load cases in this research. The conservative approach was ensured by two assumptions. These assumptions were an increase of external restraint forces due to modelling uncertainty and the use of the crack width formula from Eurocode 2 without strain reduction from tension stiffening.

The external restraint forces were increased due to the modelling uncertainty of restraint forces in the crack formation stage. This modelling uncertainty caused a risk of unsafe external restraint forces. The risk of unsafe calculations is most likely linked to the material model used in the NLFEA. The difference between varying tensile strength in the experiment, and the constant tensile strength used in the NLFEA is assumed to be one of the reasons for non-conservative restraint forces. The dissimilarity between smeared cracking caused by the solution process in the NLFEA and localized cracking in the experiment is assumed to be another reason.

The crack width formula was used without reduction from tension stiffening since an uncertain amount of tension stiffening was present in the restraint forces from NLFEA. The calculation of crack widths from Eurocode 2 usually reduces the reinforcement strain with the full contribution from tension stiffening in the uncracked concrete. A maximum tension stiffening effect is usually not the case in the NLFEA. Therefore, an exclusion of effects from tension stiffening is a conservative assumption until further examination of tension stiffening in NLFEA is performed.

The calculation of crack widths based on external restraint forces from NLFEA showed better accuracy than calculations based on the same forces from LFEA. The crack widths calculated with restraint forces from LFEA were highly overestimated. The use of the linear restraint forces are causing an unnecessarily high degree of overestimation, and it is recommended to avoid use of these forces for crack width calculations.

The results based on NLFEA were also compared to an empirical approach. The empirical crack widths were both conservative and more realistic than the crack widths from the NLFEA calculation. Therefore, it is still necessary to improve the procedure based on external restraint forces from NLFEA. A method for reduction of strains from NLFEA due to tension stiffening would most likely have caused an improvement in the calculation.

Although the crack widths from empirical calculations are more accurate than the crack widths based on NLFEA, it is recommended to perform further investigations on the reliability of the empirical calculation. It is doubtful if a factor F_t equal to 2 can be used for crack width calculations regardless of the structural stiffness. The mistrust of this factor is mainly connected to structural stiffnesses with a low number of cracks.

7 Further work

Although the nonlinear approach for crack width calculation with effects from thermal gradients is conservative, there is a need for improvement. Some areas with potential for improvement are known, and these areas can be divided into two categories. The first category is research regarding the modelling of external restraint forces. Some fields for further investigation in this category are:

- Transient or steady state thermal finite element analyses of reinforced concrete structures taking into account convection, radiation and heat generation.
- Effects of cracking due to internal restraint of thermal movement. Cracking from internal restraint was observed in the nonlinear finite element model due to variations in structural stiffness.
- Methods for conservative calculations of external restraint forces in the crack formation stage using NLFEA without implementation of the modelling uncertainty.

The second category is further examination of the implementation of external restraint forces in the crack width formula in Eurocode 2. Fields for research in this implementation are:

- Calculation procedure for average reinforcement strain based on tension stiffening acting in NLFEA.
- Implementation of creep in the crack width calculation.

It seems like the procedure based on NLFEA can predict accurate crack widths if the items above are further examined. It is assumed that an investigation of the contribution from tension stiffening in the NLFEA would lead to significant improvements of the procedure, but also creep effects are important to prevent non-conservative calculations. It is also possible that other uncertainties exist in the calculation procedure, which is not discovered in this work. Therefore, it is also necessary to validate the procedure for several structures and load cases.

8 References

Alfredsson, H. & Spåls, J. (2008). *Cracking Behaviour of Concrete Subjected to Restraint Forces*. Master's Thesis. Göteborg: Chalmers University of Technology, Department of Civil and Environmental Engineering. 219 pp.

ANSYS® Academic Research Mechanical. (Release 18.0). *Help System*. Element Reference: ANSYS,Inc.

Ariyawardena, N., Ghali, A. & El-Badry, M. (1997). Experimental Study on Thermal Cracking in Reinforced Concrete Members. *ACI Structural Journal*, 94 (4): 432-441.

Bathe, K.-J. (2014). *Finite Element Procedures*. 2 ed. United States of America: Prentice Hall, Pearson Education, Inc. 1043 pp.

Bazant, Z. P. (1975). Theory of Creep and Shrinkage in Concrete Structures: A Précis of Recent Developments. *Mechanics Today*, 2 (Chapter I): 1-93.

Brattström, N. & Hagman, O. (2017). *Reinforced Concrete Subjected To Restraint Forces : A comparison with non-linear numerical analyses*. Master's Thesis. Stockholm: Royal Institute of Technology (KTH), Department of Civil and Architectural Engineering. 128 pp.

Brekke, D.-E., Aldstedt, E. & Grosch, H. (1994, April 10-15). *Design of Offshore Concrete Structure Based On Postprocessing of Results From Finite Element Analysis (FEA): Methods, Limitations And Accuracy*. Proceedings of the Fourth (1994) International Offshore and Polar Engineering Conference, Osaka, Japan.

Brekke, D.-E. (2017). *Design for Imposed Deformation Loads*. Skøyen: Multiconsult (Presentation 01.06.2017).

Bruggeling, A. S. G. (1987). Control of crack width under imposed deformations. *IABSE Reports*, 55: 143-148.

Bruggeling, A. S. G. (1991). Restrained Imposed Deformations Versus Loads. In Grierson, D. E., Franchi, A. & Riva, P. (eds) *Progress in Structural Engineering: Proceedings of an international workshop on progress and advances in structural engineering and mechanics, University of Brescia, Italy, September 1991*, pp. 1-6. Dordrecht: Springer Netherlands.

Byron Bird, R., Stewart, W. E. & Lightfoot, E. N. (2002). *Transport Phenomena*. 2 ed. New York: John Wiley & Sons, Inc. . 895 pp.

CEN. (2002a). *Eurocode 1: Actions on structures - Part 1-1: General actions - Densities, self-weight, imposed loads for buildings*. Brussels: European Committee for Standardization.

CEN. (2002b). *Eurocode: Basis of structural design*. Brussels: European Committee for Standardization.

CEN. (2003). *Eurocode 1: Actions on structures - Part 1-5: General actions - Thermal actions*. Brussels: European Committee for Standardization.

CEN. (2004). *Eurocode 2: Design of concrete structures - Part 1-1: General rules and rules for buildings* Brussels: European Committee for Standardization.

CEN. (2005). *Eurocode 3: Design of steel structures - Part 1-1: General rules and rules for buildings* Brusseles: European Committee for Standardization.

CEN. (2006). *Eurocode 2 - Design of concrete structures - Part 3: Liquid retaining and containment structures*. Brussels: European Committee for Standardization.

Collins, M. P. & Mitchell, D. (1991). *Prestressed Concrete Structures*. 1 ed. New Jersey: Prentice-Hall, Inc. 766 pp.

Cook, R. D., Malkus, D. S., Plesha, M. E. & Witt, R. J. (2002). *Concepts and Applications of Finite Element Analysis*. United States John Wiley & Sons, Inc. . 719 pp.

Det Norske Veritas. (1980). *Rules for the design constructions and inspection of offshore structures - Appendix D - Concrete Structures*. Høvik: Det Norske Veritas.

El-Tayeb, E. H., El-Metwally, S. E., Askar, H. S. & Yousef, A. M. (2017). Thermal analysis of reinforced concrete beams and frames. *HBRC Journal*, 13 (1): 8-24.

Engen, M., Hendriks, M. A. N., Köhler, J., Øverli, J. A. & Åldstedt, E. (2017a). A quantification of the modelling uncertainty of non-linear finite element analyses of large concrete structures. *Structural Safety*, 64: 1-8.

Engen, M., Hendriks, M. A. N., Øverli, J. A. & Åldstedt, E. (2017b). Non-linear finite element analyses applicable for the design of large reinforced concrete structures. *European Journal of Environmental and Civil Engineering*: 1-23.

Hens, H. (2010). *Building Physics Heat, Air and Moisture*. 2nd ed. Berlin: Wilhelm Ernst & Sohn. 315 pp.

Holand, I., Gudmestad, O. T. & Jersin, E. (2000). *Design of Offshore Concrete Structures*. 1 ed. New York: Spon Press. 226 pp.

Huebner, K. H., Dewhirst, D. L., Smith, D. E. & Byrom, T. G. (2001). *The Finite element method for engineers*. 4th ed. New York: John Wiley and Sons, Inc. 720 pp.

Klieger, P. & Lamond, J. F. (1994). *Significance of Tests and Properties of Concrete and Concrete-Making Materials*. 1 ed. Fredericksburg: American Society for Testing and Materials. 623 pp.

Li, Y. (2010). *Predicting of the Stiffness of Cracked Reinforced Concrete Structures*. Final report. Delft: Delft University of Technology, Department Design and Construction. 153 pp.

Miji Cherian, R. & Ganesan, N. (2014). Analytical Model for the Calculation of Long Term Crack Width. *International Journal of Scientific & Engineering Research*, 5 (7): 403-407.

Nesset, J. & Skoglund, S. (2007). *Reinforced Concrete Subjected to Restraint Forces*. Master's Thesis. Göteborg: Chalmers University of Technology, Department of Civil and Environmental Engineering. 168 pp.

Newman, J. & Choo, B. S. (2003). *Advanced Concrete Technology*. 1 ed. Oxford: Elsevier Ltd. 303 pp.

Norges Standardiseringsforbund. (2003). *NS3473: Design of concrete structures. Design and detailing rules.* 6th ed. Oslo: Norges Standardiseringsforbund.

Reinhardt, H.-W. (2014). Aspects of imposed deformation in concrete structures – a condensed overview. *Structural Concrete*, 15 (4): 454-460.

Reinhardt, H. W. (1991). Imposed deformation an cracking. *IABSE Reports*, 62: 101-110.

Stolarski, T., Nakasone, Y. & Yoshimoto, S. (2006). *Engineering Analysis with ANSYS Software*. 1 ed. USA: Butterworth-Heinemann. 456 pp.

Sørensen, S. I. (2014). *Betongkonstruksjoner* 2ed. Bergen: Fagbokforlaget Vigmostad & Bjørke AS. 470 pp.

Tavares, R. M. & Camara, J. M. M. N. d. (2010). *State-of-art sobre o controlo da fendilhação devido a deformações impostas*. Lisboa: Lisboa : UTL, Instituto Superior Técnico, 2010. 11 pp.

Tipler, P. A. & Mosca, G. (2008). *Physics*. Sixth ed. New York: W. H. Freeman and Company. 1412 pp.

Vecchio, F. J. & Sato, J. A. (1990). Thermal Gradient Effects in Reinforced Concrete Frame Structures. *ACI Structural Journal*, 87 (3): 262-275.

Vecchio, F. J. (2001). Nonlinear Finite Elemenet Analysis of Reinforced Concrete: At the Crossroads?. *Structural Concrete*, 2 (4): 201-212.

Zhou, C. E. & Vecchio, F. J. (2005). Nonlinear finite element analysis of reinforced concrete structures subjected to transient thermal loads. *Computers and Concrete*, 2 (6): 455-479.

A Appendices

A.1 Calculation tie-rod temperature

A temperature was applied to the tie-rod elements in the LFEA and NLFEA to cause a pre-stress equal to the pre-stress applied in the experiment by Vecchio and Sato (1990). Dead loads and water pressures were already applied to the model at the time of pre-stressing. These loads caused slackening of the tie-rod elements in the model, since the tie-rods were given a tension-only condition. This slackening is illustrated in Figure 35.

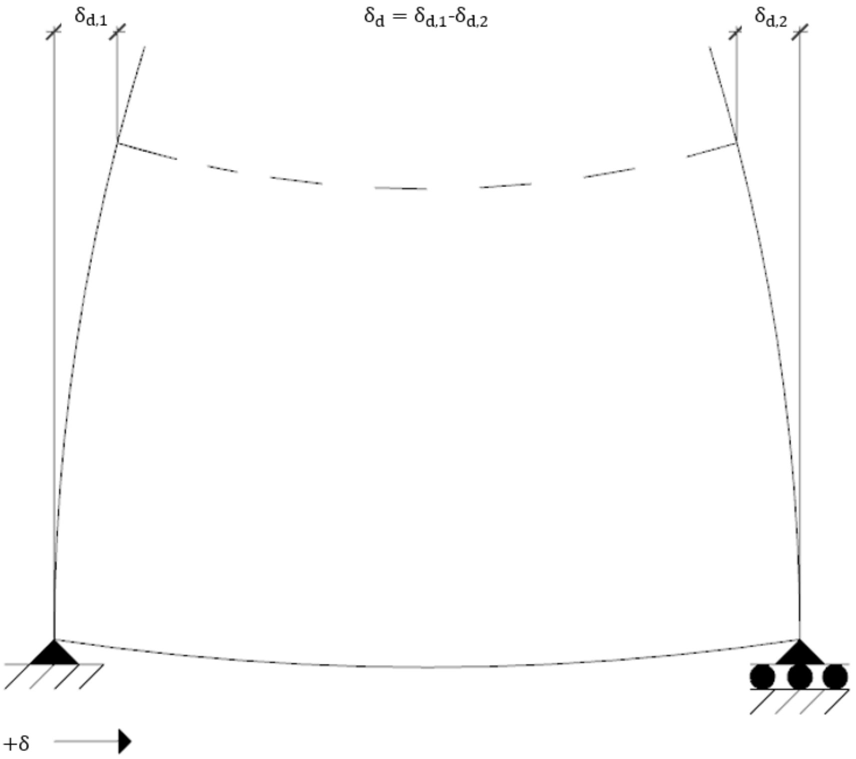

Figure 35: Slackening of tie-rods in FEA from self-weight and water pressure.

The slack of the tie-rods was removed by thermal contraction of the tie-rods. Thermal contraction was implemented by a reduction of the temperature in the tie-rod elements relative to the reference temperature in the model. This reduction was calculated based on Eq. (A.1).

$$\delta = \alpha_{tr} \cdot \Delta T \cdot l_{tr} \qquad \text{(A.1)}$$

Factors used in Eq. (A.1) are:

δ	Deformation caused by thermal contraction (mm).
α_{tr}	Coefficient of thermal expansion for tie-rod (1/°C).
ΔT	Temperature reduction (°C).
l_{tr}	Length of tie-rod (mm).

The coefficient of thermal expansion used for tie-rods was set to 12 με/K and the length of the tie-rods was 3m.

The temperature reduction was calculated based on the deformations of the tie-rod ends in the LFEA or NLFEA due to dead loads and water pressures. The sum of these deformations was set equal to the deformation in tie-rods from thermal contraction. This sum is given as δ_d in Figure 35. The equation used for calculation of the temperature reduction is given in Eq. (A.2).

$$\Delta T_s = \frac{\delta_d}{\alpha_{tr} \cdot l_{tr}} \tag{A.2}$$

New factors used in Eq. (A.2) are:

ΔT_s	Temperature decrease needed to remove slack of tie-rods (°C).
δ_d	Slackening of tie-rods due to dead load and water pressure (mm).

Tightened tie-rods were a prerequisite for the calculation of temperature reduction needed to cause a given amount of pre-stress. The pre-stress caused by thermal contraction in the tie-rods was a result of the restraint of the tie-rod deformation from the structure itself. Since the thermal contraction resulted in a deformation in both the tie-rods and the structure, the tie-rods were not fully restraint. This behavior was taken into account by calculation of a restraint factor.

A fully restrained tie-rod was compared to a partial restrained tie-rod to calculate the actual restraint of the tie-rods. A fully restrained tie-rod is illustrated in Figure 36. The ends of the tie-rod are fully restrained for deformation in this system. Because of this, the restraint forces would cause a deformation equal to and in the reversed direction of the imposed deformation. The restraint force in a fully restrained tie-rod with imposed deformations can be calculated based on Eq. (A.3).

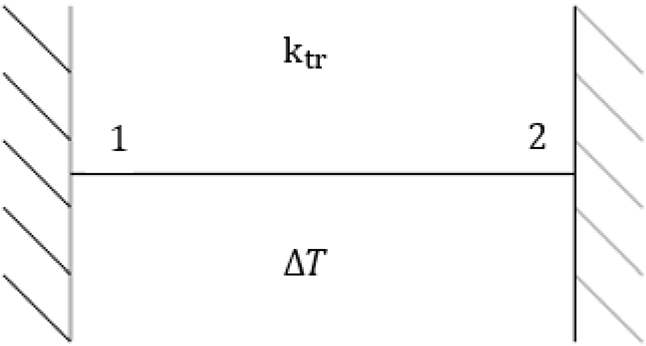

Figure 36: Fully restrained tie-rod

$$F_R = k_{tr} \cdot \delta_i \tag{A.3}$$

Factors used in Eq. (A.3) are:

F_R	Internal restraint force in tie-rod (N).
k_{tr}	Axial stiffness of tie-rod (N/mm).

δ_i	Axial deformation in tie-rod due to imposed deformation where positive values are assigned to contraction (mm).

Eq. (A.3) could have been used to calculate a temperature reduction for a given pre-stress if the structure was fully restraint, but the frame structures examined in this work were partial restrained. This behavior and a simplified system for the behavior are illustrated in Figure 37.

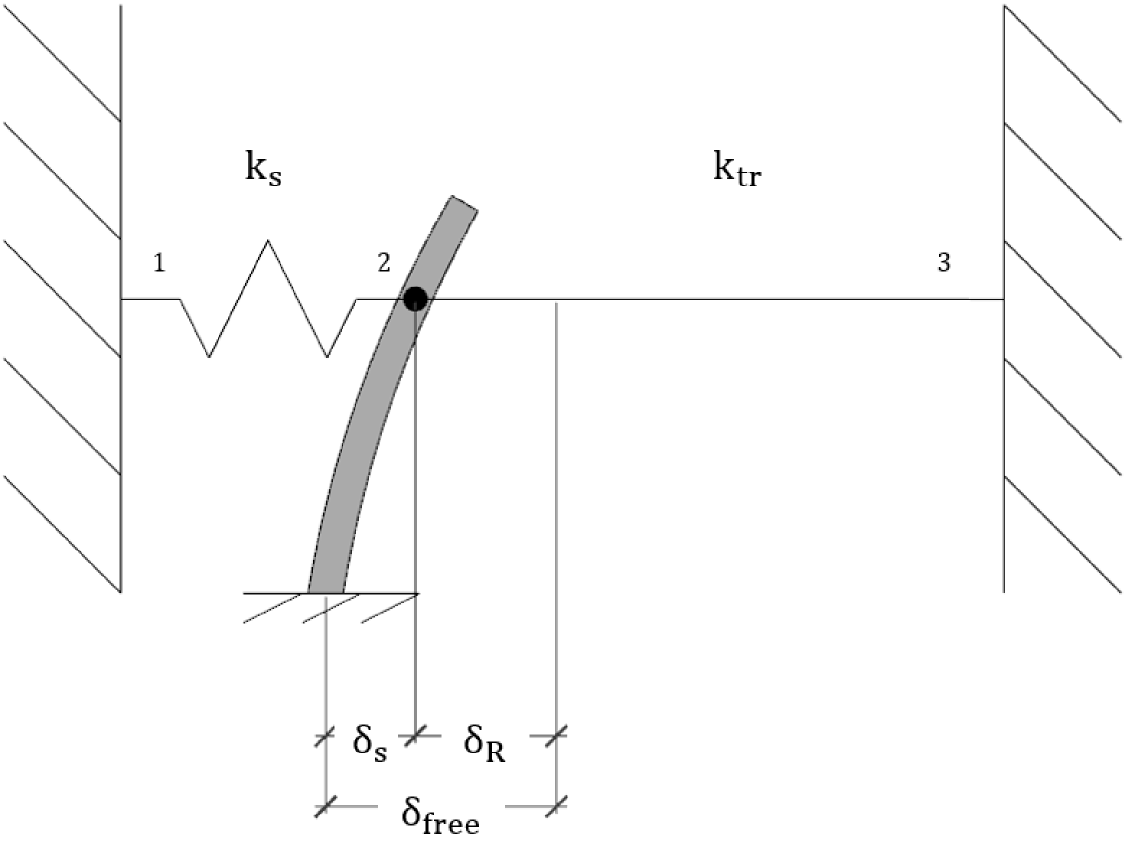

Figure 37: Partial restrained system of two elements for tie-rods.

The partial restrained behavior for the tie-rod was simplified to a fully restrained system of a spring and a rod. The spring represented the stiffness in the structure and the rod represented the stiffness in the tie-rod. The spring was used to adjust the stiffness in the structure due to a certain level of pre-stress.

The stiffness of the spring was determined in the model by application of a dummy load equal to half the level of pre-stress in each end of the two tie-rods. Half the pre-stress was used to get the stiffness of the structure for one tie-rod. The deformation in the structure due to the dummy load was registered and used to calculate the actual stiffness of the structure for the given pre-stress. This stiffness was calculated based on Eq. (A.4).

$$k_s = \frac{F_{pre}}{2 \cdot \delta_{dummy}} \tag{A.4}$$

The factors used in Eq. (A.4) are:

k_s	Stiffness of structure due to actual pre-stress (N/mm).
F_{pre}	Actual pre-stress (N).
δ_{dummy}	Sum of deformations in the ends of one tie-rod due to dummy load (mm).

The stiffness of the tie-rod was calculated based on the axial stiffness of a rod given in Eq. (A.5).

$$k_{tr} = \frac{E_{tr} \cdot A_{tr}}{l_{tr}} \tag{A.5}$$

New factors used in Eq. (A.5) are:

E_{tr}	Elastic modulus of tie-rod (GPa).
A_{tr}	Area of tie-rod cross section (mm^2).

The elastic modulus of the tie-rod was set equal to 200 GPa and the area of the cross section was set equal to 419 mm^2.

The simplified system for the partial restrained tie-rod can be represented by a set of equations based on the stiffnesses k_s and k_{tr}. These equations are given in Eq. (A.6).

$$\begin{bmatrix} k_s & -k_s & 0 \\ -k_s & k_s+k_{tr} & -k_{tr} \\ 0 & -k_{tr} & k_{tr} \end{bmatrix} \begin{Bmatrix} x_1 \\ x_2 \\ x_3 \end{Bmatrix} = \begin{Bmatrix} F_1 \\ F_2 \\ F_3 \end{Bmatrix} \tag{A.6}$$

New factors used in Eq. (A.6) are:

x_i	Deformation in node *i* (mm).
F_i	Force in node *i* (N).

A force equal to the full restraint force was applied in node 2 in the positive direction due to thermal contraction of the tie-rod. This force is implemented in the system equations in Eq. (A.7) (Cook et al. 2002).

$$\begin{bmatrix} k_s & -k_s & 0 \\ -k_s & k_s+k_{tr} & -k_{tr} \\ 0 & -k_{tr} & k_{tr} \end{bmatrix} \begin{Bmatrix} x_1 \\ x_2 \\ x_3 \end{Bmatrix} = \begin{Bmatrix} H \\ F_R \\ H - F_R \end{Bmatrix} \tag{A.7}$$

New factors used in Eq. (A.7) are:

H	Unknown reaction force (N).

The deformation in node 2 can be derived from Eq. (A.7) based on the fixed boundary conditions for node 1 and 3. The deformation is given in Eq. (A.8).

$$x_2 = \frac{F_R}{k_s+k_{tr}} \tag{A.8}$$

The deformation vector for the system is then known since the deformations in node 1 and 3 are zero due to the fixed supports. These known deformations were further used to calculate the reaction force in node 3. This reaction force equaled the internal forces in the tie-rod from the thermal contraction. The reaction force is given by Eq. (A.9).

$$R_3 = -\frac{k_{tr} \cdot F_R}{k_s + k_{tr}} \tag{A.9}$$

New factors used in Eq. (A.9) are:

R_3	Reaction force in node 3 (N).

The reaction force in node 3 was used to calculate the actual contraction of the tie-rod due to the applied force F_R. The difference between the free contraction of the tie-rod due to the force F_R and the actual contraction equaled the restrained contraction of the tie-rods. This calculation is given in Eq. (A.10).

$$\delta_R = \delta_{free} - \delta_s = \frac{F_R}{k_{tr}} - \frac{-R_3}{k_{tr}} = \frac{F_R}{k_{tr}} - \frac{F_R}{k_{tr} + k_s} \tag{A.10}$$

New factors used in Eq. (A.10) are:

δ_R	Restrained contraction of tie-rod (mm).
δ_{free}	Free contraction of tie-rod due to F_R in unrestraint system (mm).
δ_s	Free contraction of tie-rod in partial restrained system (mm).

The restraint factor was derived from Eq. (A.10). The restraint deformation was set equal to a restraint factor times the free deformation in the partial restrained system for this derivation. The derived restraint factor is given in Eq. (A.11).

$$R = \frac{k_s}{k_{tr} + k_s} \tag{A.11}$$

New factors used in Eq. (A.11) are:

R	Restraint factor.

The restraint factor was further used to calculate the restrained part of an imposed deformation from thermal contraction of the tie-rods. This restrained deformation was the only deformation causing internal forces in the tie-rod. The calculation of restrained deformation was performed by combination of Eq. (A.11) and Eq. (A.1). Eq. (A.1) represents the free deformation from a temperature reduction. The calculation of restrained deformation in the tie rod is given in Eq. (A.12).

$$\delta_{R,tc} = R \cdot \alpha_{tr} \cdot \Delta T \cdot l_{tr} \tag{A.12}$$

New factors used in Eq. (A.12) are:

$\delta_{R,tc}$	Restrained deformation from thermal contraction of tie-rod (mm).

The restrained deformation was used to derive the internal force in the tie-rod elements based on Hooke's law. This force was set equal to half the pre-stress given from the experiment since the force was divided into two tie-rods.

$$\frac{F_{pre}}{2} = k_{tr} \cdot R \cdot \alpha_{tr} \cdot \Delta T \cdot l_{tr} \tag{A.13}$$

The temperature reduction needed to cause the actual level of pre-stress was derived from Eq. (A.13) by insertion for the stiffness of the tie-rod. The calculation of this temperature reduction is given in Eq. (A.14).

$$\Delta T_{pre} = \frac{F_{pre}}{2 \cdot R \cdot E_{tr} \cdot A_{tr} \cdot \alpha_{tr} \cdot l_{tr}} \tag{A.14}$$

The application of pre-stress in the model was achieved by a reduction of the temperature in the tie-rods relative to a reference temperature in the system. The total reduction of temperature equaled the sum of Eq. (A.2) and Eq. (A.14). The temperature applied to the tie-rods was calculated based on Eq. (A.15).

$$T_{app} = T_{ref} - \left(\Delta T_s + \Delta T_{pre}\right) \tag{A.15}$$

New factors used in Eq. (A.15) are:

T_{app}	Temperature applied in tie-rods to cause pre-stress (°C).
T_{ref}	Reference temperature in model (°C).

A.2 Stress calculation for concrete in the layer-by-layer approach

The compressive stress in a concrete layer was calculated based on the nonlinear relation between strain and compressive stresses given in Eurocode 2 3.1.5. Based on this relation, a compressive stress for the layer was calculated with the function η and the parameter k. The equations for η and k are given in Eq. (A.16) and Eq. (A.17) respectively (CEN 2004).

$$\eta(\varepsilon) = \frac{\varepsilon}{\varepsilon_{c1}} \tag{A.16}$$

Factors given in Eq. (A.16) are:

$\eta(\varepsilon)$	Ratio between actual concrete strain and concrete strain corresponding to ultimate concrete stress.
ε	Actual strain in layer.
ε_{c1}	Concrete strain corresponding to ultimate concrete stress.

The strain value corresponding to the ultimate concrete stress was set equal to 2.16 ‰ for the concrete in structure PF3. This value was calculated based on the formulas given in Eurocode 2 Table 3.1 and the cylinder compression strength equal to 30.1 MPa given in the article by Vecchio and Sato (CEN 2004; Vecchio & Sato 1990).

$$k = 1.05 \cdot E_{cm} \cdot |\varepsilon_{c1}| / f_{cm} \tag{A.17}$$

New factors given in Eq. (A.17) are:

k	Parameter used in the calculation of nonlinear compression stresses.
E_{cm}	Elastic modulus of concrete (GPa).
f_{cm}	Mean compression strength of concrete (MPa).

The value of the elastic modulus was set equal to 30 GPa, which was the measured value for structure PF3 in the experiment. The value of the mean compression strength was carried out based on the formula in Eurocode 2 Table 3.1 and the cylinder compression strength measured in the experiment. This value was calculated to 38.1 MPa (Vecchio & Sato 1990).

The function η and parameter k were further used in the calculation of the compression stress corresponding to the strain value ε. The calculation of this stress is given in Eq. (A.18) (CEN 2004).

$$\sigma_c = -\frac{k \cdot \eta - \eta^2}{1 + (k - 2) \cdot \eta} \cdot f_{cm} \tag{A.18}$$

Factors given in Eq. (A.18) are:

σ_c	Concrete compression stress corresponding to the strain value ε.
k	Parameter calculated based on Eq. (A.17).
η	Function given in Eq. (A.16).
f_{cm}	Mean compression strength of concrete (MPa).

Compressive stresses were calculated in all layers with negative strain values. For layers with positive strain values, the stress was set equal to 0.

A.3 Example: Input file for frame in finite element analysis

```
! ==============================================================
! PARMETERS FOR FRAME PF1 REPORTED BY VECCHIO AND SATO (1990)
! AUTHOR: ODDGEIR OMMELSTAD
! REV.: 02.12.2017
! ==============================================================

! CONCRETE PARAMETERS
E_c = 28980
alpha_c = 0.00000986
f_c = 42.4

! REINFORCEMENT PARAMETERS
E_r = 217000
alpha_r = 0.0000124
f_y = 448

! REINFORCMENT PLACEMENT
dist_L = 55
dist_S = 40

! REINFORCEMENT AMOUNT AND SPACING
ASL_C1 = 300
SL_C1 = 200

ASL_C2 = 300
SL_C2 = 200

ASL_B = 300
SL_B = 200
```

A.4 Example: Input file for load case in finite element analysis

```
! ==============================================================
! LOAD CASE PF1-D REPORTED BY VECCHIO AND SATO (1990)
! AUTHOR: ODDGEIR OMMELSTAD
! REV.: 02.12.2017
! ==============================================================

! TEMPERATURE RESULT FILE
temp_file = 'C:\00_Bench\01_PF1\TEMP\FEM'

! INITIAL TEMPERATURE
init_temp = 16.45

! SURFACE TEMPERATURES
temp_inside = 25
temp_outside = 15.7

! PRE-STRESS
F_tr = 3170
```

A.5 Example: Script for thermal finite element analysis

```
! ==============================================================
! INPUT FILE FOR: THERMAL FINITE ELEMENT ANALYSIS
! AUTHOR: ODDGEIR OMMELSTAD
! REV.: 02.12.2017
! ==============================================================

FINISH
/CLEAR
/FILENAME,FEM
/PREP7
SELTOL,0.0001

! ==============================================================
! DEFINE SCENARIO VARIABLES
! ==============================================================

/INP,MODEL,INP
/INP,STADIUM,INP

! ==============================================================
! DEFINE GEOMETRY
! ==============================================================

! BEAM

BEAMHEIGHT = 300
LENGTH = 3000
WIDTH = 800

! COLUMN

COLHEIGHT = 2500
THICKNESS = 300

! WATER

WATERLEVEL = 1800

! TIE - ROD

T_ROD_LEVEL = 2200

! ==============================================================
! SET MESH SIZE
! ==============================================================

NDIVL = 48
NDIVCOL_BOT = 30
NDIVCOL_TOP_1 = 8
NDIVCOL_TOP_2 = 6
NDIVTHICK = 6
NDIVWIDTH = 4

! ==============================================================
! SET CONCRETE PROPERTIES
! ==============================================================

lambda_c = 0.00186

! ==============================================================
! DEFINE MATERIALS
! ==============================================================

MP,KXX,1,lambda_c
```

```
! ===================================================================
! DEFINE REAL CONSTANTS
! ===================================================================

R,1

! ===================================================================
! DEFINE ELEMENTTYPES
! ===================================================================

ET,1,SOLID70

! ===================================================================
! GENERATE KEYPOINTS
! ===================================================================

XMAX = 4
*DIM,X,ARRAY,XMAX
X(01) = 0
X(02) = X(01) + THICKNESS
X(03) = X(02) + LENGTH - 2*THICKNESS
X(04) = X(03) + THICKNESS

YMAX = 2
*DIM,Y,ARRAY,YMAX
Y(01) = 0
Y(02) = WIDTH

ZMAX = 5
*DIM,Z,ARRAY,ZMAX
Z(01) = 0
Z(02) = BEAMHEIGHT
Z(03) = WATERLEVEL
Z(04) = T_ROD_LEVEL
Z(05) = COLHEIGHT

*DO,ZZZ,1,zmax
 *DO,YYY,1,ymax
 *DO,XXX,1,xmax
  K,10000*ZZZ+100*YYY+XXX,x(XXX),y(YYY),z(ZZZ)
 *ENDDO
 *ENDDO
*ENDDO

! ===================================================================
! GENERATE VOLUMS
! ===================================================================

V_TOP,10101,1,1,100,1,10000,4
V_TOP,10102,1,1,100,1,10000,1
V_TOP,10103,1,1,100,1,10000,4

! ===================================================================
! GENERATE MESH GRID
! ===================================================================

LD_TOP,NDIVWIDTH,,10101,100,1,1,4,10000,4
LD_TOP,NDIVTHICK,,10101,1,1,100,2,10000,5
LD_TOP,NDIVTHICK,,10103,1,1,100,2,10000,5
LD_TOP,NDIVTHICK,,10101,10000,1,100,2,1,4
LD_TOP,NDIVL,,10102,1,1,100,2,10000,2
LD_TOP,NDIVCOL_BOT,,20101,10000,1,100,2,1,4
LD_TOP,NDIVCOL_TOP_1,,30101,10000,1,100,2,1,4
LD_TOP,NDIVCOL_TOP_2,,40101,10000,1,100,2,1,4
```

```
! ===============================================================
! ASSIGN CONCRETE PROPERTIES TO VOLUMES
! ===============================================================

VSEL,ALL
VATT,1,1,1
ALLSEL

! ===============================================================
! GENERATE MESH
! ===============================================================

VSEL,ALL
ESIZE,,1
VMESH,ALL

! ===============================================================
! BOUNDARY CONDITIONS
! ===============================================================

ALLSEL
NSEL,S,LOC,Z,Z(01),Z(05)
NSEL,U,LOC,X,X(01)+0.001,X(04)-0.001
NSEL,A,LOC,Z,Z(01)
D,ALL,TEMP,temp_outside

ALLSEL
NSEL,S,LOC,Z,Z(02),Z(05)
NSEL,R,LOC,X,X(02),X(03)
D,ALL,TEMP,temp_inside

! ===============================================================
! SOLUTION
! ===============================================================

ALLSEL
/SOLU
ALLSEL
ERESX,NO
SOLVE
FINI
ALLSEL
SAVE,,,ALL
/EOF
```

A.6 Example: Script for nonlinear finite element analysis

```
! ============================================================
! INPUT FILE FOR: NONLINEAR FINITE ELEMENT ANALYSIS
! AUTHOR: ODDGEIR OMMELSTAD
! REV.: 02.12.2017
! ============================================================

FINISH
/CLEAR
/FILENAME,FEM
/PREP7
SELTOL,0.0001

! ============================================================
! DEFINE VARIABLES
! ============================================================

/INP,MODEL,INP
/INP,STADIUM,INP
NUMSUBST = 30

! ============================================================
! DEFINE GEOMETRY
! ============================================================

! BEAM
BEAMHEIGHT = 300
LENGTH = 3000
WIDTH = 800

! COLUMN
COLHEIGHT = 2500
THICKNESS = 300

! WATER
WATERLEVEL = 1800

! TIE – ROD
T_ROD_LEVEL = 2200

! ============================================================
! SET MESH SIZE
! ============================================================

NDIVL = 48
NDIVCOL_BOT = 30
NDIVCOL_TOP_1 = 8
NDIVCOL_TOP_2 = 6
NDIVTHICK = 6
NDIVWIDTH = 4

! ============================================================
! SET CONCRETE PROPERTIES
! ============================================================

v_c = 0.2
rho_c = 0.000002400

! ============================================================
! SET REINFORCEMENT PROPERTIES
! ============================================================

v_r = 0.3
rho_r = 0.000007775
```

```
! ==============================================================
! SET TIE ROD PROPERTIES
! ==============================================================

E_tr = 200000
A_tr = 419
alpha_tr = 0.000012

! ==============================================================
! SET OTHER PROPETIES
! ==============================================================

gravity = 9.81
rho_w = 0.000001000
WATERSLOPE = gravity*rho_w

! ==============================================================
! SET REIFORCEMENT AMOUNT AND PLACEMENT
! ==============================================================

counter_=0
counter_S=0

*IF,dist_L,GT,THICKNESS/NDIVTHICK,THEN
	counter_=1
*ENDIF

*IF,dist_S,GT,THICKNESS/NDIVTHICK,THEN
	counter_S=1
*ENDIF

rat_L = (dist_L-counter_*(THICKNESS/NDIVTHICK)) / (THICKNESS/NDIVTHICK)
rat_S_s = dist_S / (WIDTH/NDIVWIDTH)
rat_S_tb = (dist_S-counter_S*(THICKNESS/NDIVTHICK)) / (THICKNESS/NDIVTHICK)

! AREA AND SPACING FOR SHEAR REINFORCEMENT
ASS = 100
SS = 150

! ==============================================================
! DEFINE CONCRETE MATERIAL
! ==============================================================

MP,DENS,1,rho_c
MP,ALPX,1,alpha_c
TB,USER,1,1,2
TBTEMP,1.0
TBDATA,1,f_c,3
TB,STATE,1,,50

! ==============================================================
! DEFINE REINFORCEMENT MATERIAL
! ==============================================================

MP, DENS,3,rho_r
MP,ALPX,3,alpha_r
MP, EX, 3,E_r
MP, NUXY, 3,v_r
TB,BISO,3,1
TBTEMP,0
TBDATA,1,f_y,2000

! ==============================================================
! DEFINE TIE-ROD MATERIAL
! ==============================================================

MP,EX,50,E_tr
```

```
MP,ALPX,50,alpha_tr

! ==============================================================
! OTHER MATERIALS
! ==============================================================

MP,DENS,99,0
MP,DENS,100,0

! ==============================================================
! REFERENCE TEMPERATURE
! ==============================================================

TREF,init_temp

! ==============================================================
! DEFINE REAL CONSTANTS
! ==============================================================

R,1
R,99
R,100

! ==============================================================
! DEFINE CONCRETE ELEMENTTYPE
! ==============================================================

ET,1,SOLID185
KEYOPT,1,2,3

! ==============================================================
! DEFINE REINFORCEMENT ELEMENTTYPE
! ==============================================================

ET,3,REINF265

! ==============================================================
! DEFINE TIE-ROD ELEMENTTYPE
! ==============================================================

ET,5,LINK180

! ==============================================================
! OTHER ELEMENTTYPES
! ==============================================================

ET,99,SURF154
KEYOPT,99,2,0

ET,100,MASS21
KEYOPT,100,3,0

! ==============================================================
! DEFINE GEOMETRY
! ==============================================================

XMAX = 4
*DIM,X,ARRAY,XMAX
X(01) = 0
X(02) = X(01) + THICKNESS
X(03) = X(02) + LENGTH - 2*THICKNESS
X(04) = X(03) + THICKNESS

YMAX = 2
*DIM,Y,ARRAY,YMAX
Y(01) = 0
Y(02) = WIDTH
```

```
ZMAX = 5
*DIM,Z,ARRAY,ZMAX
Z(01) = 0
Z(02) = BEAMHEIGHT
Z(03) = WATERLEVEL
Z(04) = T_ROD_LEVEL
Z(05) = COLHEIGHT

*DO,ZZZ,1,zmax
 *DO,YYY,1,ymax
 *DO,XXX,1,xmax
  K,10000*ZZZ+100*YYY+XXX,x(XXX),y(YYY),z(ZZZ)
 *ENDDO
 *ENDDO
*ENDDO

! ==============================================================
! GENERATE VOLUMS
! ==============================================================

V_TOP,10101,1,1,100,1,10000,4
V_TOP,10102,1,1,100,1,10000,1
V_TOP,10103,1,1,100,1,10000,4

! ==============================================================
! GENERATE MESH GRID
! ==============================================================

LD_TOP,NDIVWIDTH,,10101,100,1,1,4,10000,4
LD_TOP,NDIVTHICK,,10101,1,1,100,2,10000,5
LD_TOP,NDIVTHICK,,10103,1,1,100,2,10000,5
LD_TOP,NDIVTHICK,,10101,10000,1,100,2,1,4
LD_TOP,NDIVL,,10102,1,1,100,2,10000,2
LD_TOP,NDIVCOL_BOT,,20101,10000,1,100,2,1,4
LD_TOP,NDIVCOL_TOP_1,,30101,10000,1,100,2,1,4
LD_TOP,NDIVCOL_TOP_2,,40101,10000,1,100,2,1,4

! ==============================================================
! GENERATE END NODES FOR TIE-RODS
! ==============================================================

! Right side
K,10,X(01)-0.1,200,T_ROD_LEVEL
K,11,X(01)-0.1,600,T_ROD_LEVEL

! Left side
K,12,X(04)+0.1,200,T_ROD_LEVEL
K,13,X(04)+0.1,600,T_ROD_LEVEL

! ==============================================================
! ASSIGN CONCRETE PROPERTIES TO VOLUMES
! ==============================================================

ALLSEL
VSEL,ALL
VATT,1,1,1
ALLSEL

! ==============================================================
! GENERATE MESH
! ==============================================================

ALLSEL
VSEL,ALL
ESIZE,,1
VMESH,ALL
```

```
! ============================================================
! GENERATE LOAD SURFACES
! ============================================================

ALLSEL
TYPE,99
REAL,99
MAT,99
ESURF

! ============================================================
! GENERATE REINFORCEMENT
! ============================================================

ALLSEL
TYPE,3

! ============================================================
! X – DIRECTION (DIRECTION OF BEAM LENGTH)
! ============================================================

LOCAL,11,0,0,0,0
SECTYPE,21,REINF,SMEAR,XREINF1,0
SECDATA,3,ASL_B,SL_B,11,0,ELEF,1,rat_L
ESEL,S,TYPE,,1
ESEL,R,CENT,Y,Y(01),Y(02)
ESEL,R,CENT,Z,Z(01)+counter_*(THICKNESS/NDIVTHICK),Z(02)-((NDIVTHICK-
1)/NDIVTHICK)*THICKNESS+counter_*(THICKNESS/NDIVTHICK)
SECN,21
MAT,3
EREINF

LOCAL,11,0,0,0,0
SECTYPE,22,REINF,SMEAR,XREINF2,0
SECDATA,3,ASL_B,SL_B,11,0,ELEF,1,1-rat_L
ESEL,S,TYPE,,1
ESEL,R,CENT,Y,Y(01),Y(02)
ESEL,R,CENT,Z,Z(01)+((NDIVTHICK-1)/NDIVTHICK)*THICKNESS-counter_*(THICKNESS/NDIVTHICK),Z(02)-
counter_*(THICKNESS/NDIVTHICK)
SECN,22
MAT,3
EREINF

LOCAL,11,0,0,0,0
SECTYPE,23,REINF,SMEAR,XREINF3,0
SECDATA,3,ASS,SS,11,0,ELEF,3,rat_S_s
ESEL,S,TYPE,,1
ESEL,R,CENT,Y,Y(01),Y(01)+(1/NDIVWIDTH)*WIDTH
ESEL,U,CENT,X,X(02),X(3)
SECN,23
MAT,3
EREINF

LOCAL,11,0,0,0,0
SECTYPE,24,REINF,SMEAR,XREINF4,0
SECDATA,3,ASS,SS,11,0,ELEF,3,1-rat_S_s
ESEL,S,TYPE,,1
ESEL,R,CENT,Y,Y(02)-(1/NDIVWIDTH)*WIDTH,Y(02)
ESEL,U,CENT,X,X(02),X(3)
SECN,24
MAT,3
EREINF
```

```
! ==============================================================
! Z – DIRECTION (DIRECTION OF COLUMN LENGTH)
! ==============================================================
LOCAL,12,0,0,0,0,90,0,-90
SECTYPE,25,REINF,SMEAR,ZREINF1,0
SECDATA,3,ASL_C1,SL_C1,12,0,ELEF,2,rat_L
CSYS,0
ESEL,S,TYPE,,1
ESEL,U,CENT,X,X(01)*counter_,counter_*(THICKNESS/NDIVTHICK)
ESEL,U,CENT,X,X(02)-((NDIVTHICK-1)/NDIVTHICK)*THICKNESS+counter_*(THICKNESS/NDIVTHICK),X(04)
SECN,25
MAT,3
EREINF

LOCAL,12,0,0,0,0,90,0,-90
SECTYPE,26,REINF,SMEAR,ZREINF1,0
SECDATA,3,ASL_C2,SL_C2,12,0,ELEF,2,rat_L
CSYS,0
ESEL,S,TYPE,,1
ESEL,U,CENT,X,X(01),X(03)+counter_*(THICKNESS/NDIVTHICK)
ESEL,U,CENT,X,X(04)-((NDIVTHICK-1)/NDIVTHICK)*THICKNESS+counter_*(THICKNESS/NDIVTHICK),X(04)
SECN,26
MAT,3
EREINF

LOCAL,12,0,0,0,0,90,0,-90
SECTYPE,27,REINF,SMEAR,ZREINF2,0
SECDATA,3,ASL_C1,SL_C1,12,0,ELEF,2,1-rat_L
CSYS,0
ESEL,S,TYPE,,1
ESEL,U,CENT,X,X(01),X(01)+((NDIVTHICK-1)/NDIVTHICK)*THICKNESS-counter_*(THICKNESS/NDIVTHICK)
ESEL,U,CENT,X,X(02)-counter_*(THICKNESS/NDIVTHICK),X(04)
SECN,27
MAT,3
EREINF

LOCAL,12,0,0,0,0,90,0,-90
SECTYPE,28,REINF,SMEAR,ZREINF2,0
SECDATA,3,ASL_C2,SL_C2,12,0,ELEF,2,1-rat_L
CSYS,0
ESEL,S,TYPE,,1
ESEL,U,CENT,X,X(01),X(03)+((NDIVTHICK-1)/NDIVTHICK)*THICKNESS-counter_*(THICKNESS/NDIVTHICK)
ESEL,U,CENT,X,counter_*X(04)-counter_*(THICKNESS/NDIVTHICK),counter_*X(04)
SECN,28
MAT,3
EREINF

LOCAL,12,0,0,0,0,90,0,-90
SECTYPE,29,REINF,SMEAR,ZREINF3,0
SECDATA,3,ASS,SS,12,0,ELEF,3,rat_S_s
CSYS,0
ESEL,S,TYPE,,1
ESEL,R,CENT,Y,Y(01),Y(01)+(1/NDIVWIDTH)*WIDTH
ESEL,U,CENT,Z,Z(02),Z(05)
SECN,29
MAT,3
EREINF

LOCAL,12,0,0,0,0,90,0,-90
SECTYPE,30,REINF,SMEAR,ZREINF4,0
SECDATA,3,ASS,SS,12,0,ELEF,3,1-rat_S_s
CSYS,0
ESEL,S,TYPE,,1
ESEL,R,CENT,Y,Y(02)-(1/NDIVWIDTH)*WIDTH,Y(02)
ESEL,U,CENT,Z,Z(02),Z(05)
SECN,30
MAT,3
```

```
EREINF

! ============================================================
! Y – DIRECTION (WIDTH OF FRAME)
! ============================================================

ALLSEL
LOCAL,13,0,0,0,0, 90,90,0
SECTYPE,31,REINF,SMEAR,YREINF1,0
SECDATA,3,ASS,SS,13,0,ELEF,2,rat_S_tb
CSYS,0
ESEL,S,TYPE,,1
ESEL,U,CENT,X,X(02)-((NDIVTHICK-
1)/NDIVTHICK)*THICKNESS+counter_S*(THICKNESS/NDIVTHICK),X(03)+counter_S*(THICKNESS/NDIVTHICK)
ESEL,U,CENT,X,X(04)-((NDIVTHICK-1)/NDIVTHICK)*THICKNESS+counter_S*(THICKNESS/NDIVTHICK),X(04)
ESEL,U,CENT,X,X(01),X(01)+counter_S*(THICKNESS/NDIVTHICK)
SECN,31
MAT,3
EREINF

LOCAL,13,0,0,0,0, 90,90,0
SECTYPE,32,REINF,SMEAR,YREINF2,0
SECDATA,3,ASS,SS,13,0,ELEF,2,1-rat_S_tb
CSYS,0
ESEL,S,TYPE,,1
ESEL,U,CENT,X,X(01),X(01)+((NDIVTHICK-1)/NDIVTHICK)*THICKNESS-counter_S*(THICKNESS/NDIVTHICK),
ESEL,U,CENT,X,X(02)-counter_S*(THICKNESS/NDIVTHICK),X(03)+((NDIVTHICK-1)/NDIVTHICK)*THICKNESS-
counter_S*(THICKNESS/NDIVTHICK)
ESEL,U,CENT,X,X(04)-counter_S*(THICKNESS/NDIVTHICK),X(04)
SECN,32
MAT,3
EREINF

LOCAL,13,0,0,0,0, 90,90,0
SECTYPE,33,REINF,SMEAR,YREINF3,0
SECDATA,3,ASS,SS,13,0,ELEF,1,rat_S_tb
CSYS,0
ESEL,S,TYPE,,1
ESEL,R,CENT,Y,Y(01),Y(02)
ESEL,R,CENT,Z,Z(01)+counter_S*(THICKNESS/NDIVTHICK),Z(02)-((NDIVTHICK-
1)/NDIVTHICK)*THICKNESS+counter_S*(THICKNESS/NDIVTHICK)
SECN,33
MAT,3
EREINF

LOCAL,13,0,0,0,0, 90,90,0
SECTYPE,34,REINF,SMEAR,YREINF4,0
SECDATA,3,ASS,SS,13,0,ELEF,1,1-rat_S_tb
CSYS,0
ESEL,S,TYPE,,1
ESEL,R,CENT,Z,Z(01)+((NDIVTHICK-1)/NDIVTHICK)*THICKNESS-counter_S*(THICKNESS/NDIVTHICK),Z(02)-
counter_S*(THICKNESS/NDIVTHICK)
SECN,34
MAT,3
EREINF
CSYS,0

! ============================================================
! GENERATE TIE RODS
! ============================================================

ALLSEL
L,10,12
L,11,13
ALLSEL
SECTYPE,50,LINK,,TIEROD
SECDATA,A_tr
```

```
SECCONTROL,0,1
LSEL,S,LENGTH,,X(04)-X(01) + 0.2
LATT,50,,5,,,,50
LMESH,ALL

*DO,KEP,10,13
        ALLSEL
        KSEL,S,KP,,KEP
        NSLK
        *GET,node_num,NODE,0,NUM,MAX
        TYPE,100
        MAT,100
        REAL,100
        E,node_num
*ENDDO

! ==============================================================
! GENERATE multi-point constraint FOR TIE-ROD CONNECTION
! ==============================================================

! Right side
ALLSEL
KSEL,S,KP,,10
NSLK
*GET,node_num_1,NODE,0,NUM,MAX
ALLSEL
NSEL,S,LOC,X,X(01)
NSEL,R,LOC,Z,Z(04)-150,Z(04)+150
NSEL,R,LOC,Y,0,400
NSEL,A,NODE,,node_num_1
CERIG,node_num_1,ALL,UX

ALLSEL
KSEL,S,KP,,11
NSLK
*GET,node_num_2,NODE,0,NUM,MAX
ALLSEL
NSEL,S,LOC,X,X(01)
NSEL,R,LOC,Z,Z(04)-150,Z(04)+150
NSEL,R,LOC,Y,400,800
NSEL,A,NODE,,node_num_2
CERIG,node_num_2,ALL,UX

! Left side
ALLSEL
KSEL,S,KP,,12
NSLK
*GET,node_num_3,NODE,0,NUM,MAX
ALLSEL
NSEL,S,LOC,X,X(04)
NSEL,R,LOC,Z,Z(04)-150,Z(04)+150
NSEL,R,LOC,Y,0,400
NSEL,A,NODE,,node_num_3
CERIG,node_num_3,ALL,UX

ALLSEL
KSEL,S,KP,,13
NSLK
*GET,node_num_4,NODE,0,NUM,MAX
ALLSEL
NSEL,S,LOC,X,X(04)
NSEL,R,LOC,Z,Z(04)-150,Z(04)+150
NSEL,R,LOC,Y,400,800
NSEL,A,NODE,,node_num_4
CERIG,node_num_4,ALL,UX
```

```
! ==========================================================
! APPLY BOUNDARY CONDITIONS
! ==========================================================

! PINNED SUPPORT
NSEL,S,LOC,X,THICKNESS/2
NSEL,R,LOC,Z,Z(01)
D,ALL,UX,,,,,UZ
NSEL,R,LOC,Y,Y(01)
D,ALL,UY

! ROLLER SUPPORT
NSEL,S,LOC,X,LENGTH-(THICKNESS/2)
NSEL,R,LOC,Z,Z(01)
D,ALL,UZ
NSEL,R,LOC,Y,Y(01)
D,ALL,UY

! ==========================================================
! CALCULATION OF TIE-ROD RESTRAINT
! ==========================================================

/SOLU

! ==========================================================
! LOAD CASE 1: SELF-WEIGHT AND WATER PRESSURE
! ==========================================================

! ==========================================================
! WATERPRESSURE
! ==========================================================

ALLSEL
SFGRAD
SFGRAD,PRES,0,Z,WATERLEVEL,-WATERSLOPE
ESEL,S,TYPE,,99
ESEL,R,CENT,Z,Z(02),Z(03)
ESEL,R,CENT,X,X(02),X(03)
SFE,ALL,1,PRES,0,0
SFGRAD

! ==========================================================
! SELF-WEIGHT
! ==========================================================

ALLSEL
ACEL,,,gravity

! ==========================================================
! SOLUTION 1: BASED ON ITERATIVE PROCESS ACCORDING TO ENGEN (2017)
! ==========================================================

ALLSEL
/INP,USERMAT_SETTINGS,ANS,,:SOLPAR
TIME,1
SOLVE

! ==========================================================
! LOAD CASE 2: DUMMY LOAD
! ==========================================================

ALLSEL
KSEL,S,KP,,10,11
NSLK
F,ALL,FX,F_tr/2
```

```
ALLSEL
KSEL,S,KP,,12,13
NSLK
F,ALL,FX,-F_tr/2

! ============================================================
! SOLUTION 2: BASED ON ITERATIVE PROCESS ACCORDING TO ENGEN (2017)
! ============================================================

ALLSEL
/INP,USERMAT_SETTINGS,ANS,,:SOLPAR
TIME,2
SOLVE

FINISH

! ============================================================
! TIE-ROD RESTRAINT CALCULATION
! ============================================================

! ============================================================
! READING DEFORMATION FROM LOAD CASE 1
! ============================================================

/POST1
SET,1,30
ALLSEL
KSEL,S,KP,,10
NSLK
*GET,node_num,NODE,0,NUM,MAX
*GET,DELTA_DEAD_LEFT,NODE,node_num,U,X
ALLSEL
KSEL,S,KP,,12
NSLK
*GET,node_num,NODE,0,NUM,MAX
*GET,DELTA_DEAD_RIGHT,NODE,node_num,U,X
DELTA_DEAD = DELTA_DEAD_LEFT - DELTA_DEAD_RIGHT

! ============================================================
! READING DEFORMATION FROM LOAD CASE 1 + 2
! ============================================================

SET,2,30
ALLSEL
KSEL,S,KP,,10
NSLK
*GET,node_num,NODE,0,NUM,MAX
*GET,DELTA_TOT_LEFT,NODE,node_num,U,X
ALLSEL
KSEL,S,KP,,12
NSLK
*GET,node_num,NODE,0,NUM,MAX
*GET,DELTA_TOT_RIGHT,NODE,node_num,U,X
DELTA_TOT = DELTA_TOT_LEFT - DELTA_TOT_RIGHT

! ============================================================
! CALCULATION OF RESTRAINT AND TEMP. FOR SLACKENING
! ============================================================

DELTA_DUMMY = DELTA_TOT - DELTA_DEAD
K_NLFEA = F_tr/(2*DELTA_DUMMY)
K_TIEROD = E_tr*A_tr/(LENGTH+0.2)
R_NLFEA = K_NLFEA / (K_NLFEA + K_TIEROD)
T_DEAD = DELTA_DEAD/(alpha_tr*(LENGTH+0.2))

*CFOPEN,'RESTRAINT',INP
*VWRITE,'R_NLFEA',R_NLFEA
```

```
(A7,'=',F12.10)
*VWRITE,'T_DEAD',T_DEAD
(A6,'=',F12.8)
*CFCLOS

! ===============================================================
! READING INITIAL DEFLECTION OF BEAM
! ===============================================================

ALLSEL
NSEL,S,LOC,X,LENGTH/2
NSEL,R,LOC,Z,BEAMHEIGHT/2
NSEL,R,LOC,Y,WIDTH/2
*GET,node_num,NODE,0,NUM,MAX
*GET,DELTA_B_TOT,NODE,node_num,U,Z
DELTA_B_INI = - DELTA_B_TOT

! ===============================================================
! READING INITIAL EXPANSION IN BEAM
! ===============================================================

ALLSEL
NSEL,S,LOC,X,X(01)
NSEL,R,LOC,Z,BEAMHEIGHT/2
NSEL,R,LOC,Y,WIDTH/2
*GET,node_num,NODE,0,NUM,MIN
*GET,DELTA_A_LEFT_TOT,NODE,node_num,U,X
ALLSEL
NSEL,S,LOC,X,X(04)
NSEL,R,LOC,Z,BEAMHEIGHT/2
NSEL,R,LOC,Y,WIDTH/2
*GET,node_num,NODE,0,NUM,MIN
*GET,DELTA_A_RIGHT_TOT,NODE,node_num,U,X
DELTA_A_INI = DELTA_A_RIGHT_TOT - DELTA_A_LEFT_TOT

! ===============================================================
! IMPLEMENTING RESTRAINT AND CALCULATE TEMP. FOR PRE-STRESS
! ===============================================================

/PREP7
/INP,RESTRAINT,INP
del_temp = -F_tr/(E_tr*alpha_tr*2*A_tr)/R_NLFEA + init_temp - T_DEAD

! ===============================================================
! SOLUTION OF EXPERIMENTAL LOAD CASE
! ===============================================================

/SOLU

! ===============================================================
! DELETE DUMMY LOADS
! ===============================================================

ALLSEL
KSEL,S,KP,,10,11
NSLK
F,ALL,FX,0

ALLSEL
KSEL,S,KP,,12,13
NSLK
F,ALL,FX,0
```

```
! ============================================================
! LOAD CASE 3: PRE-STRESSED TIE-ROD
! ============================================================

TREF,init_temp
ESEL,S,TYPE,,5
NSLE
BFE,ALL,TEMP,1,del_temp

ALLSEL
/INP,USERMAT_SETTINGS,ANS,,:SOLPAR
TIME,1
SOLVE

! ============================================================
! LOAD CASE 4: THERMAL EXPANSION
! ============================================================

ALLSEL
LDREAD,TEMP,,,,,temp_file,RTH

ALLSEL
/INP,USERMAT_SETTINGS,ANS,,:SOLPAR
TIME,2
SOLVE


! ============================================================
! WRITING RESULTS TO FILE
! ============================================================


/POST1
SET,LAST

ALLSEL
KSEL,S,KP,,10
NSLK
*GET,node_num,NODE,0,NUM,MAX
*GET,DELTA_C_LEFT,NODE,node_num,U,X

ALLSEL
KSEL,S,KP,,12
NSLK
*GET,node_num,NODE,0,NUM,MAX
*GET,DELTA_C_RIGHT,NODE,node_num,U,X

DELTA_C = DELTA_C_RIGHT - DELTA_C_LEFT

ALLSEL
NSEL,S,LOC,X,X(01)
NSEL,R,LOC,Z,BEAMHEIGHT/2
NSEL,R,LOC,Y,WIDTH/2
*GET,node_num,NODE,0,NUM,MIN
*GET,DELTA_A_LEFT,NODE,node_num,U,X

ALLSEL
NSEL,S,LOC,X,X(04)
NSEL,R,LOC,Z,BEAMHEIGHT/2
NSEL,R,LOC,Y,WIDTH/2
*GET,node_num,NODE,0,NUM,MIN
*GET,DELTA_A_RIGHT,NODE,node_num,U,X

DELTA_A = DELTA_A_RIGHT - DELTA_A_LEFT
```

```
ALLSEL
NSEL,S,LOC,X,LENGTH/2
NSEL,R,LOC,Z,BEAMHEIGHT/2
NSEL,R,LOC,Y,WIDTH/2
*GET,node_num,NODE,0,NUM,MAX
*GET,DELTA_B_MID,NODE,node_num,U,Z
DELTA_B = - DELTA_B_MID

ALLSEL
ESEL,S,TYPE,,5
*GET,elem_num,ELEM,0,NUM,MIN

ALLSEL
KSEL,S,KP,,10
NSLK
*GET,node_num,NODE,0,NUM,MAX
*GET,FORCE_TIEROD,ELEM,elem_num,EFOR,node_num,FX
FORCE_R =2*FORCE_TIEROD

SET,1,30

ALLSEL
ESEL,S,TYPE,,5
*GET,elem_num,ELEM,0,NUM,MIN

ALLSEL
KSEL,S,KP,,10
NSLK
*GET,node_num,NODE,0,NUM,MAX
*GET,PRE-STRESS_TIEROD,ELEM,elem_num,EFOR,node_num,FX

PRE_STRESS =2*PRE-STRESS_TIEROD
DELTA_C_DIFF = DELTA_C + DELTA_TOT
DELTA_A_DIFF = DELTA_A - DELTA_A_INI
DELTA_B_DIFF = DELTA_B - DELTA_B_INI


*CFOPEN,'RESULTS',INP
*VWRITE,'DELTA_A',DELTA_A
(A7,' = ',F12.8)
*VWRITE,'DELTA_B',DELTA_B
(A7,' = ',F12.8)
*VWRITE,'DELTA_C',DELTA_C
(A7,' = ',F12.8)
*VWRITE,'FORCE',FORCE_R
(A7,' = ',F9.2)
*VWRITE,'PRESTRE',PRE_STRESS
(A7,' = ',F9.2)
*VWRITE,'DEL_A_D',DELTA_A_DIFF
(A7,' = ',F12.8)
*VWRITE,'DEL_B_D',DELTA_B_DIFF
(A7,' = ',F12.8)
*VWRITE,'DEL_C_D',DELTA_C_DIFF
(A7,' = ',F12.8)
*CFCLOS

FINISH
ALLSEL
SAVE,,,ALL

/EOF
```

Norges miljø- og biovitenskapelige universitet
Noregs miljø- og biovitskapelege universitet
Norwegian University of Life Sciences

Postboks 5003
NO-1432 Ås
Norway